BELL CREEK TEST SITE – SIMULATION REPORT

Plains CO_2 Reduction (PCOR) Partnership Phase III
Task 9 – Deliverable D66, Update 4

Originally Submitted: August 2011; Update 1 Submitted: August 2012; Update 2 Submitted: August 2013; Update 3 Submitted: August 2014

Prepared for:

Andrea M. Dunn

National Energy Technology Laboratory
U.S. Department of Energy
626 Cochrans Mill Road
PO Box 10940
Pittsburgh, PA 15236-0940

DOE Cooperative Agreement No. DE-FC26-05NT42592

Prepared by:

Nicholas W. Bosshart
Lu Jin
Neil W. Dotzenrod
Shaughn A. Burnison
Jun Ge
Jun He
Matthew E. Burton-Kelly
Scott C. Ayash
Charles D. Gorecki
John A. Hamling
Edward N. Steadman
John A. Harju

Energy & Environmental Research Center
University of North Dakota
15 North 23rd Street, Stop 9018
Grand Forks, ND 58202-9018

August 2015
Approved

2016-EERC-10-09

EERC DISCLAIMER

LEGAL NOTICE This research report was prepared by the Energy & Environmental Research Center (EERC), an agency of the University of North Dakota, as an account of work sponsored by the U.S. Department of Energy (DOE) National Energy Technology Laboratory (NETL). Because of the research nature of the work performed, neither the EERC nor any of its employees makes any warranty, express or implied, or assumes any legal liability or responsibility for the accuracy, completeness, or usefulness of any information, apparatus, product, or process disclosed or represents that its use would not infringe privately owned rights. Reference herein to any specific commercial product, process, or service by trade name, trademark, manufacturer, or otherwise does not necessarily constitute or imply its endorsement or recommendation by the EERC.

ACKNOWLEDGMENTS

This work was performed under DOE NETL Cooperative Agreement No. DE-FC26-05NT42592. The EERC would like to thank Denbury Resources Inc. (Denbury) for providing necessary data to perform this work. Special thanks go to the members of Denbury's Bell Creek team for their valuable input and fruitful discussions.

DOE DISCLAIMER

This report was prepared as an account of work sponsored by an agency of the United States Government. Neither the United States Government, nor any agency thereof, nor any of their employees, makes any warranty, express or implied, or assumes any legal liability or responsibility for the accuracy, completeness, or usefulness of any information, apparatus, product, or process disclosed, or represents that its use would not infringe privately owned rights. Reference herein to any specific commercial product, process, or service by trade name, trademark, manufacturer, or otherwise does not necessarily constitute or imply its endorsement, recommendation, or favoring by the United States Government or any agency thereof. The views and opinions of authors expressed herein do not necessarily state or reflect those of the United States Government or any agency thereof.

NDIC DISCLAIMER

This report was prepared by the EERC pursuant to an agreement partially funded by the Industrial Commission of North Dakota, and neither the EERC nor any of its subcontractors nor the North Dakota Industrial Commission nor any person acting on behalf of either:

(A) Makes any warranty or representation, express or implied, with respect to the accuracy, completeness, or usefulness of the information contained in this report or that the use of any information, apparatus, method, or process disclosed in this report may not infringe privately owned rights; or

(B) Assumes any liabilities with respect to the use of, or for damages resulting from the use of, any information, apparatus, method, or process disclosed in this report.

Reference herein to any specific commercial product, process, or service by trade name, trademark, manufacturer, or otherwise does not necessarily constitute or imply its endorsement, recommendation, or favoring by the North Dakota Industrial Commission. The views and opinions of authors expressed herein do not necessarily state or reflect those of the North Dakota Industrial Commission.

TABLE OF CONTENTS

LIST OF FIGURES

Continued . . .

LIST OF FIGURES (continued)

LIST OF TABLES

BELL CREEK TEST SITE – SIMULATION REPORT

EXECUTIVE SUMMARY

The Plains CO_2 Reduction (PCOR) Partnership is working with Denbury Resources Inc. (Denbury) to evaluate the effectiveness of large-scale injection of carbon dioxide (CO_2) into the Bell Creek oil field for CO_2 enhanced oil recovery (EOR) and to study long-term associated CO_2 storage.

With the goal of providing a comprehensive assessment of associated CO_2 storage behavior, the PCOR Partnership has initiated a modeling and numerical simulation effort as part of its adaptive management approach to CO_2 storage program development. The modeling and simulation efforts include 1) characterizing and modeling the study area; 2) developing a robust pressure, volume, and temperature model to predict the miscibility behavior of the system and to aid in compositional simulation; 3) history-matching the constructed dynamic reservoir models; and 4) running predictive simulations to aid in monitoring long-term behavior of injected CO_2.

This report encompasses the modeling and simulation work completed since August 2014 and includes 1) the construction of a Bell Creek reference model to enable consistency across the various geologic modeling efforts, 2) the incorporation of 33 baseline and 19 repeat pulsed-neutron logs (PNLs) to improve the static and dynamic geocellular models, 3) history-matching and predictive simulations of the combined Phase 1 and 2 area (clipped from the Version (V) 2 geologic model), and 4) construction of a V3 geologic model, developed to incorporate 3-D surface seismic data and portray a new understanding of the reservoir's depositional history.

The reference model has been constructed to house key data sets associated with the Bell Creek Field, including 751 wells, field and processed logs, core analyses, structural tops, cultural surface boundaries, completed simulation results, ground surface elevation from lidar, and 3-D surface seismic data. The reference model will be important for future Bell Creek efforts to provide a foundation to ensure consistency across various modeling efforts.

Individual Phase 1 and 2 simulation models, previously developed and reported in Liu and others[1], have been combined to form a new simulation model that enables simulated fluid flow between the phases. Simulation work discussed in this report includes 1) history-matching 47 years of field records with primary production, waterflooding, and CO_2 EOR in the Phase 1 and 2 areas; 2) analyzing fluid saturation distribution in the reservoir; 3) identifying cross-boundary fluid flow between Phases 1 and 2; and 4) predictive simulations of continuous CO_2 injection

[1] Liu, G., Braunberger, J.R., Pu, H., Gao, P., Gorecki, C.D., Ge, J., Klenner, R.C.L., Bailey, T.P., Dotzenrod, N.W., Bosshart, N.W., Ayash, S.C., Hamling, J.A., Steadman, E.N., and Harju, J.A., 2014, Bell Creek test site – simulation report: Plains CO_2 Reduction (PCOR) Partnership Phase III Task 9 Deliverable D66 Update 4 for U.S. Department of Energy National Energy Technology Laboratory Cooperative Agreement No. DE-FC26-05NT42592, August.

(CCI) and water alternating gas (WAG) in both Phase 1 and 2 areas to assess oil recovery, CO_2 storage, and CO_2 utilization factor.

Results of predictive simulations for the Bell Creek project include the following:

- The WAG case results in less hydrocarbon pore volumes injected (HCPVI) than CCI for the same injection time (WAG injects 3 HCPVs, while CCI injects 4.65 HCPVs). This is because CO_2 has lower density and viscosity than water; more pore volumes of CO_2 can be injected into the reservoir (in comparison to water) under the same pressure constraints.

- CCI results in approximately twice the injected CO_2 in comparison to the WAG case and approximately 1.7 times more CO_2 stored (however, more CO_2 is produced with oil in CCI mode). Also, CCI requires more injected CO_2 to produce the same amount of oil in comparison to the WAG case.

- During the simulated WAG case, the CO_2 utilization factor (i.e., amount of CO_2 needed to produce 1 barrel of oil) dropped below 10 MMscf/bbl after 1 HCPVI. This decreased to 7 MMscf/bbl when 3 HCPVs were injected in the WAG mode. The value remains above 10 MMscf/bbl, even after 4 HCPVI, in CCI mode. These results agree with similar results published in Ettehadtavakkol and others.[2]

- The incremental oil recovery from CCI and WAG is almost the same, while the HCPVI of WAG is 35% less than that of CCI. Thus WAG has higher sweep efficiency and can utilize CO_2 better than CCI in the EOR process.

It should be noted that the previously developed V1 and V2 geologic models (and subsequently the simulation results discussed above) have roots in the conventional Bell Creek depositional interpretation of stacked barrier bar sands within a large, Galveston Island-style depositional environment oriented approximately northeast to southwest. Recent investigations discussed within this report (history-matching during simulation efforts, incorporation and interpretation of 3-D and 4-D seismic surveys, and comparison of PNL measured oil saturations with modeled oil saturations) have indicated this interpretation should be reexamined in renewed (V3) modeling efforts.

Integration and interpretation of the Bell Creek 3-D baseline surface seismic data lend support to a new depositional model with an interpreted local, transgressive barrier bar (as seen to be related to character in the upper Bell Creek sand interval) in Phases 1 and 2, indicating a large shift in inferred shoreline orientation from previous studies (approximately northwest to southeast). As such, a V3 model is under construction which will incorporate the new geophysical data, results from the history-matched simulation model, and the new geological interpretation. This model will then be used along with the V2 model in the history-matching and predictive simulation efforts to better understand the long-term fate of the injected CO_2.

[2] Ettehadtavakkol, A., Lake, L.W., and Bryant, S.L., 2014, CO_2 EOR and storage design optimization: International Journal of Greenhouse Gas Control, v. 25, p. 79–92.

BELL CREEK TEST SITE – SIMULATION REPORT

INTRODUCTION

The Plains CO_2 Reduction (PCOR) Partnership, led by the Energy & Environmental Research Center (EERC), is working with Denbury Resources Inc. (Denbury) to determine the effect of large-scale injection of carbon dioxide (CO_2) into a deep clastic reservoir for the purpose of CO_2 enhanced oil recovery (EOR) and to monitor associated CO_2 storage at the Bell Creek oil field, which is operated by Denbury Onshore LLC. A technical team that includes Denbury, the EERC, and others is conducting a variety of activities to determine the baseline reservoir characteristics and perform predictive simulations of CO_2 injection. The results of these activities will facilitate the assessment of various potential injection schemes, guide monitoring strategies, and help determine the ultimate fate of injected CO_2. Denbury is carrying out the injection and production operations, while the EERC provides support for site characterization, modeling and simulation, risk assessment, and the development of the monitoring, verification, and accounting (MVA) plan to address key technical subsurface risks (Gorecki and others, 2012).

The Bell Creek oil field in southeastern Montana is a subnormally pressured reservoir with significant hydrocarbon charge that lies near the northeastern boundary of the Powder River Basin (PRB) (Figure 1). Exploration and production activities for mineral and energy resources in the area over the last 55 years have yielded a significant amount of information about the geology of southeastern Montana and the northern PRB, which has been cataloged in a literature review. Decades of oil and gas production through primary and secondary recovery (waterflood and polymer flood pilot tests) have resulted in reservoir decline and have led to the current CO_2 injection-based tertiary oil recovery project. CO_2 is being delivered to the site via the 232-mile Greencore Pipeline from the ConocoPhilips Lost Cabin natural gas-processing plant and from ExxonMobil's Shute Creek gas-processing plant in LaBarge, Wyoming (Figure 1). Currently, around 50 million standard cubic feet (MMscf) of CO_2 a day is delivered to the field for EOR operations.

CO_2 is being injected into the oil-bearing sandstone reservoir of the Lower Cretaceous Muddy (Newcastle) Formation at a depth of approximately 4500 feet (1372 meters) (Figure 2). Nine stages of injection are scheduled to occur across the field (Figure 3). Laboratory studies (minimum miscibility pressure [MMP] analysis, slim-tube studies, and core sample oil extractions) indicate the reservoir is suitable for miscible flooding conditions, with an incremental oil production target of 40–50 million barrels (MMbbl). The activities at the Bell Creek oil field will inject an estimated 1 million tons (Mt) of purchased CO_2 annually, much of which will be permanently stored at the end of the EOR project.

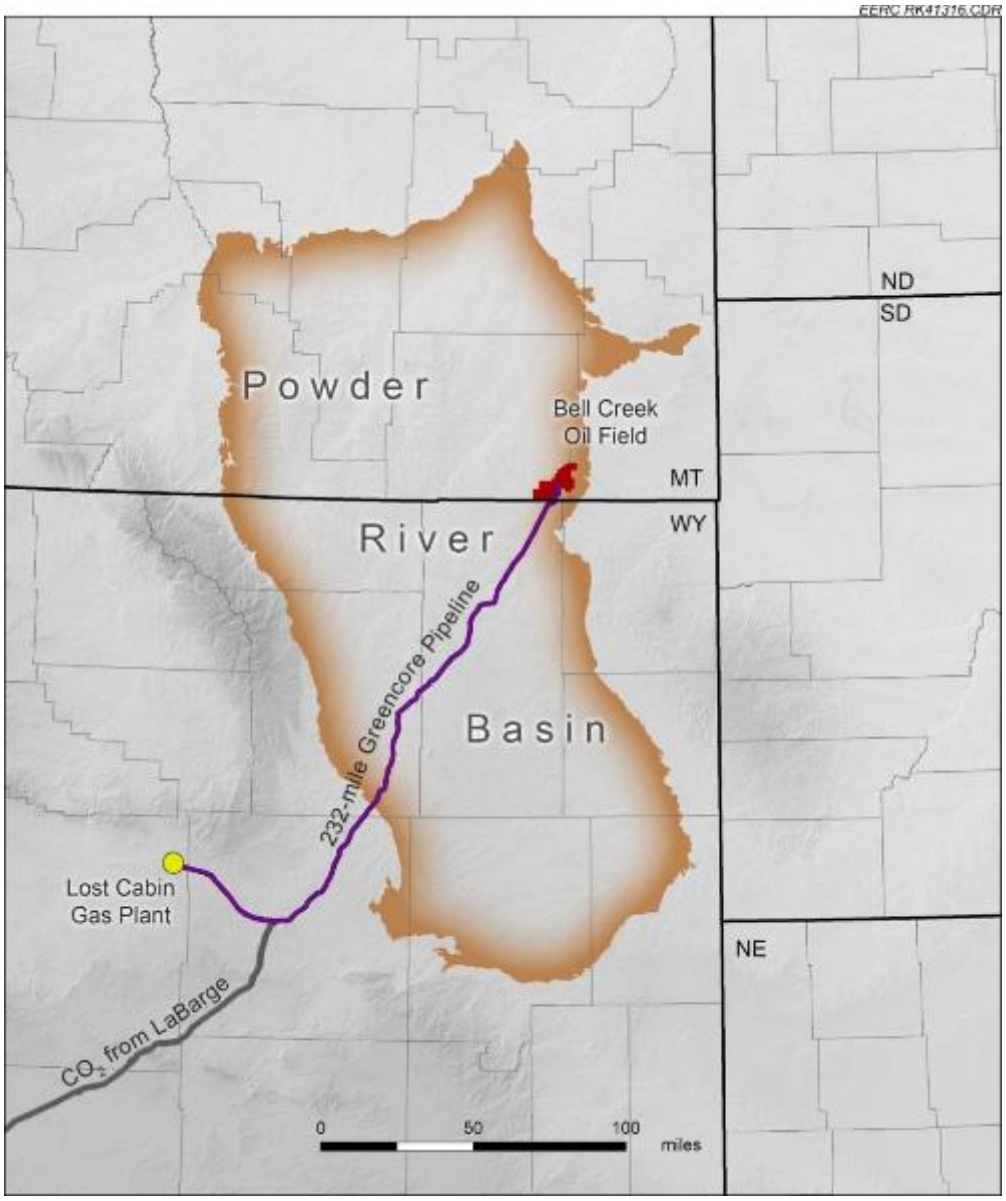

Figure 1. Map depicting the location of the Bell Creek oil field in relation to the PRB and the completed pipeline route to the site from the Lost Cabin gas plant.

Within the Bell Creek oil field, the Muddy Formation is dominated by high-porosity (25%–35%), high-permeability (150–1175 mD) sandstones deposited in a nearshore marine environment (Saini and others, 2012). The initial reservoir pressure was approximately 1200 psi, which is significantly lower than the regional hydrostatic pressure regime (2100 psi at 4500 feet). The oil field is located structurally on a shallow monocline with a 1°–2° dip to the northwest and with an axis trending southwest to northeast for a distance of approximately 20 miles. Stratigraphically, the Muddy Formation in the Bell Creek oil field features an updip sand facies pinch-out into shale facies serving as a trap.

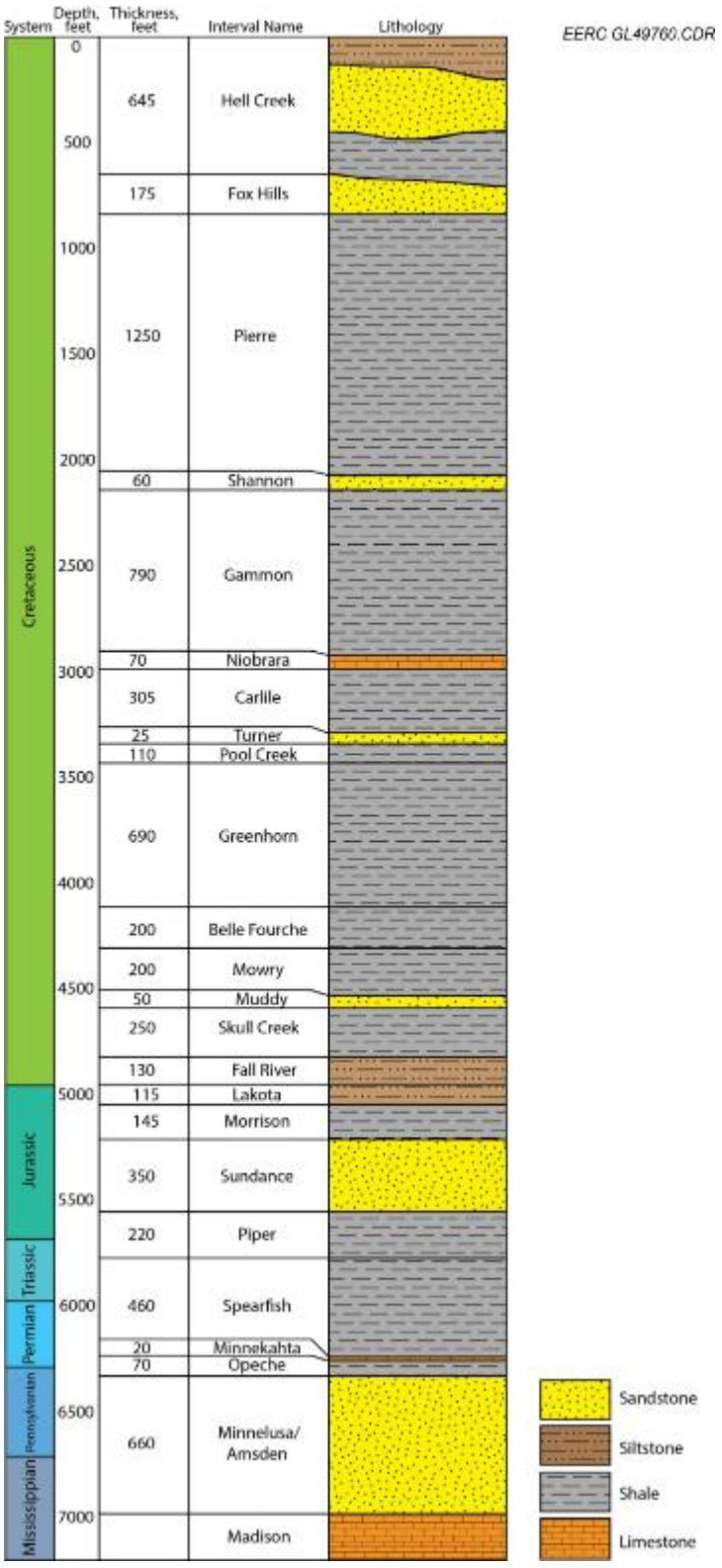

Figure 2. Local stratigraphy of the Bell Creek development area.

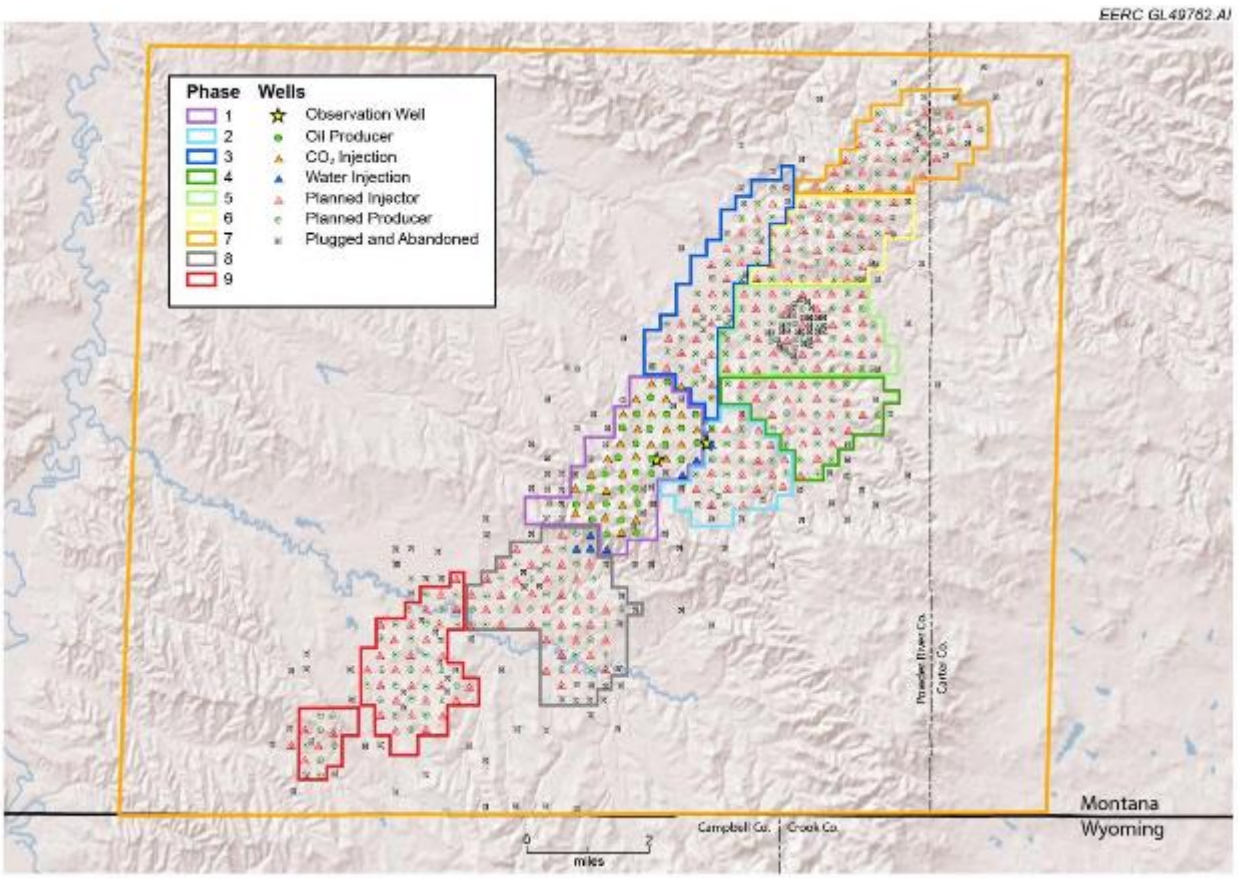

Figure 3. Study area of the Bell Creek oil field showing the nine phases of scheduled injection.

The Muddy Formation of the Bell Creek Field has been divided into four informal members, consisting of (in ascending order) the Rozet Member (lowermost silty interval overlying the Skull Creek Shale), Bell Creek Sand Interval, Coastal Plain Interval (this interval is not considered a separate member in this study, instead included within the Bell Creek Sand Interval), and Springen Ranch Member (estuarine and shallow marine locally sandy siltstone/shale; see Figure 4). Recent efforts to understand the Muddy Formation of the field have shown the Bell Creek Sand Interval can, generally, be divided into (up to) four intervals: 1) a lowermost, laterally extensive sand appearing to have high connectivity throughout the field (interpreted from production logs) and thought to be prodelta or lower shoreface deposits (deposited during regression/relative sea-level fall); 2) a silty sand-to-siltstone interval possibly representing a slight deepening in water depth (relative sea-level rise); 3) a sand interval appearing similar to the lower sand and likely deposited in a similar manner (during regression/relative sea-level fall) but appearing to have an erosional unconformity at the top (as evidenced by change in grain sorting and composition, bedding character and, in some places, the presence of thin coals, indicating subaerial exposure); and 4) if present, an upper sand lying unconformably upon Interval 3 with variable thickness and thought to be deposited during a final transgression (relative sea-level rise), likely deposited in barrier bar-to-shoreline environments. An estuarine/shallow marine siltstone (lower Springen Ranch) overlaps the sandstone, deposited as transgression continued.

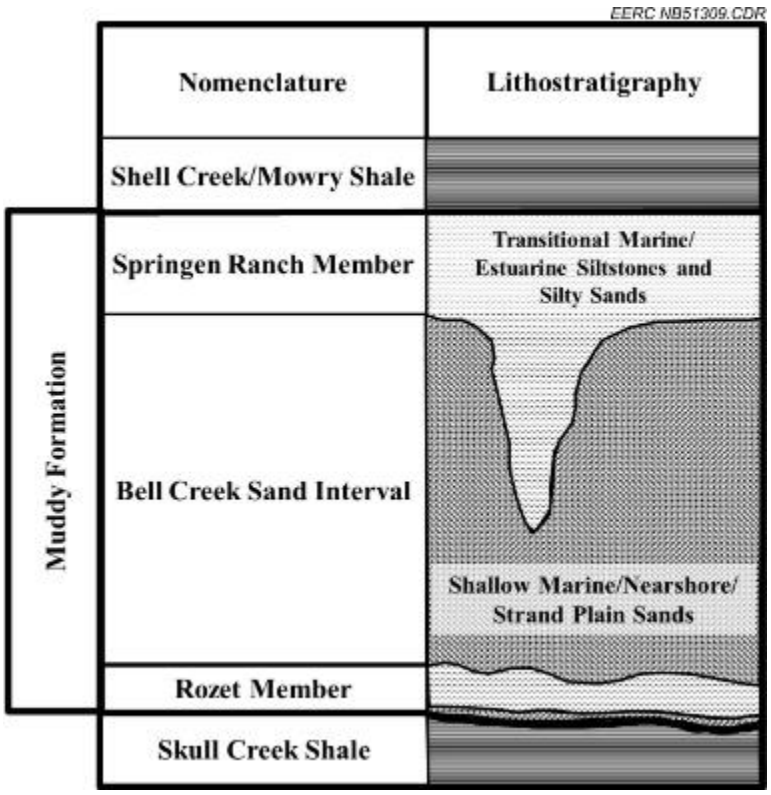

Figure 4. Muddy Formation reservoir stratigraphy (adapted from Molnar, 1990).

The overlying Lower Cretaceous Mowry Formation provides the primary seal, preventing fluid migration to overlying aquifers and to the surface. On top of the Mowry Formation are several thousand feet of low-permeability strata, including the Belle Fourche, Greenhorn, Niobrara, and Pierre Formations, which provide redundant layers of protection in the unlikely event that the primary seal fails to prevent upward fluid migration (Figure 2).

The Version (V) 3 static geologic model is being constructed to include these new interpretations, representing the full-field study area centered on Phase 1.

The simulation activities during this reporting period pertain to the V2 geologic model and were mostly focused on the Phase 1 and 2 areas for history-matching production/injection and pressure records and various predictive simulations. The simulation efforts using the V2 geologic model experienced difficulties during the history-matching process, indicating that the modeled reservoir geology (developed and supporting the conventional thought of deposition as part of a large-scale, Galveston Island-style barrier bar) may not be an accurate representation of the actual reservoir geology. As such, renewed efforts have focused on increasing our understanding of the Muddy Formation sand deposition and the construction of a new (V3) geologic model. These efforts will, upon completion of the V3 model, enable more accurate predictive estimates of fluid flow and pressure response and will provide valuable data to support the design and implementation of a monitoring program to track the injected CO_2 in the Bell Creek Field.

PURPOSE

The PCOR Partnership is employing an adaptive management approach for large-scale CO_2 storage projects consisting of four main components: site characterization, modeling and simulation, risk assessment, and MVA. Each component is continually evaluated and updated throughout the lifetime of a project. The results of each evaluation then serve as input for the remaining components (Figure 5). This iterative cycle is repeated throughout all project phases, from feasibility study through postclosure monitoring. The PCOR Partnership's adaptive management approach allows the site-specific nature of any carbon storage project to be taken into account and creates a dynamic environment where monitoring strategies, for example, can be adjusted to accommodate an evolving risk and operational profile. Thus the MVA techniques deployed will always target relevant technical risks and ensure that the most cost-effective,

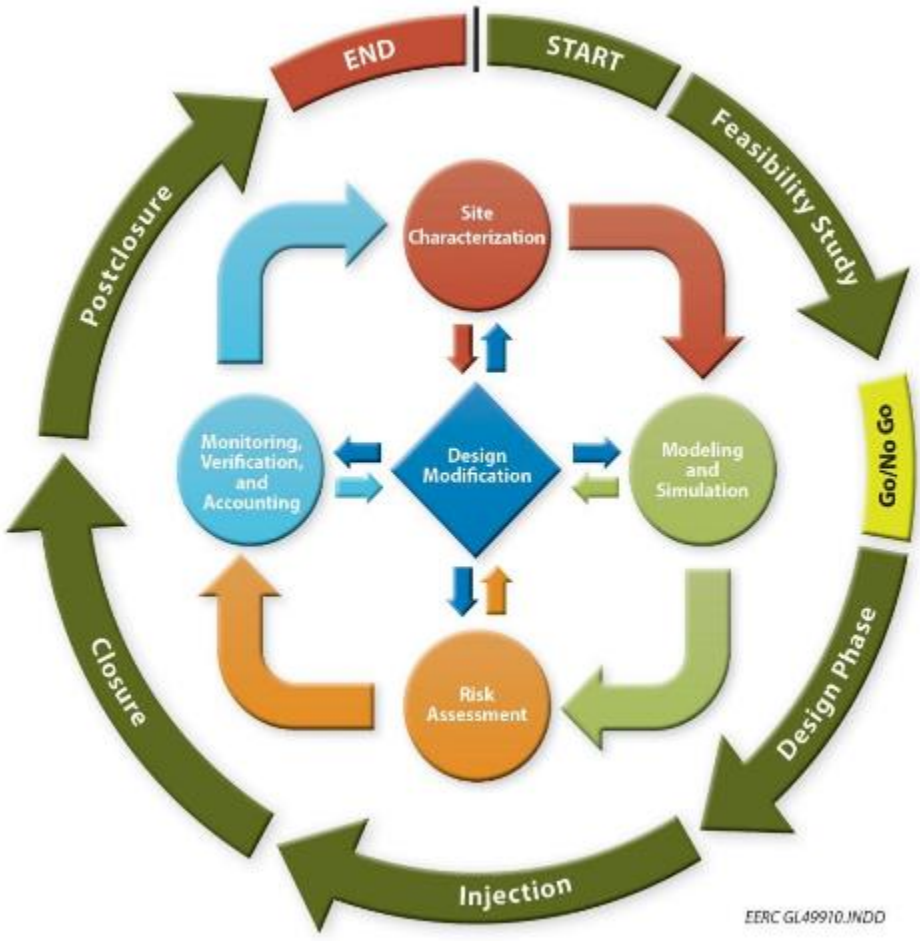

Figure 5. Project elements of the Bell Creek CO_2 storage and EOR project. Each element feeds into another, iteratively improving results and efficiency of evaluation (modified from Gorecki and others, 2012).

technically viable, site-specific strategies will be used throughout the life of a project. This integrated process is refined through each incremental stage of the project, from initial planning, to injection, and through postclosure.

The EERC's geologic modeling of the subsurface assists in understanding and predicting the behavior of the injected CO_2 and reservoir fluids over the injection and postinjection period. To aid in the validation of the reservoir model, history matching is performed on a numerically tuned dynamic reservoir model that is constructed using a completed 3-D static geologic model. This is followed by simulation work, which is a valuable tool for assessing scenarios of fluid migration within the reservoir and the potential for out-of-zone fluid migration. Additionally, simulation activities provide a means to evaluate the sweep and storage efficiency and the applicability of various monitoring activities related to both associated CO_2 storage and CO_2 EOR in different scenarios.

Performing geologic characterization, geocellular modeling, and numerical simulation is essential input for risk identification and to guide MVA. This approach lays the foundation for a project-specific, risk-based, goal-oriented MVA plan. The goal of the MVA plan is to effectively monitor the behavior of the injected CO_2 and reservoir fluids in the subsurface throughout the project life. Predictive simulations assist with targeted deployment of MVA data acquisitions at optimal geographic locations and time intervals to maximize the knowledge gained and minimize expenditures. The results and experience gained at the Bell Creek oil field will provide insight and knowledge that can be directly and readily applied to similar projects within the PCOR Partnership region and throughout the world (Steadman and others, 2011; Hamling and others, 2013).

BACKGROUND

Following the adaptive management philosophy developed by the PCOR Partnership (Figure 5), modeling and simulation activities have been updated annually based on available site characterization data and field injection/production records to improve risk identification and the MVA plan. All elements have been integrated into an iterative process to produce meaningful results for large-scale CO_2 storage and EOR projects. To date, four versions of the modeling and simulation reports have been produced to cover the highlights of activities since 2011. A brief description of each report follows:

- **Bell Creek Test Site Simulation Report: PCOR Partnership Phase III Task 9 Deliverable D66, 2011, approved (Pu and others, 2011)**

  The V1 3-D geologic model was developed based on the available site characterization data and was focused on the Phase 1 area. A generalized lithology and stratigraphic framework in the Bell Creek oil field were interpreted that include four distinct lithofacies, Springen Ranch shale, coastal plain, Bell Creek sand, and Rozet shale in the Muddy Formation. The structure and properties were populated based on the 154 wells within the study boundary. Available data were analyzed, interpreted, and incorporated into the 3-D static geologic and dynamic reservoir models to represent geologic and reservoir properties in order to provide a solid groundwork for simulation activities.

The PVT (pressure, volume, and temperature) data from three fluid samples were analyzed and lumped as seven components that matched the laboratory data. The results indicate that miscibility for oil samples can be achieved at approximately 2800 psi.

- **Bell Creek Test Site Simulation Report: PCOR Partnership Phase III Task 9 Deliverable D66, 2012, approved (Saini and others, 2012)**

  A 1-D compositional simulation of the experimental slim-tube tests was performed to ensure the robustness of the seven-component Peng–Robinson (PR) equation of state (EOS) developed in 2011. MMP estimated from slim-tube simulation is about 2750 psia at 108°F, which agrees with the experimental results.

  The constructed geologic model was validated through history matching of oil rate, water cut, and gas/oil ratio (GOR) and was used for various predictive simulation scenarios for the Phase 1 area. A total of 12 cases based on a five-spot, a quarter five-spot, and the entire Phase 1 pattern were designed to address associated CO_2 storage and CO_2 breakthrough at the monitoring well, 05-06 OW, from a CO_2 water alternating gas (WAG) injection scenario.

- **Bell Creek Test Site Simulation Report: PCOR Partnership Phase III Task 9 Deliverable D66, 2013, pending approval (Braunberger and others, 2013)**

  A detailed 3-D static geocellular model of the Bell Creek oil field area (V2 model) was constructed using pertinent reservoir characterization data gathered in an extensive literature review and existing core analysis work for the entire Bell Creek oil field and surrounding area. Seven hundred forty-eight wells with wireline logs and many with core data were analyzed, interpreted, and incorporated into the 3-D static geocellular and dynamic reservoir models to represent geologic stratigraphy, petrophysical facies, and reservoir properties for simulation activities.

  The seven-component PR EOS model was tuned and matched to both original oil and depleted oil from slim-tube test and laboratory data. This produced an acceptable EOS for both matching historic production/injection and for performing predictive simulations.

  The Phase 1 area and immediately adjacent area were clipped from the V2 model and matched to production and injection historical records for a total of 46 years to validate the model and to get a good estimate of the current saturations and pressures in the model. Five predictive simulation cases were run to evaluate WAG and continuous CO_2 injection (CCI) at two injection bottomhole pressure (BHP) constraints and varying WAG cycle lengths.

- **Bell Creek Test Site Simulation Report: PCOR Partnership Phase III Task 9 Deliverable D66, 2014, pending approval (Liu and others, 2014)**

  Thirty-three baseline pulsed-neutron logs (PNLs) and seven repeat PNLs were used to update the stratigraphy and formation thicknesses from the reservoir to the surface throughout the V2 geologic model. Changes in fluid saturations for CO_2, water, and oil were identified through the repeat logs and incorporated into the model. In addition, a comprehensive reference model was created to serve as a repository for all relevant Bell Creek data used in the modeling and simulation activities. The existing V1 and V2 models, PNLs, historic and newly acquired logs, and core data were included in the reference model.

  A Phase 2 area simulation model was created from the V2 fieldwide 3-D geologic model and validated by history-matching oil, water, and gas production; water injection; and reservoir pressure data. The history-matched Phase 1 and 2 models were used to conduct predictive simulations to estimate the CO_2 storage potential of the Bell Creek Field as well as better understand sweep efficiency, recovery factor, and CO_2 utilization. Five simulation cases for Phases 1 and 2 (ten cases total) were performed to investigate WAG and CCI for two injection BHP constraints and varying WAG cycle lengths. Results indicated that WAG yields faster oil recovery and better sweep efficiency than CCI in Phase 1 and Phase 2, while CCI results in more CO_2 being stored.

SCOPE OF WORK

In order to evaluate the efficiency of large-scale CO_2 injection for CO_2 EOR and to monitor the associated CO_2 storage in the Muddy Formation at the Bell Creek oil field, several iterations of a 3-D geologic modeling coupled with dynamic simulation work were completed as submitted in the previous four D66 reports (2011, 2012, 2013, and 2014). This report documents the modeling and simulation activities completed over the course of the past year (August 2014–August 2015), which includes 1) updating of a Bell Creek reference model housing all relevant modeling data and serving as a foundation for consistency across various modeling efforts; 2) geological interpretation based on the newly acquired PNL, seismic, and core data; 3) beginning efforts in the construction of a new (V3) geologic model to more accurately capture the reservoir heterogeneity; and 4) the history-matching and simulation of a combined Phase 1 and 2 model (from the V2 geologic model).

Repeat pulsed-neutron well logging was performed through casing from the surface to the reservoir, primarily to identify changes in fluid saturations of CO_2, water, and oil for fluid movement monitoring and characterization in, above, and below the reservoir. These data also help to identify geologic formation breaks, which are critical to understanding the local stratigraphy of the Bell Creek Field from the reservoir to the surface.

Integration of the baseline 3-D surface seismic data set with high lateral resolution (~82 feet) has provided an increased understanding of the Muddy Formation deposition and enabled a higher degree of accuracy in capturing the reservoir geology in V3 modeling efforts.

Previously developed, separate Phase 1 and 2 simulation models have been combined in an integrated model, which has been used to 1) history-match field records, including primary production, waterflooding, and CO_2 EOR in Phase 1 and 2 areas for 47 years; 2) run predictive simulations of CCI and WAG in both Phase 1 and 2 areas to assess oil recovery, CO_2 storage, and CO_2 utilization factor; and 3) provide a foundation for ongoing work in another iteration of modeling and simulation activities, which has been integrated into the PCOR Partnership's adaptive management plan (Figure 5).

Bell Creek Reference Model

EERC efforts relating to the Bell Creek project have been ongoing for several years, have involved a large number of research staff, and have included several different types and iterations of modeling activities. Long-term projects such as Bell Creek generate large amounts of data, which can create a challenge in the storage and organization of those data. These efforts also require the ability for multiple individuals to examine and interpret the data (potentially simultaneously). Additionally, awareness and access to the most up-to-date and accurate data sometimes becomes an issue, especially when involving new researchers and during data transmission between individuals. Under these circumstances, it is important for project teams to efficiently and methodically manage and store these data. To overcome these challenges, the EERC modeling and simulation group has created (using Schlumberger's Petrel) a 3-D Bell Creek reference model (or repository) of quality-controlled, up-to-date modeling data from which data may be transferred or new models may be built. This enables efficiency in future modeling and simulation activities and acts as a foundation to ensure consistency between various modeling efforts. The Bell Creek reference model has already been used to assist in the development of the EERC's V3 geologic, geomechanical, PNL, and near-surface models.

Data stored in the reference model have been obtained from multiple sources, including previous modeling and simulation results (see Appendix A). The model has been constructed to house associated Bell Creek data, including 751 wells, field and processed logs, core analyses, structural tops, cultural surface boundaries, completed simulation results, ground surface elevation from lidar, and 3-D surface seismic data.

Prior to November 2012, 33 baseline PNLs were acquired in Phases 1 and 2 of the Bell Creek Field. Since that time, several repeat PNL campaigns (resulting in 19 additional repeat/monitor PNL data sets; see Figure 6) have been completed to measure changes in oil, water, and gas saturations. Each logging campaign generates a large volume of data (field and processed logs) that will be quality-checked and analyzed by multiple individuals for various investigations (e.g., for use in the EERC's MVA efforts in assessing containment effectiveness by monitoring saturations in overlying formations, to calibrate history-matching efforts during dynamic simulation, etc.). To help facilitate these diverse activities, the logs are stored within the reference model to ensure ease of access and ability to incorporate the most up-to-date iterations of these logs.

With regard to use of the PNLs in the Bell Creek project's MVA program, the EERC's Modeling and Simulation Group has been working with Schlumberger and Denbury to evaluate

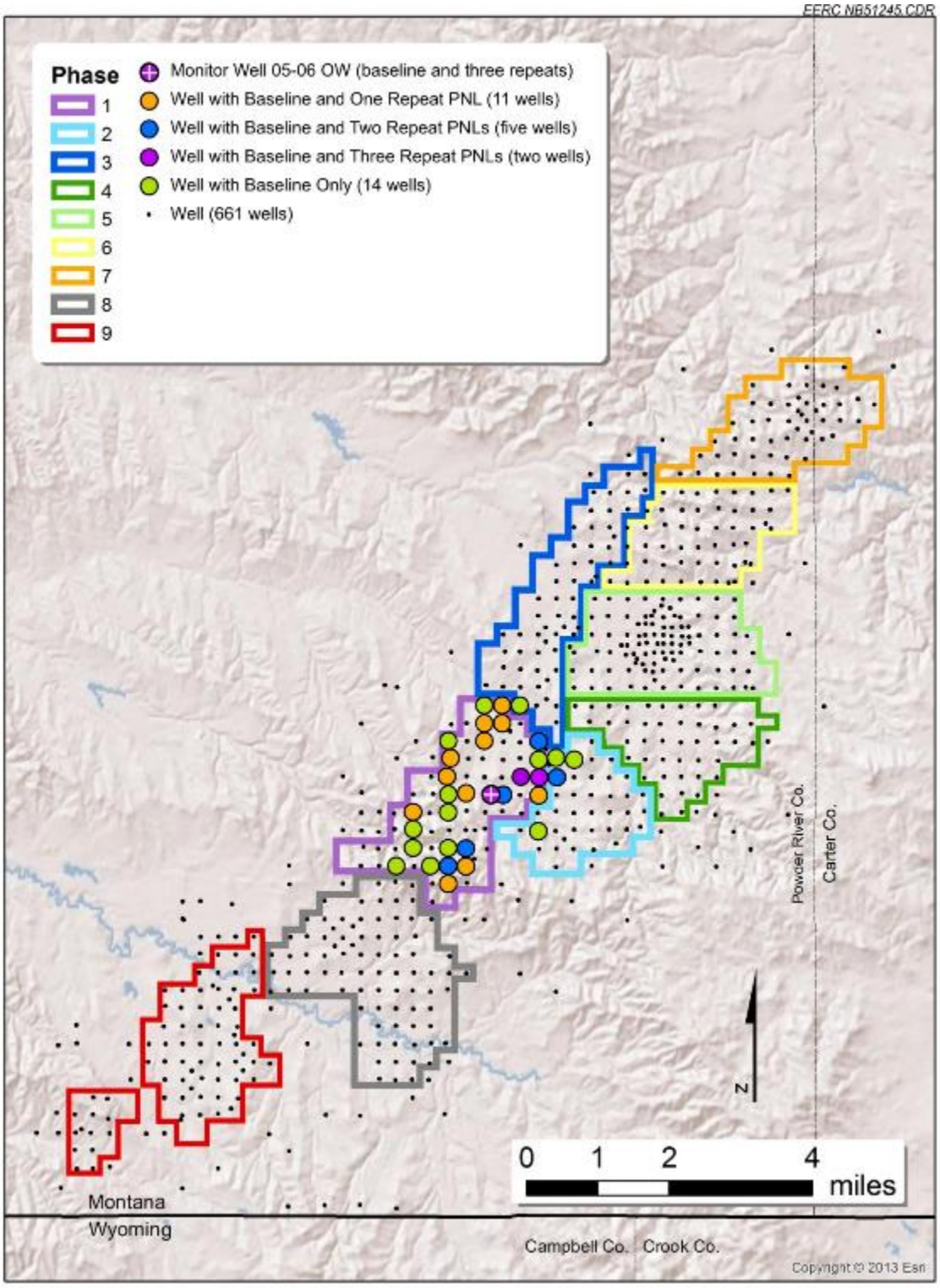

Figure 6. Map of wells showing where baseline and monitor pass PNLs were collected within the Bell Creek Field.

and interpret the accuracy and practical utility of these logs with respect to geologic and geophysical aspects of the reservoir. As part of this effort, the logs were reinterpreted from the original processing of the field logs. This was necessary for the following reasons:

1. The results from the original processing (from reservoir to surface) were acquired using only the sigma values (matrix and fluid) calculated from the reservoir. This resulted in unrealistic characterization of overlying formations (increased sand content and anomalously high effective porosity estimates existing in shale-rich intervals, etc.). Comparing these estimates with available cores has made such inaccuracies clear.

2. PNL acquisition occurs using two modes: sigma and carbon/oxygen (C/O). The C/O model is used to monitor fluid saturations, and data for this model have only been acquired in the reservoir interval. The sigma mode, while not useful in providing detailed (quantitative) fluid saturation measurements, may still be used to identify potential zones of unintended CO_2 saturation (qualitative) outside of the reservoir. Thus accuracy in overlying formations is of importance and necessary for implementation within a successful MVA framework.

Examples of PNL results from Wells 32-11 (injection well) and 32-02 (production well) are shown in Figures 7 and 8, respectively.

An added benefit in PNL acquisition in Bell Creek has been increasing confidence in the understanding of the field's subsurface stratigraphic and structural character, which previously relied on (for the most part) legacy resistivity and spontaneous potential logs (resistivity and spontaneous potential well logs were acquired from reservoir to surface; gamma ray and other select well logs were acquired for only the reservoir and short intervals of the overlying strata). The recent PNL campaigns, which run from the reservoir to within 200 ft of the surface (sigma mode), have presented an opportunity to adjust formation tops with higher confidence, and these formation tops have been incorporated into the Bell Creek reference model.

The PNL-informed formation tops are contributing to the development of a near-surface model (currently under construction; see Figure 9), which will provide a structural framework and property model of the Pierre, Fox Hills, and Lower Hell Creek aquifer intervals and Upper Hell Creek (exposed at the surface) Formation of the Bell Creek Field and nearby areas. This model's purpose lies in the integration of near-surface monitoring data into the management and assessment of the site's evolving risk profile. This model may also be used in the future for simulations of possible CO_2 migration from the reservoir, helping to inform and adapt MVA efforts and, ultimately, enable rapid response in the event of out-of-zone CO_2 movement.

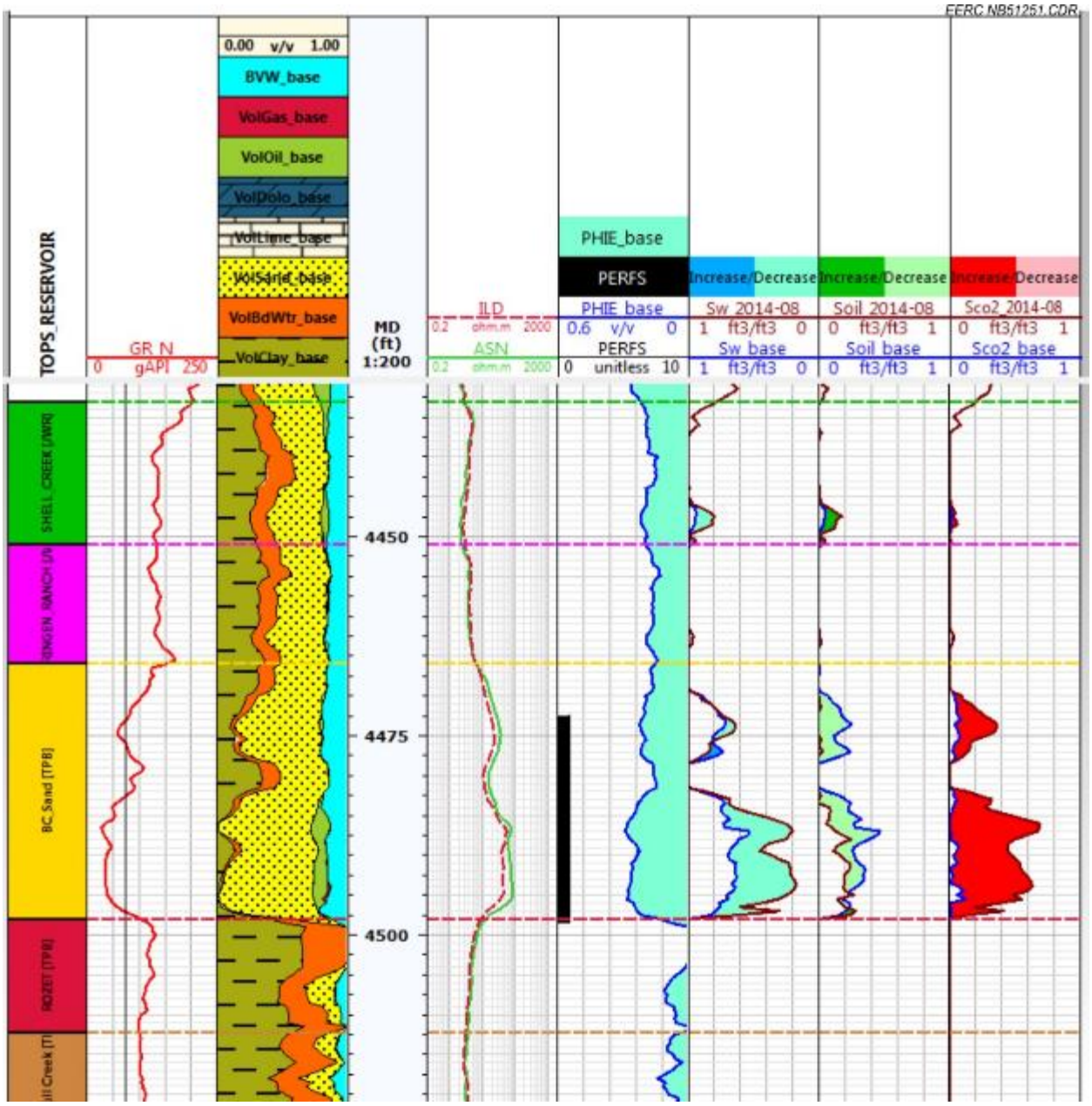

Figure 7. 32-11 injection well log display within the Muddy Formation interval. Track descriptions are (from left to right) member tops, gamma ray (GR) log, component volumes, reference track (measured depth in feet), resistivity log, perforations, effective porosity, water saturation, facies, oil saturation, and CO_2 saturation. For the saturations, color fill is indicative of increase or decrease in repeat PNL measurement (in comparison to baseline PNL measurement prior to CO_2 injection). Interval tops shown are (from bottom to top) Skull Creek, Rozet, Bell Creek sand, Springen Ranch, and Shell Creek shale.

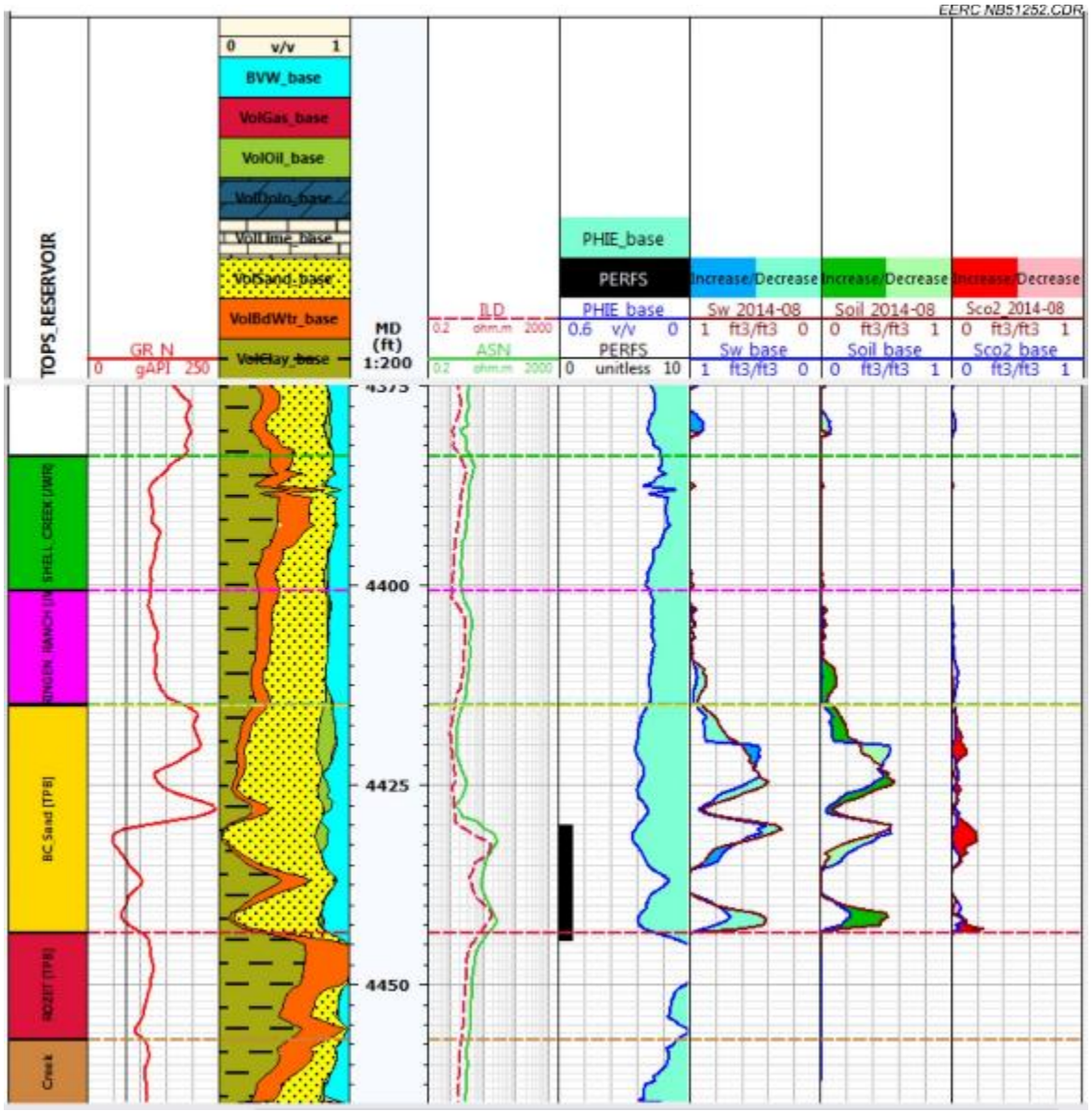

Figure 8. 32-02 production well log display within the Muddy Formation interval. Track descriptions are (from left to right) member tops, GR log, component volumes, reference track (measured depth in feet), resistivity log, perforations, effective porosity, water saturation, facies, oil saturation, and CO_2 saturation. For the saturations, color fill is indicative of increase or decrease in repeat PNL measurement (in comparison to baseline PNL measurement prior to CO_2 injection). Interval tops shown are (from bottom to top) Skull Creek, Rozet, Bell Creek sand, Springen Ranch, and Shell Creek shale.

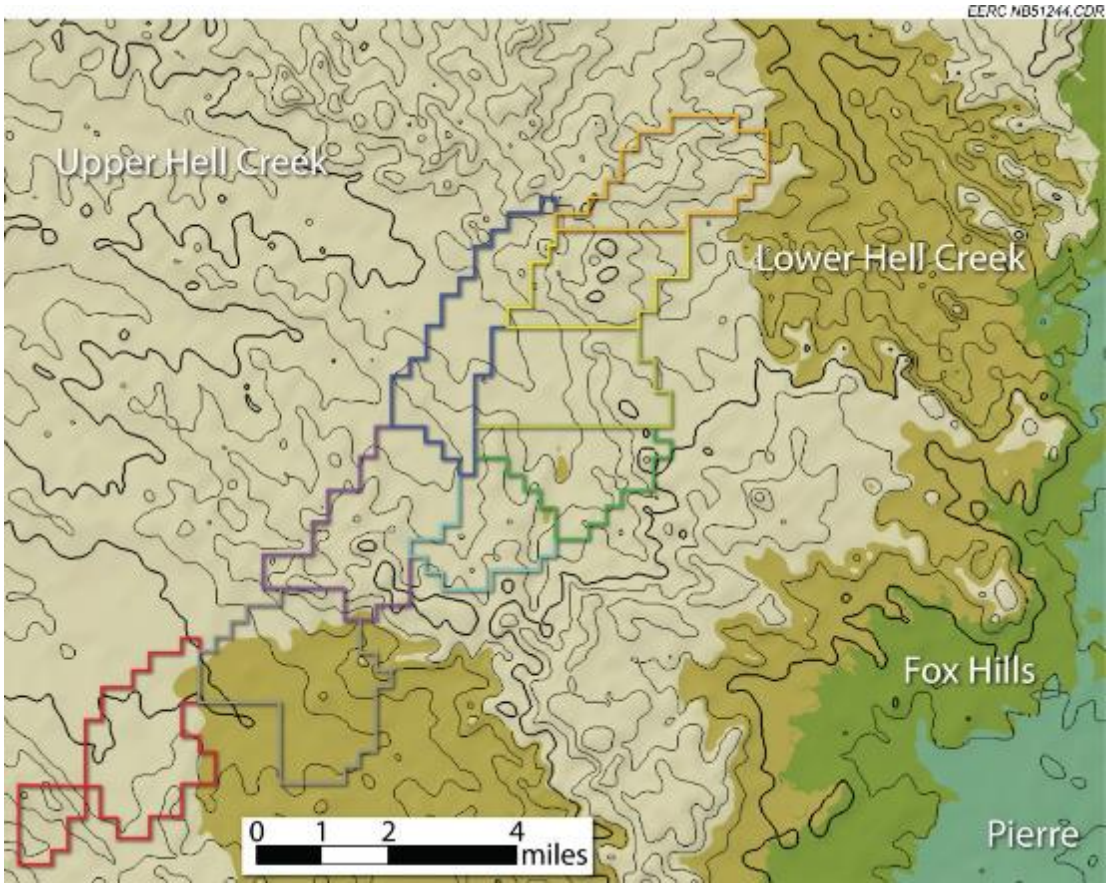

Figure 9. Map view of Bell Creek near-surface model. Relief is that of ground surface (1× vertical exaggeration). The Fox Hills and Pierre Formations outcrop on the east side of the Bell Creek Field because of structural dip to the west.

3-D surface seismic data have also been acquired during Bell Creek project activities, including both a baseline survey (acquired in 2012, prior to the start of CO_2 injection) and a repeat survey acquired in October 2014 (Figure 10). The 3-D reference model has been updated to include both surveys and continues to be updated with seismically derived results as they become available (i.e., surface and volume attribute data, AVO (amplitude versus offset) angle stacks, inversion volumes, etc.).

Reservoir Simulation

Since discovery in 1967, the Bell Creek oil field in southeastern Montana has undergone primary production (solution gas drive), waterflooding, and two micellar–polymer pilot tests. CO_2 EOR has been carried out in the field since 2013, which is anticipated to recover 30 million barrels of oil from the reservoir. To ensure safe, long-term CO_2 storage and maximize oil production, reservoir simulation is needed to help analyze production performance, make production/injection plans, evaluate containment effectiveness, and predict CO_2 migration.

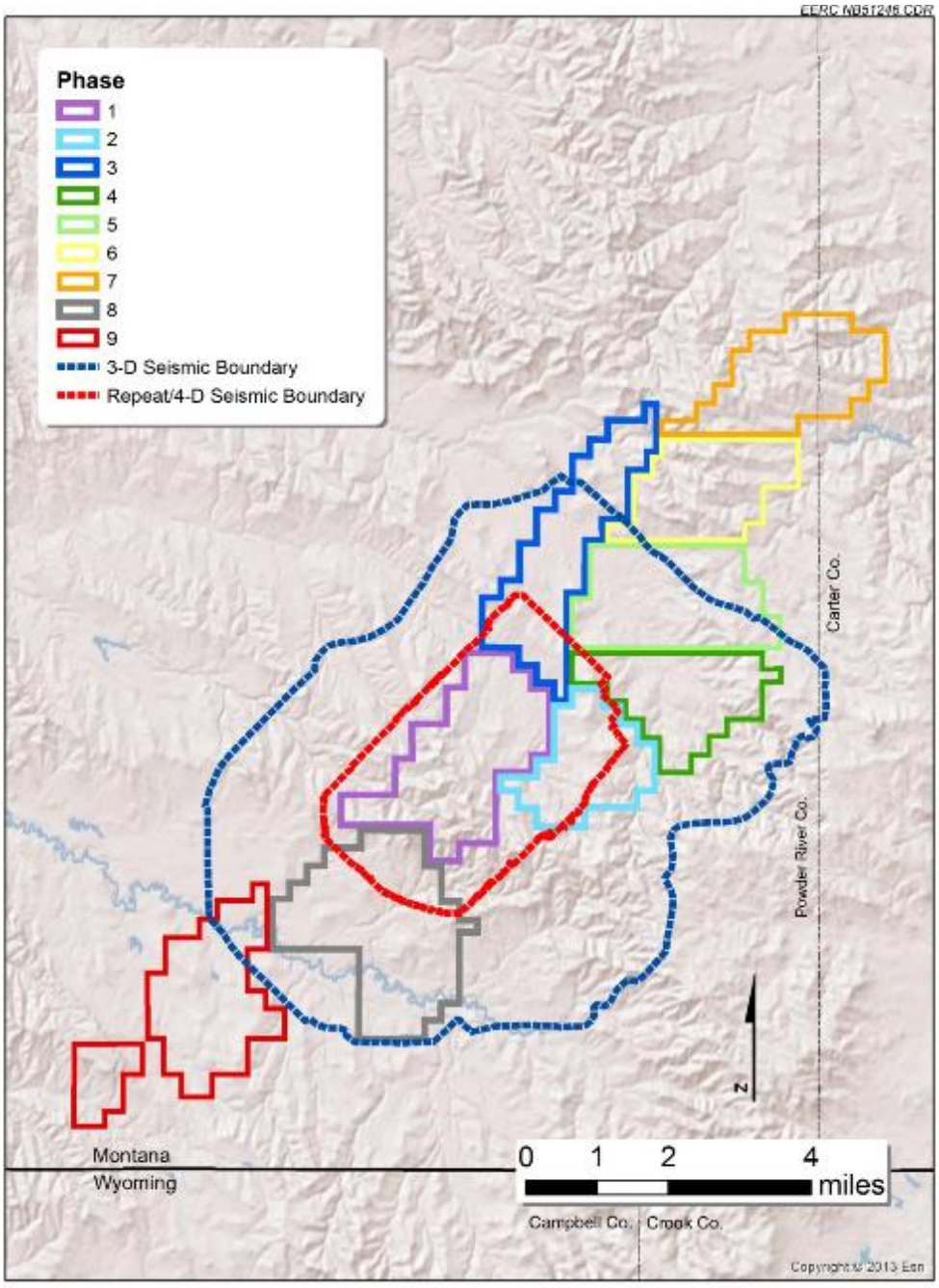

Figure 10. Map illustration of the approximate areal extent of both the baseline 3-D surface seismic (outlined in blue) and repeat (outlined in red) seismic surveys in the Bell Creek Field.

So far, two versions of static geologic models have been developed to characterize the reservoir structure. The V1 model mainly focuses on the Phase 1 area and its surrounding area, while the V2 model covers a 200-square-mile study area centered on Phase 1. In order to better understand the reservoir dynamics and flow behavior, as well as make reasonable predictions, two dynamic simulation models were developed separately for the Phase 1 and Phase 2 areas based on

the geologic models. Based on the results of the two models, the boundary between the areas is not perfectly sealed, implying fluid flow between Phases 1 and 2. Thus it was necessary to develop a combined simulation model that includes both areas.

As shown in Figure 11, the 10-square-mile area shaded in red and blue was clipped from the V2 geologic model to build the combined dynamic reservoir model. The rock–fluid properties, such as PVT data and relative permeability data, as well as production and injection history were brought into Computer Modelling Group Ltd.'s (CMG's) Builder, which converted the static model into a dynamic flow model. CMG's full compositional reservoir simulator (GEM) was then used to simulate the primary depletion, waterflooding, and CO_2 EOR processes. Numerical tuning of the reservoir model was conducted in the history matching to achieve meaningful predictions. This study focused on the history matching of the combined model, which included primary depletion, waterflooding, and CO_2 flooding (including data through April 2015). The processes of reservoir modeling, production/injection analysis, and history matching are described in the following sections.

Reservoir Modeling

Individual simulation of Phase 1 and Phase 2 areas showed that grid size and cell count had significant impact on compositional flow simulation. Based on sensitivity analyses, a cell size of 100 feet × 100 feet (length and width) and average thickness of 1 foot was selected. Results showed that 21 layers in the vertical direction could capture the overall flow behavior in the field. A combined Phase 1 and 2 model grid contained a total of 859,362 cells with dimensions of 259 × 158 × 21 cells. The Phase 1 and 2 combined model extent encompassed a total of 102 wells: 26 producers and 27 injectors in the Phase 1 area, 17 producers and 18 injectors in the Phase 2 area, and ten producers and four injectors in the areas beyond these phases. Figure 12 shows the well distribution in the Phase 1 and 2 areas, which were used as references in the history match.

Production/Injection Analysis

Generally, the reservoir structure dips from east–southeast to west–northwest at about 100 feet/mile (~1°), with a complex of deltaic and nearshore-deposited sands (Burt and others, 1975). Edgewater (water encroachment during production from the downdip aquifer) is evident from the production behavior of wells in the west boundary of the Phase 1 area. Figure 13 shows the early breakthrough of water to wells in this region at the primary depletion stage. However, the quick pressure drop in the reservoir indicates that the edgewater is not strong enough to support the production without artificial lift. Comparison of nearby well pairs in Figure 14 shows the limited extent of edgewater in the reservoir. From the figure, we can see that although Wells 3202 and 3203 are close to each other (about 1500 feet apart), water breakthrough to Well 3203 occurs in the first day, while it takes 4.5 years for the edgewater to arrive at Well 3202. Similar phenomena are observed in Well Pair 5607 and 5608.

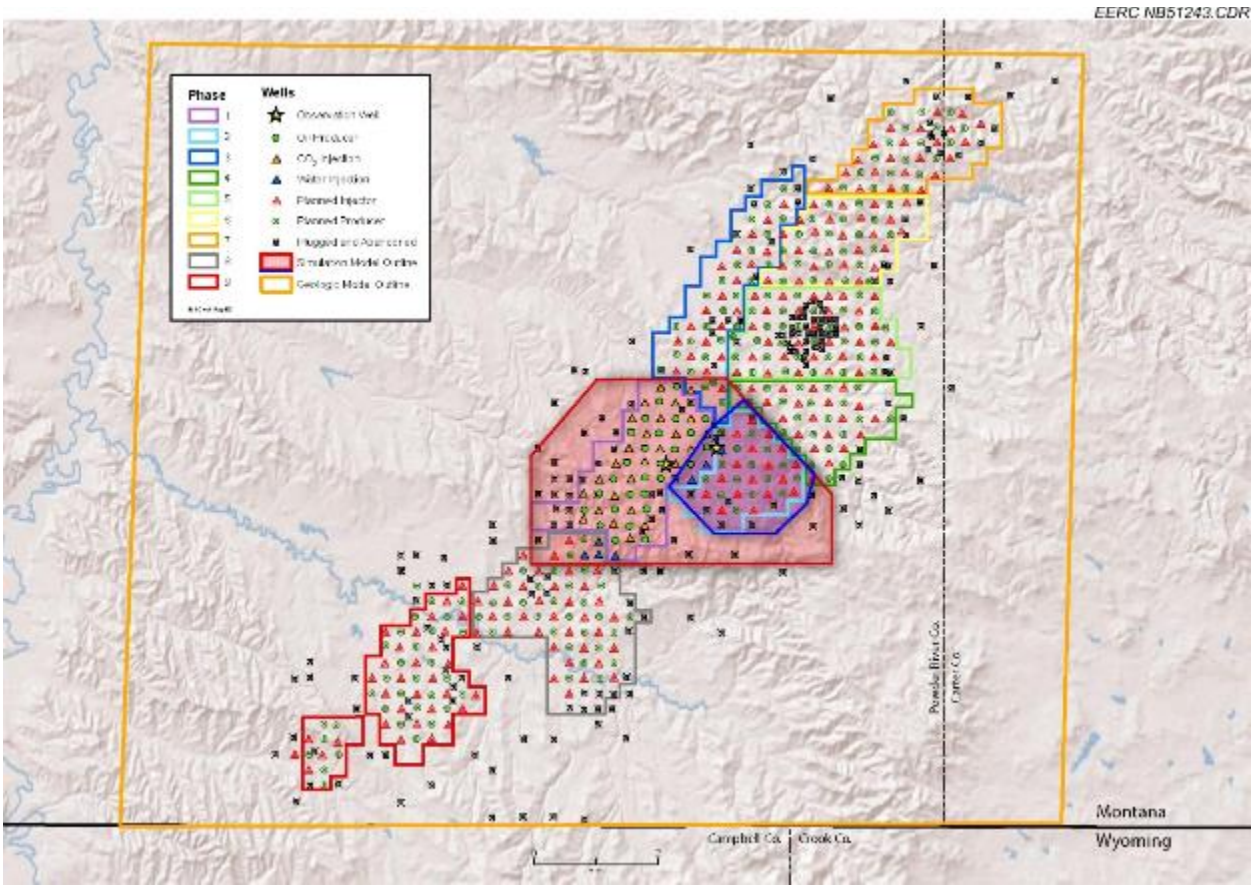

Figure 11. Schematic of the V2 combined Phase 1 and 2 simulation model extent (the area shaded in red; the area shaded in blue represents the extent of the previously developed individual Phase 2 simulation model).

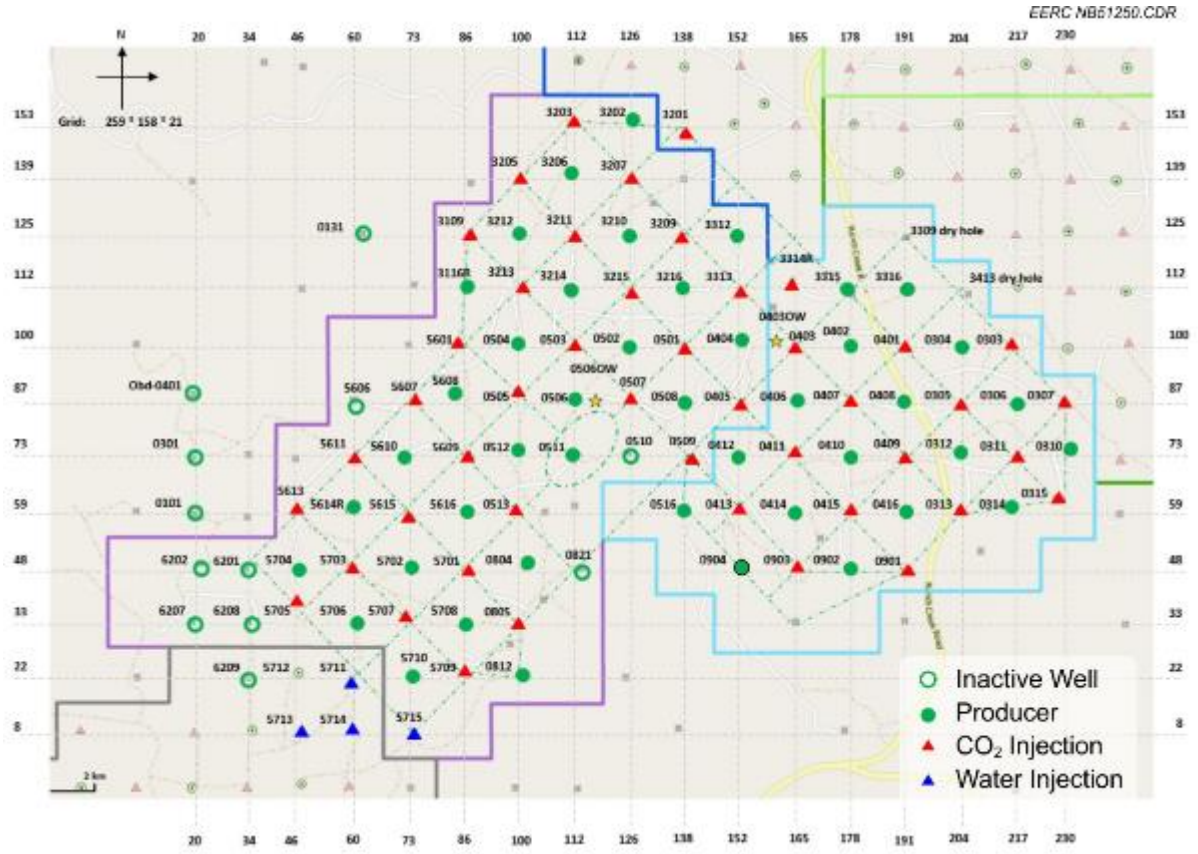

Figure 12. Well distribution in Phases 1 and 2. The numbers at the picture margins represent V2 model grid coordinates.

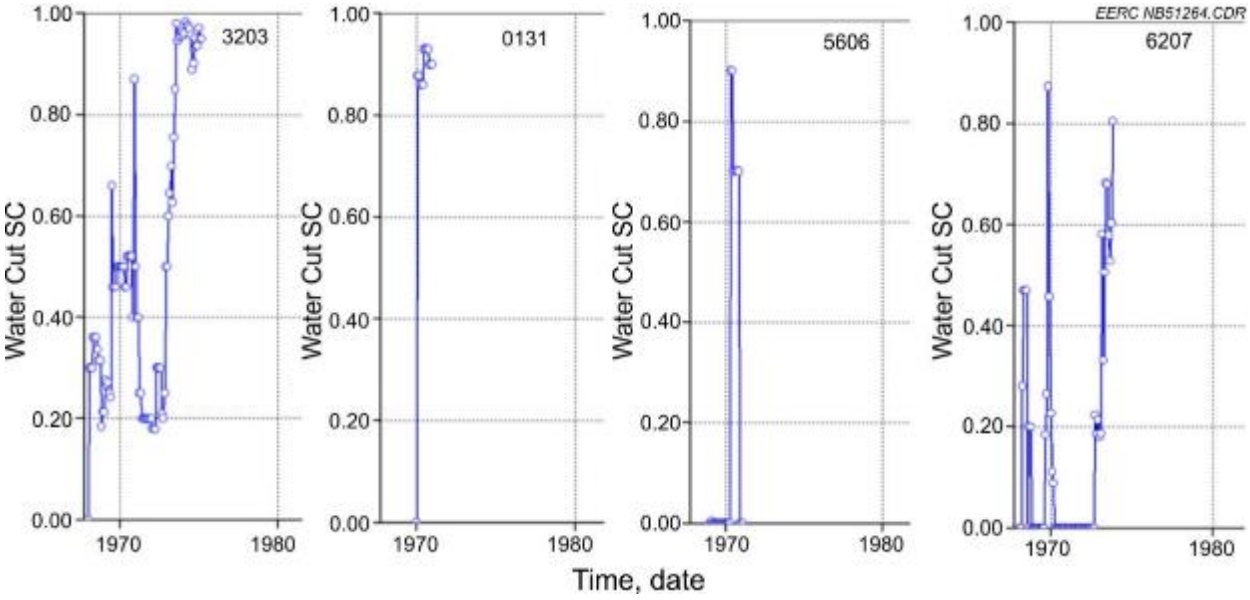

Figure 13. Early water breakthrough to wells in the west boundary of Phase 1 area (SC is standard conditions).

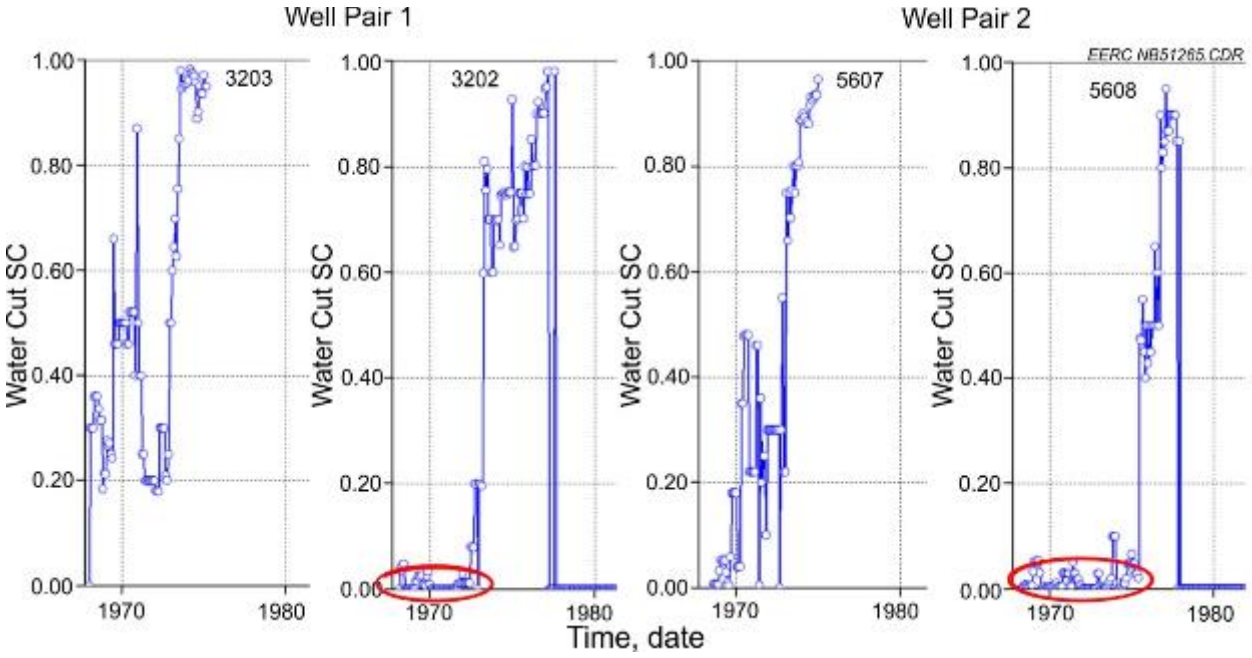

Figure 14. Comparison of water cut for nearby well pairs.

Although edgewater effects occur along the west boundary of the reservoir, the impact of local water invasion is also noted in production performance, especially for wells in the western and southern areas of Phase 2. It is clear that water breakthrough to these wells occurs in the very beginning of production (Figure 15), indicating there is considerable water invasion or initial water saturations were greater in this part of the reservoir.

Boundary sealability is also an important factor for waterflooding and CO_2 flooding design and operations as it relates to the pressure response and sweep efficiency. Results from Phase 2 area simulation showed possible fluid connection between the Phase 1 and 2 areas. This effect could not be fully simulated in the previous model as it did not include wells in the Phase 1 area. By comparing well pairs located on both sides of the boundary, the interphase (Phases 1 and 2) fluid channel could be estimated. Because the reservoir dip trend is from Phase 2 toward Phase 1, water would break through to wells in Phase 1 faster than wells in Phase 2 during primary depletion if there was no flow barrier between phases. Actual production showed that water breakthrough was 5.5 years faster in Well 0403 of Phase 2 than in Well 0404 in Phase 1 (Figure 16), indicating good sealability between Wells 0403 and 0404. Similar good sealability was observed between Wells 0511 and 0516. However, when Water Injector 0405 was turned on, the water cut in its nearby wells, such as 0406, 0412 (in the Phase 2 area), and 0508 (in the Phase 1 area), shown in Figure 17, soon reached 98%, which indicates good connectivity between these wells.

Solution gas was the driving force in the primary depletion stage. Regional gas caps were detected in some parts of the field. PVT analyses in the early stages of development showed that the crude was saturated, with saturation pressures ranging from 665 to 760 psi. Solution GOR varied from 200 to 306 scf/bbl, which contributed to driving oil from the reservoir to wells before waterflooding (Burt and others, 1975).

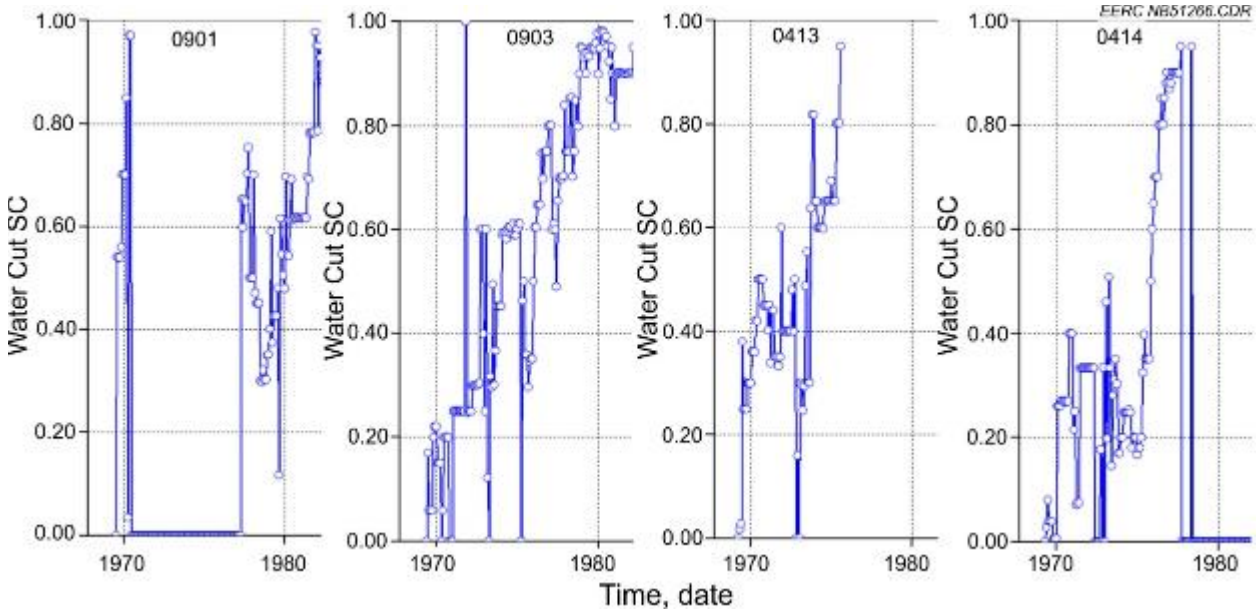

Figure 15. Early water breakthrough to wells in the south boundary of the Phase 2 area.

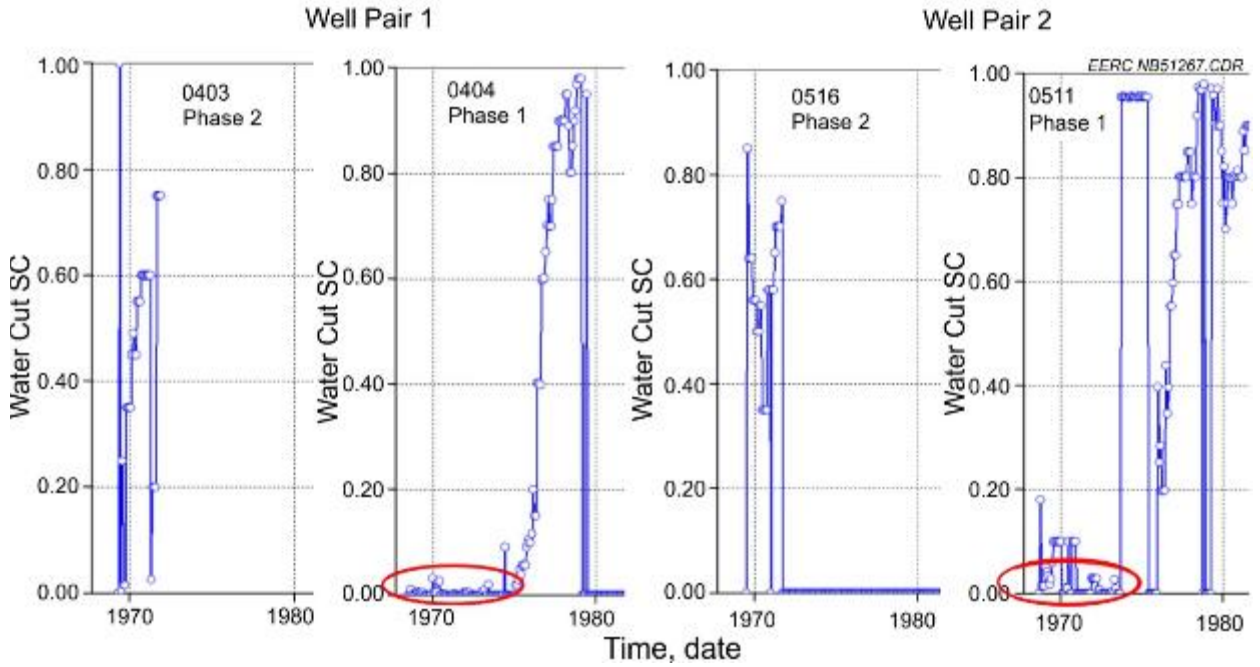

Figure 16. Comparison of water cut in nearby wells for boundary sealability analysis.

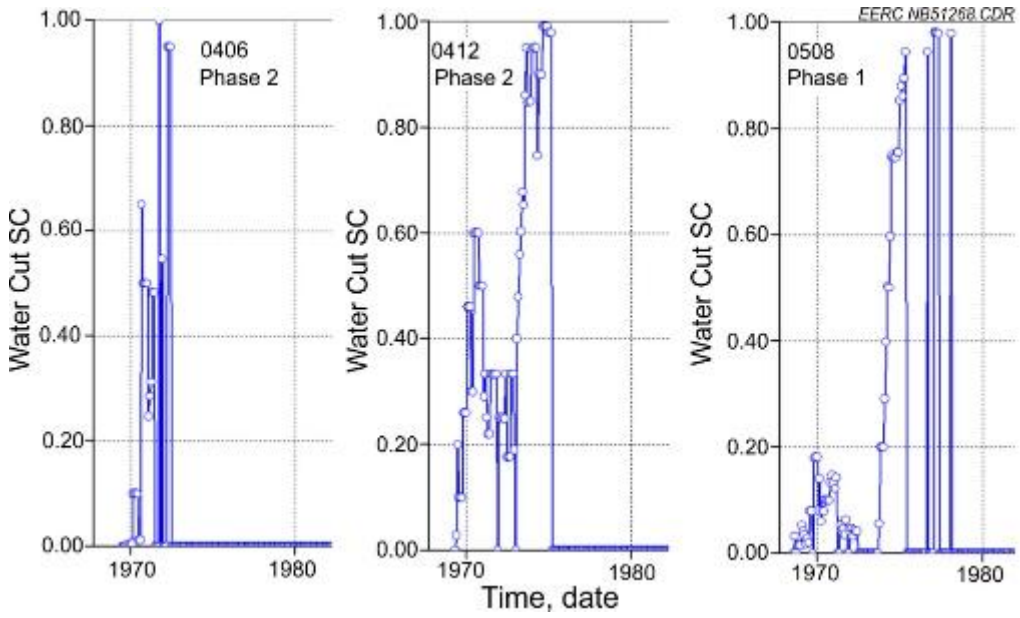

Figure 17. Fast water cut development in wells near Water Injector 0405 showing good connectivity between these wells.

History Matching

The purpose of history matching is to get a good estimation of fluid saturations and pressure distribution profiles in the reservoir at current conditions and for providing a reference for CO_2 flooding design, field operation, and performance prediction. Because of the uncertainty of reservoir parameters and conditions, a number of simulation runs are usually required to match historical field data. The number of simulation runs can be quite large, especially when there are many wells in a large field with a long production/injection history. Although the history-matching process is time-consuming and resource-demanding, it yields insight to better understand the reservoir, produces results important in optimizing reservoir management, and provides the foundation for predictive simulation cases (i.e., CCI vs. WAG injection) necessary to improve future production performance.

Previous history-matching efforts in individual Phase 1 and Phase 2 models (reported in Liu and others, 2014) identified substantial difficulties in the process, including adjustment of fluid flow boundaries; adjustment of near-wellbore fluid saturations, porosities, permeabilities, etc.; and even the necessity of additional pseudowells for pressure support to achieve acceptable history-matched conditions. The adjustment of fluid flow boundaries was necessary along the eastern edge of Phase 1 and the western edge of Phase 2 to achieve fluid volume balance, indicating there may be local hydraulic connectivity between the two phases. These issues indicated that the reservoir geology had not been captured accurately in the previous modeling efforts, and predictive estimates resulting from these individual phase numerical simulations may have decreased accuracy. Thus it was decided to construct a simulation model combining Phases 1 and 2.

More than 20 reservoir and production parameters, such as permeability, porosity, oil/water/gas saturations, production rate, injection rate, and pressure, were involved in the combined Phase 1 and 2 simulation study. The Bell Creek simulation model contained nearly 1 million cells, and as a result, the method of handling these parameters was a key factor for effective simulation. Geostatistical methods offered a great way to collapse the number of variables in the model. Such methods were used to assign geological and reservoir parameters to the V2 static model; however, these methods can only reduce uncertainty so much, the degree of which strongly depends on available data such as well logs, core measurements, seismic surveys.

As previously stated, the combined model covers a large area (10 square miles) with a complex geologic framework, uncertain reservoir features, and many long-history wells. A systematic history match methodology using dimensionless groups was applied in this study to analyze the reservoir condition and match the field data.

In order to assess the CO_2-flooding process, the governing equations of Wood and others (2008), which were constructed by modifying the waterflooding governing equations and boundary conditions of Shook and others (1992) and rederiving the dimensionless groups using inspectional analysis, were used to identify ten groups for CO_2 flooding, as shown in Table 1. Further discussion of the dimensionless grouping process is in Appendix B.

By reducing 20+ parameters to ten groups with clear physical meanings, the problem becomes much easier to analyze. The effective aspect ratio measures the rate of communication between fluids in the horizontal direction versus that in the vertical direction. Lower aspect ratio means that fluids flow easier in the vertical direction relative to the horizontal direction, which leads to segregation of fluids in the reservoir. Increased segregation means a smaller swept zone and lower flooding efficiency. Thus it is favorable to have larger aspect ratios in the reservoir. The dip angle group is a purely geometrical group without any rock or fluid properties. Long and thin reservoirs have high values of the dip angle group, which is favorable for both water and CO_2 flooding as it reduces the impact of gravity override. The buoyancy number is a ratio of gravity force to viscous force; a higher value in this category means greater density difference between fluids and, therefore, greater potential for fluids to segregate in the reservoir and smaller sweep

Table 1. Dimensionless Groups for CO_2 Flooding (Wood and others, 2008)

Name	Expression	Name	Expression
Effective Aspect Ratio	$R_L = \frac{L}{H}\sqrt{\frac{k_z}{k_x}}$	Mobility ratio (water)	$M_W^* = \frac{k_{rw}^* \mu_o}{k_{ro}^* \mu_w}$
Dip Angle Group	$N_\alpha = \frac{L}{H} tan\ \alpha$	Mobility ratio (CO_2)	$M_g^* = \frac{k_{rg}^* \mu_o}{k_{ro}^* \mu_g}$
Buoyancy Number (gas)	$N_g^* = \frac{H \Delta \rho g cos\ \alpha}{\Delta P}$	Initial oil saturation	S_{oi}
Injection Pressure Group	$P_{injD} = \frac{P_{inj}}{P_{MM}}$	Residual oil saturation to water	S_{orw}
Producing Pressure Group	$P_{pD} = \frac{P_p}{P_{MM}}$	Residual oil saturation to gas	S_{org}

efficiency. Injection and producing groups are the measurements of pressure control in the wells. Both of them relate to MMP, which is the lowest pressure for CO_2 and oil to be miscible, as traditionally measured by slim-tube experiments, where CO_2 develops miscibility through a multicontact process with a given reservoir oil at the reservoir temperature. At MMP, the interfacial tension is zero and no interface exists between the fluids.

The five groups from the left-hand column of Table 1 (discussed in the preceding paragraph) are closely related to reservoir geometry and operational constraints, which are more deterministic than the following rock–fluid related groups (right-hand column of Table 1). The initial oil saturation and residual oil saturations to water and gas were measured from lab experiments, but the accuracy of their distribution in the reservoir remained uncertain. A mobility ratio characterized the moving abilities of fluids in the reservoir as the ratio of the viscous forces of one fluid to the viscous forces of another. The water/CO_2 mobility ratios were functions of fluids viscosities and relative permeability curves, which had higher uncertainty but considerable impact on oil recovery. Thus relative permeability and end point fluid saturation of fluids were the major parameters for adjustment in the history match process. Also, skin factor was used to mimic the formation damage/stimulation effects near wellbores.

To date, three sets of oil–water and five sets of gas–liquid relative permeability curves have been experimentally measured from core samples taken from two wells (BC 22-03 and 05-06 OW). Core properties are described in Table 2 (see Appendix B Figures B-2 and B-3 for BC 22-03 and 05-06 OW well log displays with sample depths plotted). Appendix B Figures B-4 to B-6 show the oil–water relative permeability curves for Core Samples #1, #5, and #6 from Well BC 22-03, respectively. The figures demonstrate significant variation of connate water saturation (S_{wc}) and end point oil relative permeability to water (K_{row}^*). In these cores, S_{wc} decreases from 0.433 to 0.211, while K_{row}^* increases from 0.447 to 0.927. For the gas–liquid relative permeability curves, three sets were measured using Core Samples #3, #7, and #10 from Well BC 22-03, and two other sets were measured using composite cores (long core sample constructed by assembling three shorter samples), numbered Composite 1 and 2 from Well BC 05-06 OW. Similar variation was observed for residual oil to gas (S_{org}), end point gas relative permeability (K_{rg}^*), and end point oil relative permeability to gas (K_{rog}^*). As shown in Appendix B Figures B-7–B-11, S_{org} varies from 0.33 to 0.7, K_{rg}^* varies from 0.1 to 0.87, and K_{rog}^* varies from 0.5 to 1.0. Such drastic variation in

Table 2. Basic Properties for Cores Used in Relative Permeability Measurement

No.	Core Name	Depth, feet	Porosity, V/V	Permeability, mD
1	BC 22-03, #1	4470–4471	0.301	224
2	BC 22-03, #3	4472–4473	0.250	237
3	BC 22-03, #5	4474–4475	0.308	1190
4	BC 22-03, #6	4475–4476	0.315	1940
5	BC 22-03, #7	4476–4477	0.330	2870
6	BC 22-03, #10	4481–4482	0.299	1560
7	BC 05-06 OW, Composite #1	4534–4537	0.253	1260
8	BC 05-06 OW, Composite #2	4520–4525	0.244	175

rock–fluid properties not only shows the high heterogeneity of the reservoir but also gives a wide range for parameter tuning in history matching.

After dividing the production history into three clear stages (primary depletion, waterflooding, and CO_2 flooding) as well as sorting the parameters into compact dimensionless groups, the history match was carried out using the EERC's high-performance computing cluster, which allows parallel simulation of different cases to improve simulation efficiency. During simulation, liquid production rates were used as primary constraints, and BHPs were used as secondary constraints. Historic data, including oil production, water production rates, and water cut, were used to compare with the simulations. In the primary depletion stage, local water saturation was adjusted to match the water breakthrough time. In the waterflooding stage, some possible high-permeability channels and barriers were adjusted. In the CO_2 flooding stage, relative permeability curves and endpoint saturations were the most efficient parameters to tune as they related to the EOR mechanisms.

A reasonably good match of the production history was obtained after systematic parameter tuning and production/injection analysis. Figure 18 shows the liquid production rate input to the simulation as the primary control constraint. Figures 19–24 show the history match results for oil production rate, water production rate, gas production rate, GOR, water cut, and average reservoir pressure, respectively. The results show that the model can capture the overall reservoir performance trends, but some local points are not able to be matched.

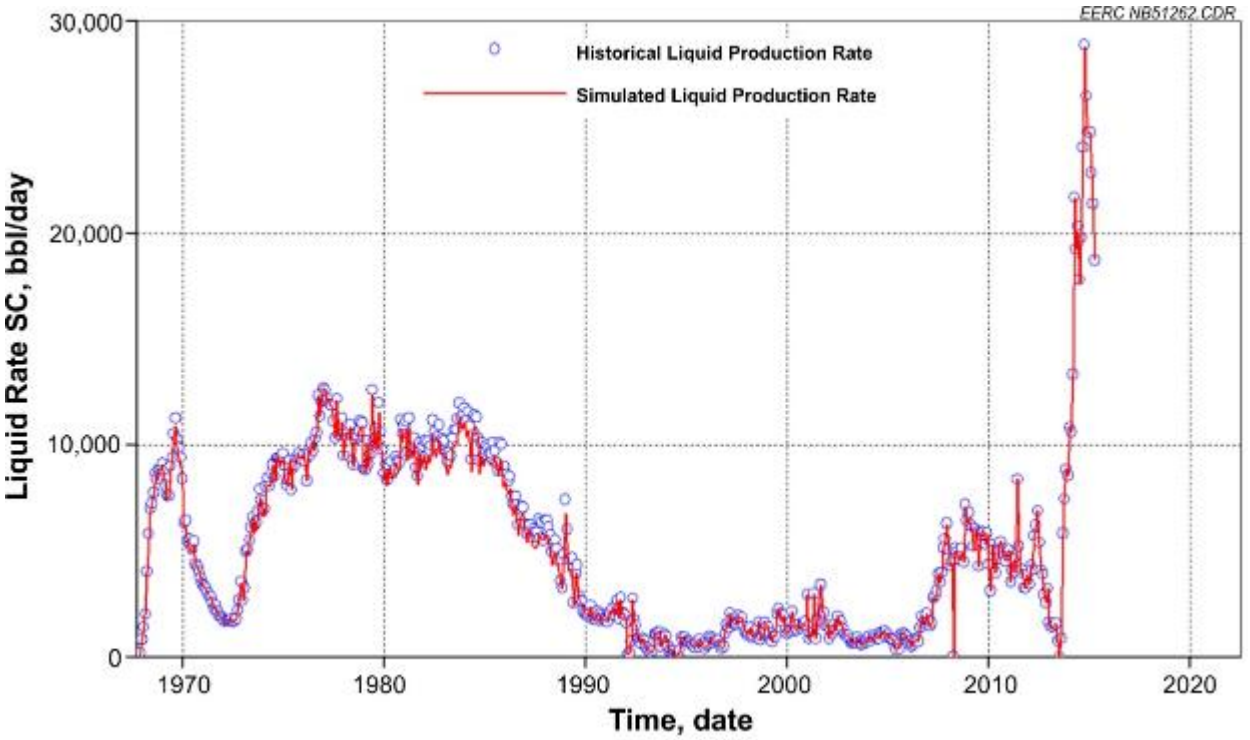

Figure 18. Liquid production rate input to the simulation as a primary control constraint.

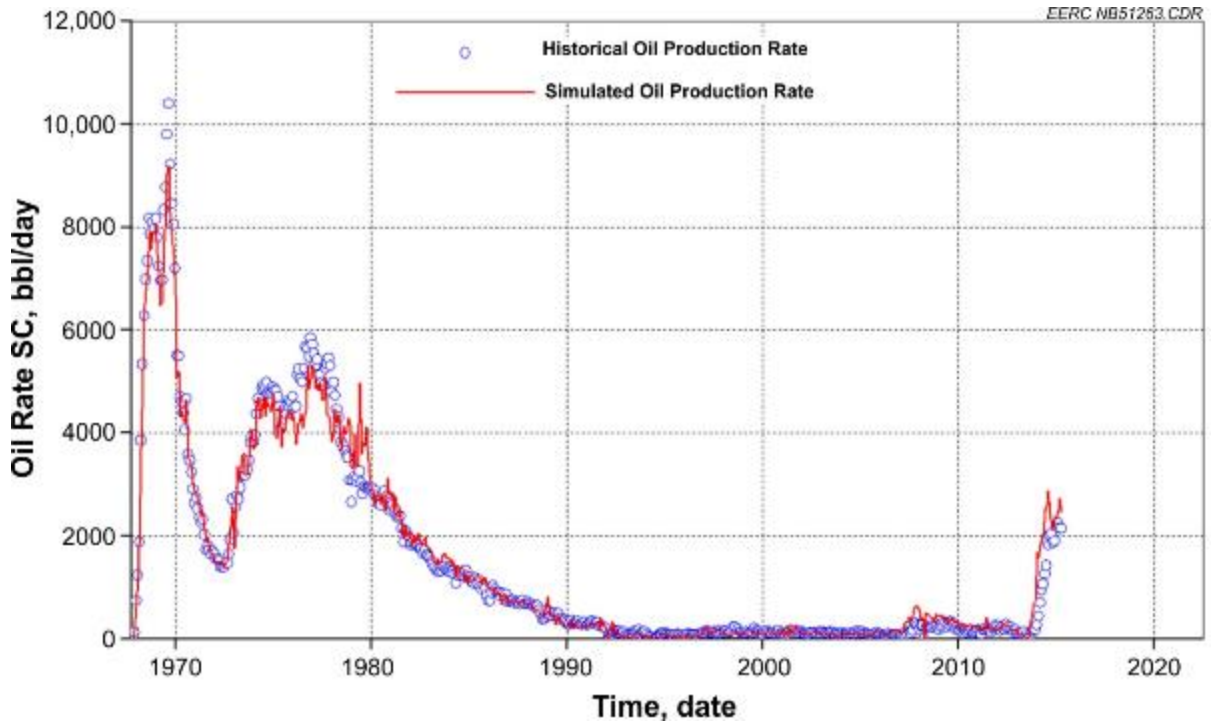

Figure 19. Oil production rate history match results.

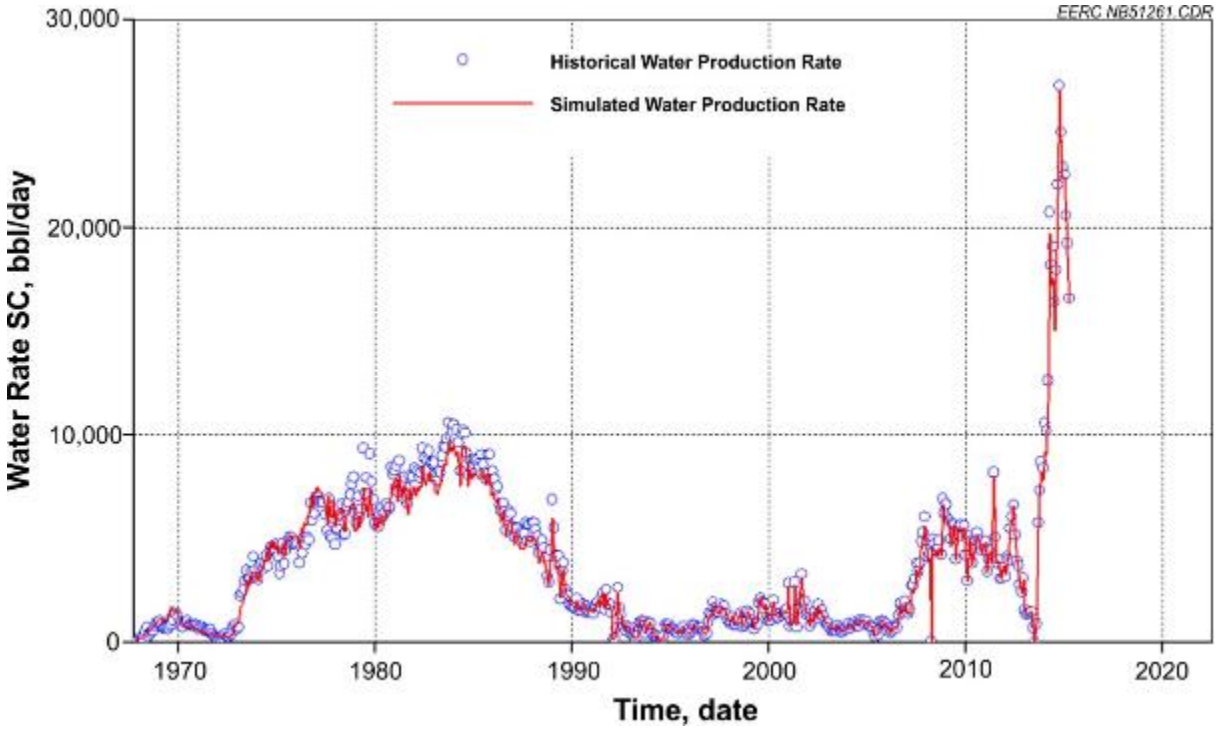

Figure 20. Water production rate history match results.

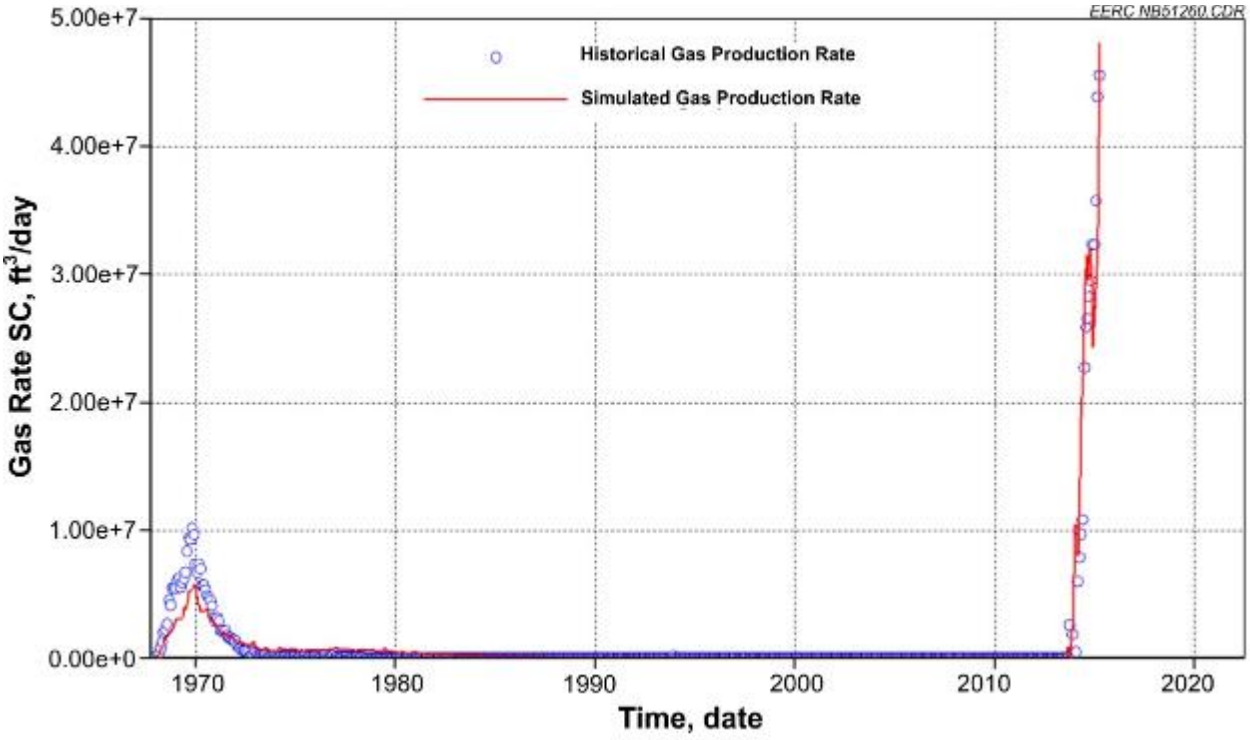

Figure 21. Gas production rate history match results.

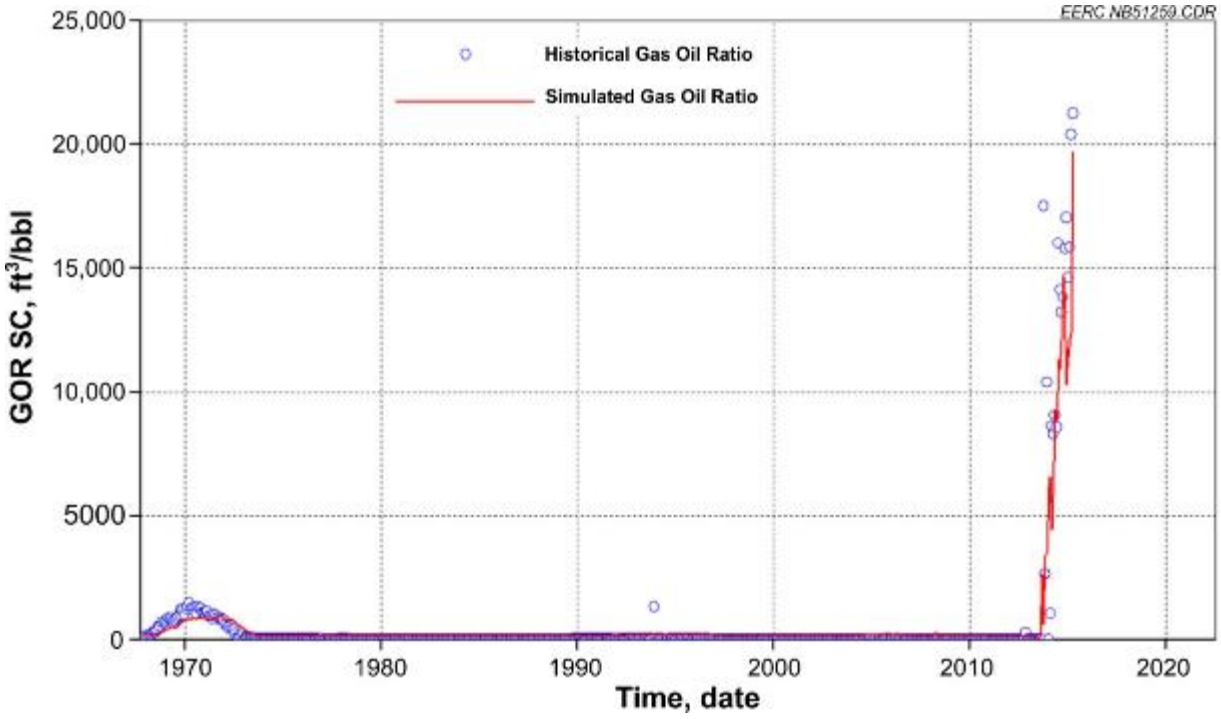

Figure 22. GOR history match results.

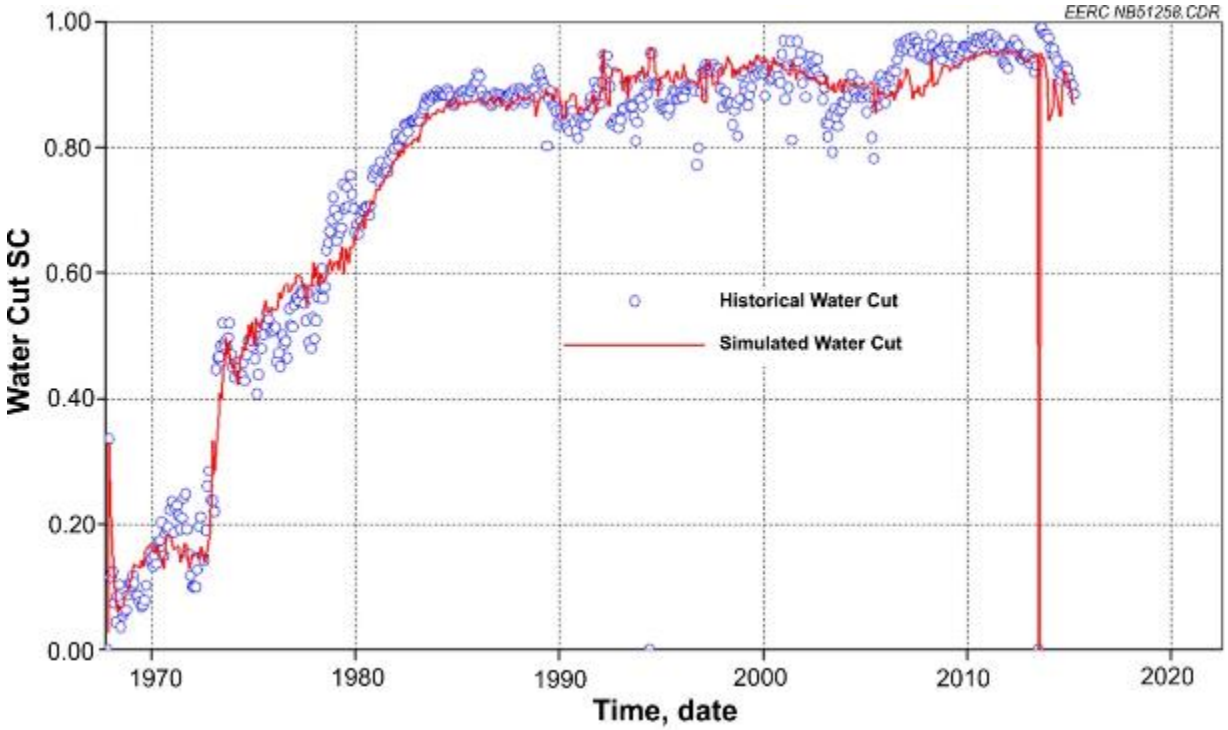

Figure 23. Water cut history match results.

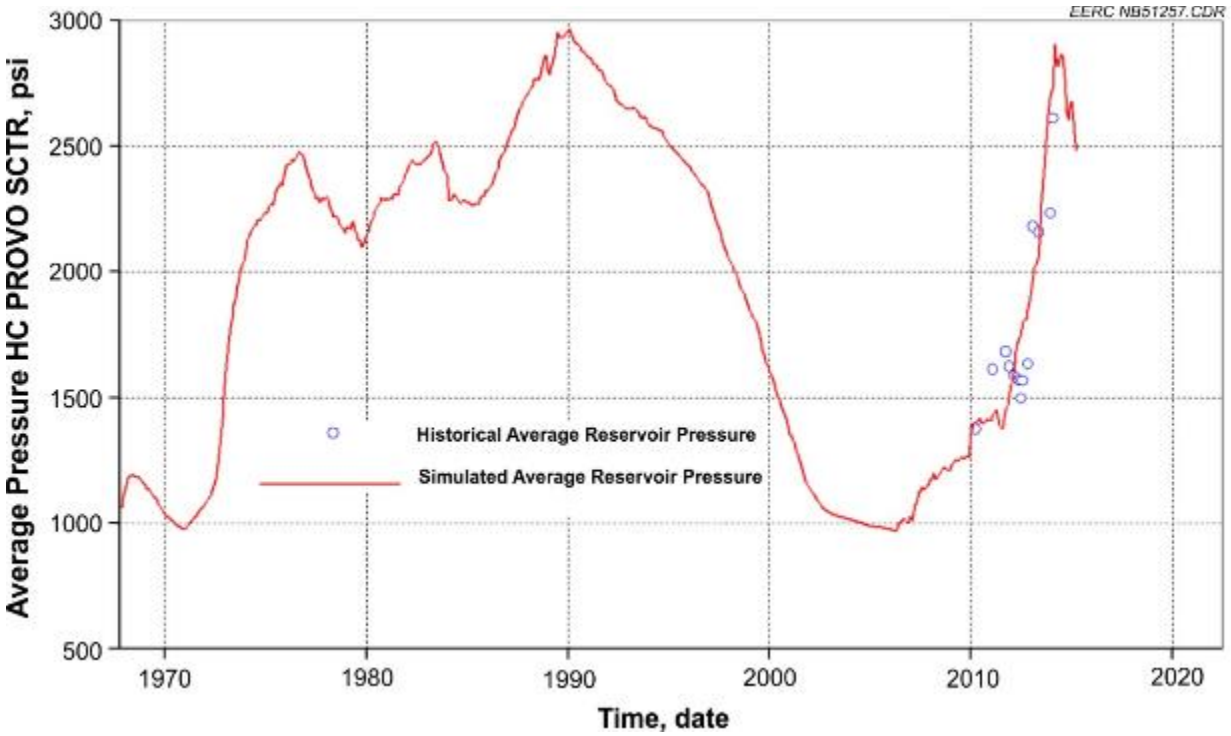

Figure 24. Average reservoir pressure history match results.

Predictive Simulation

Both theoretical study and field practice have shown that many factors, such as injection mode (CCI or WAG), operational constraints (injection rate and pressure), have important effects on CO_2 flooding performance, especially for reservoirs with a complex geologic structure (Harpole and Hallenbeck, 1996; Wood and others, 2008; Zhou and others, 2012; Han and Gu, 2014). The strong reservoir heterogeneity and complicated fluid saturation distribution in the Bell Creek Field make it difficult to determine the best operational schedule. Thus it was necessary to carry out predictive simulations under different scenarios for performance evaluation. Based on the history-matched model, one CCI and one WAG case were simulated to observe reservoir response.

In both cases, the minimum BHP constraint was set at 2300 psi for all producers. The maximum injection pressure constraint was 2800 psi for all injectors in Phases 1 and 2. The CO_2 injection rate for each well was set at the previous 6-month average value of that well. According to the previous WAG simulation study, the water injection rate was set at 1675 bpd and 1110 barrels per day (bpd) for injectors in the Phase 1 and 2 areas, respectively (Braunberger and others, 2013). The operational schedule of the WAG case was set as a 3-month, 1:1 cycle for water and CO_2 injection. Simulation parameter tables for the CCI and WAG cases can be found in Appendix B, Tables B-3–B-5.

It should be noted that the relative permeability hysteresis effect was not included in the two simulation cases discussed in this report. Hysteresis refers to the directional saturation phenomena exhibited by relative permeability curves. In many types of porous media, the relative permeability values are a nonunique function of saturation, having different values when a given phase saturation is being increased than when it is being reduced because of phase trapping (Bennion and others, 1996). It has been reported that phase trapping is a mechanism detrimental to productivity/injectivity in many reservoir applications (Rogers and Grigg, 2000; Jin and Wojtanowicz, 2014).

Previous studies to determine the extent of oil and gas trapping by water during WAG have shown that rock wettability strongly affects this trapping, thus the performance of WAG operations (oil recovery and associated CO_2 storage) varies between different oil fields (Huang and Holm, 1988; Rogers and Grigg, 2000). Each reservoir has its unique hysteresis curves, which relate to rock fluid properties and reservoir conditions. Several models have been used to describe the hysteresis phenomena; however, lab measurements are required to calibrate the curves for model accuracy. A comprehensive model for the complicated Bell Creek reservoir has not been constructed at this time. Previous study of Phase 1 and Phase 2 models showed that cases including hypothetical relative permeability hysteresis curves for the gas phase resulted in slightly lower oil recovery than the cases without considering hysteresis.

Experimental measurements of relative permeability curves with hysteresis were recommended to tune the WAG process (Fatemi and others, 2012). To better assess the impact of hysteresis on WAG performance in Bell Creek, laboratory floods will be carried out under reservoir conditions, and the measured relative permeability curves will be integrated within the next iteration of numerical simulations.

Figure 25 shows the hydrocarbon pore volume injected (HCPVI) for the CCI and WAG cases from 2015 to 2060 with the production/injection settings discussed above. The WAG case results in less HCPVI than CCI for the same injection time (WAG injects 3 HCPVs, while CCI injects 4.65 HCPVs). This is because CO_2 has lower density and viscosity than water; more pore volumes of CO_2 can be injected into the reservoir than water under the same pressure conditions. Thus it may be better to compare the reservoir performance and evaluate sweep efficiency based upon HCPVI rather than injection duration for the two cases. Similar plots graphed over time can be found in Appendix B.

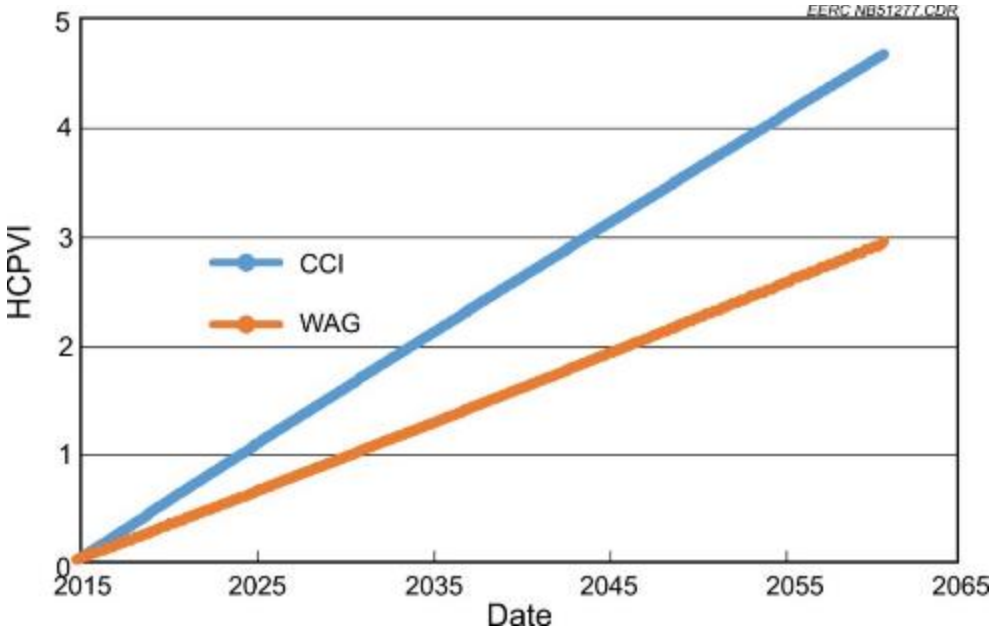

Figure 25. HCPVI for the simulated CCI and WAG cases.

Figures 26 and 27 show the cumulative CO_2 injected and stored by CCI and WAG versus HCPVI, respectively. The CCI case results in injection of approximately twice the amount of CO_2 in comparison to the WAG case and roughly 1.7 times greater mass of stored CO_2 (however, more CO_2 is produced with oil in the CCI mode). In addition, CCI requires more CO_2 to produce the same amount of oil in comparison to the WAG case.

The GOR and CO_2 utilization factor (amount of CO_2 needed to produce one barrel of oil) for both cases are shown in Figures 28 and 29, respectively. In Figure 29, we see that the CO_2 utilization factor for the WAG case drops below 10 MMscf/bbl after 1 HCPVI. This decreases to 7 MMscf/bbl when 3-HCPV fluids are injected in WAG mode, while the value remains above 10 MMscf/bbl even after 4 HCPV in CCI mode.

From Figure 30, it is clear that the incremental oil recovery from CCI and WAG is almost the same (although CCI seems to produce oil more quickly; see Appendix B, Figure B-16), while

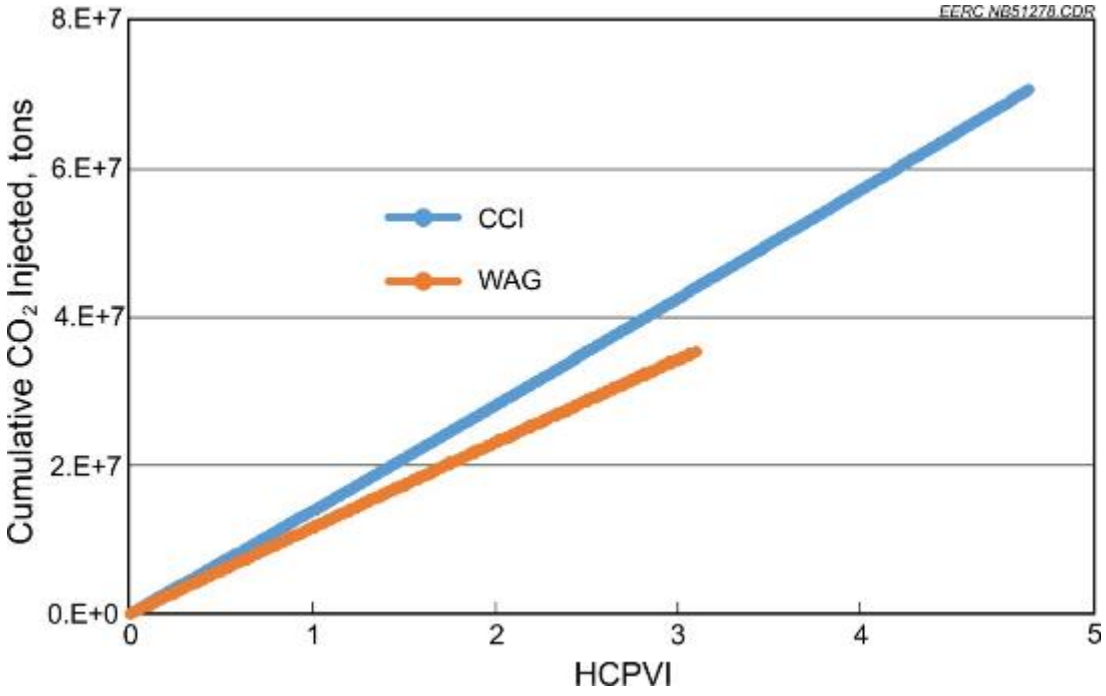

Figure 26. Cumulative CO_2 injected during CCI and WAG.

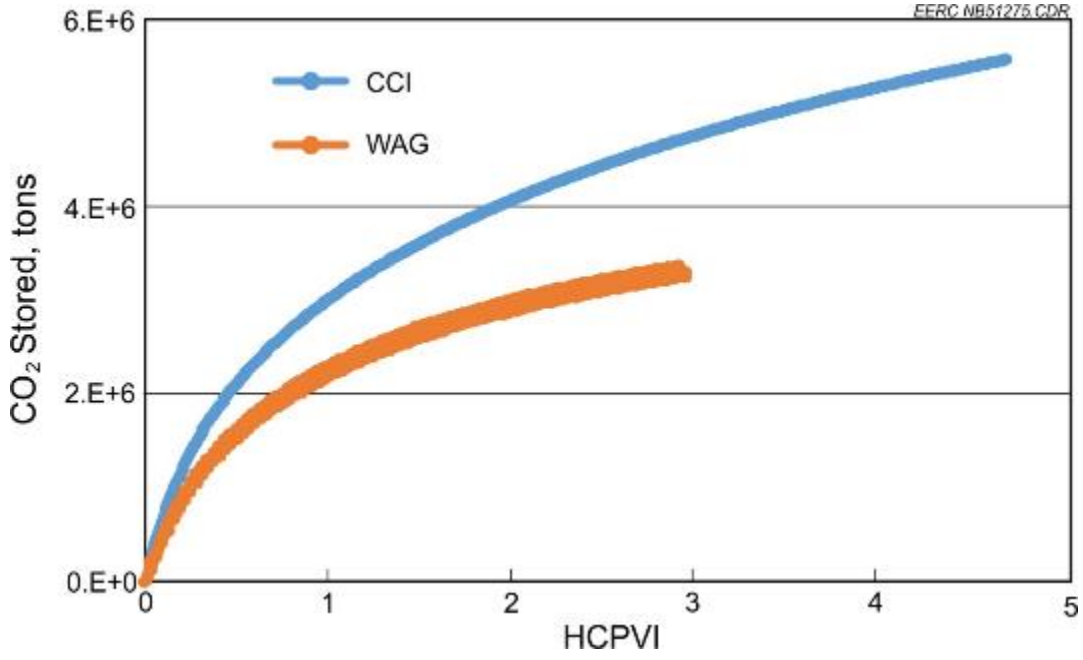

Figure 27. Cumulative CO_2 stored during CCI and WAG.

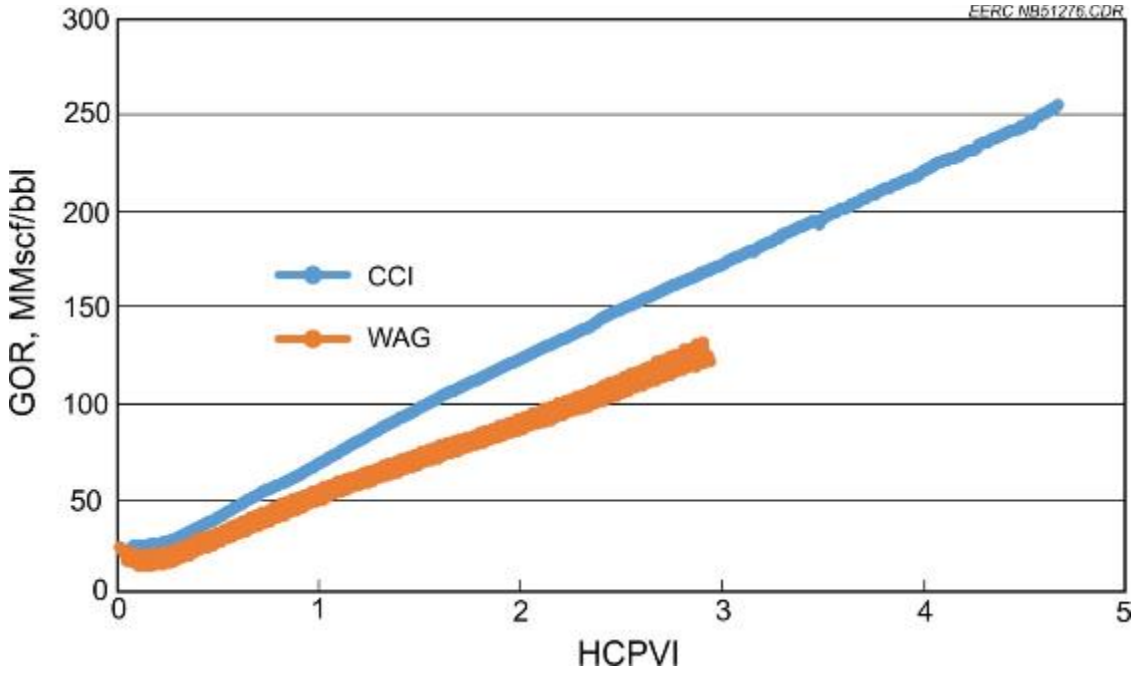

Figure 28. GOR during CCI and WAG.

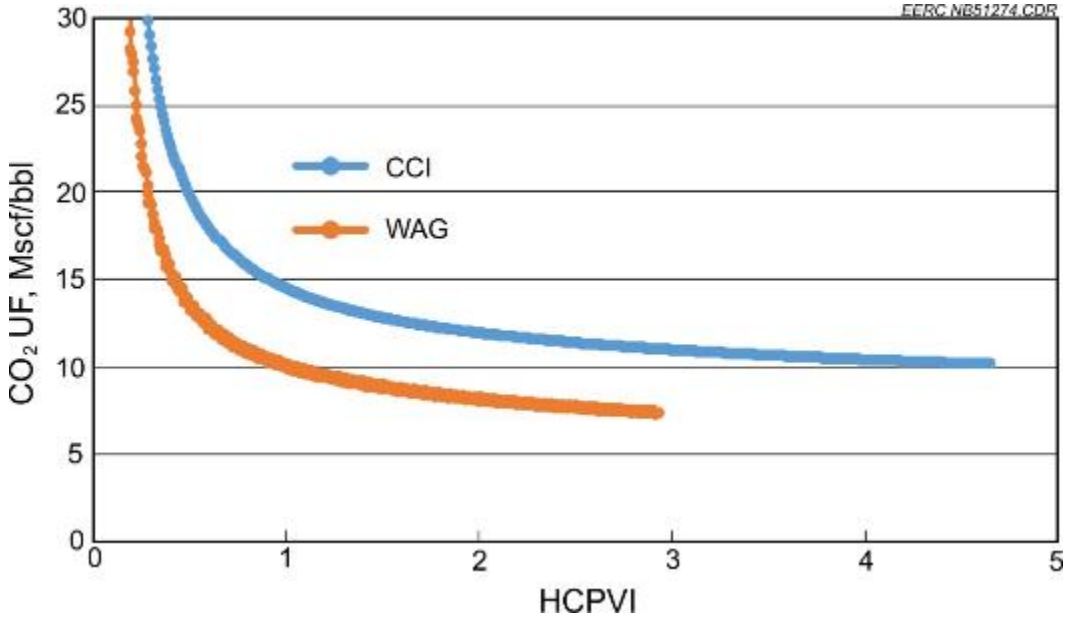

Figure 29. Comparison of CO_2 utilization factor during CCI and WAG.

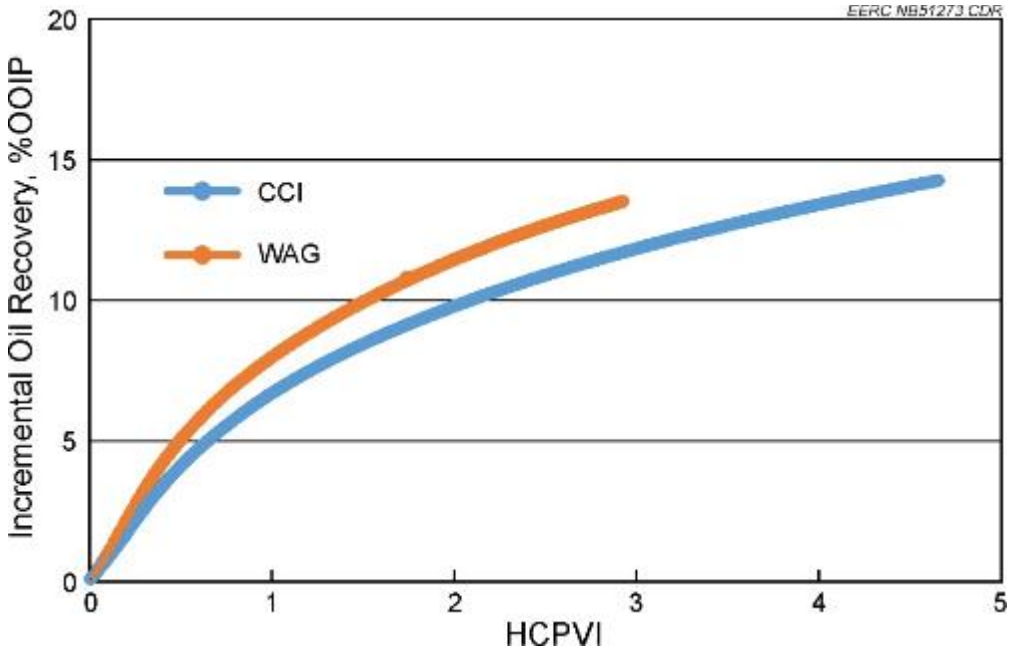

Figure 30. Incremental oil recovery by CCI and WAG.

the HCPVI of WAG is 35% less than that of CCI. Thus the WAG case has higher sweep efficiency per unit of injected volume, as shown in Figure 30, which indicates that WAG can utilize CO_2 better than CCI in the EOR process. This agrees with results published in Ettehadtavakkol and others (2014).

Figures 31 and 32 show the predicted oil production rate and gas injection rate for both the CCI and WAG cases over the simulation duration, respectively. The oil rate curves for both cases are similar, with peak productions of nearly 2500 bbl/day occurring approximately 2–3 years into the simulation time frame. These curves are meant to represent two hypothetical scenarios and are not intended for use in SEC (Securities & Exchange Commission).

Figures 33 to 35 illustrate the CO_2 plume distribution profiles for CCI and WAG after 1, 2, and 3 HCPVs of fluids are injected into the reservoir.

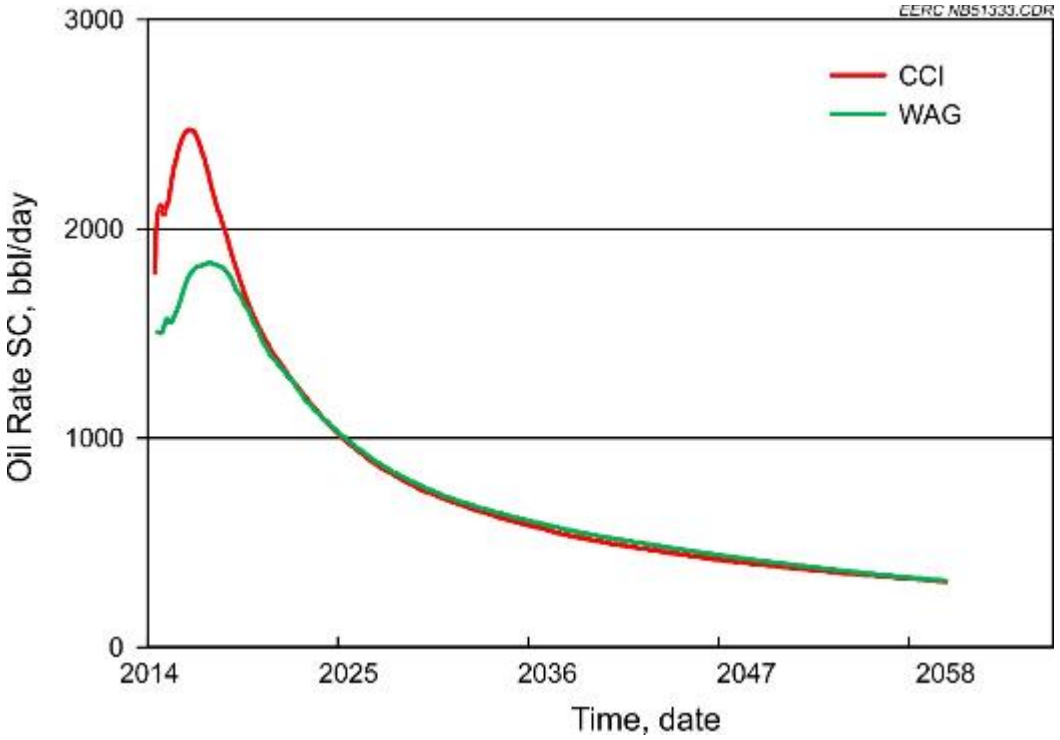

Figure 31. Predicted oil production rate for both the CCI and WAG cases over the simulation time frame.

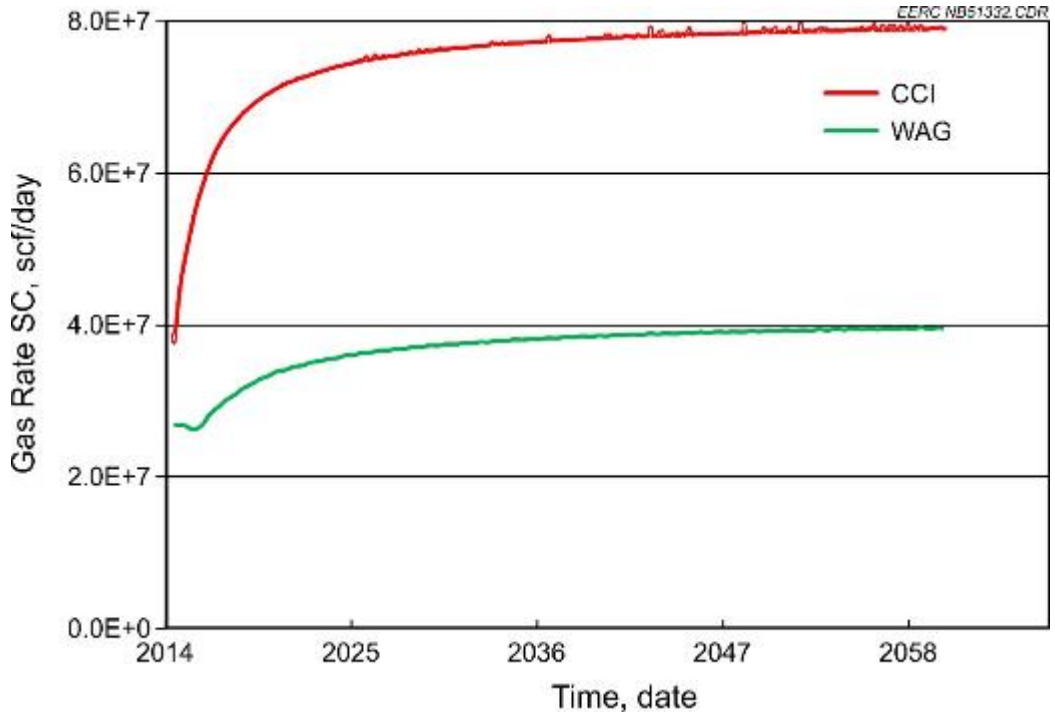

Figure 32. Predicted CO_2 injection rate for both the CCI and WAG cases over the simulation time frame.

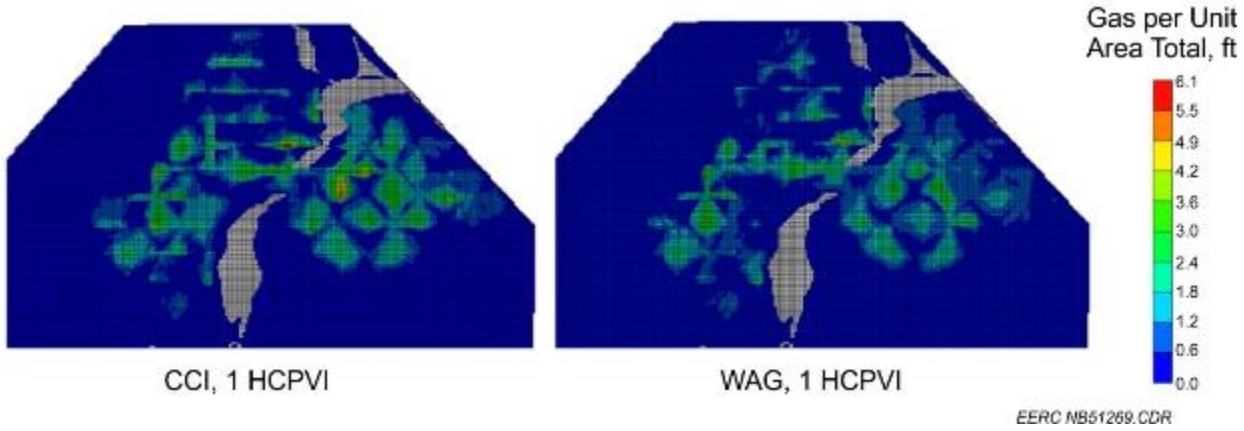

Figure 33. CO_2 plume distribution for CCI and WAG after 1 HCPVI.

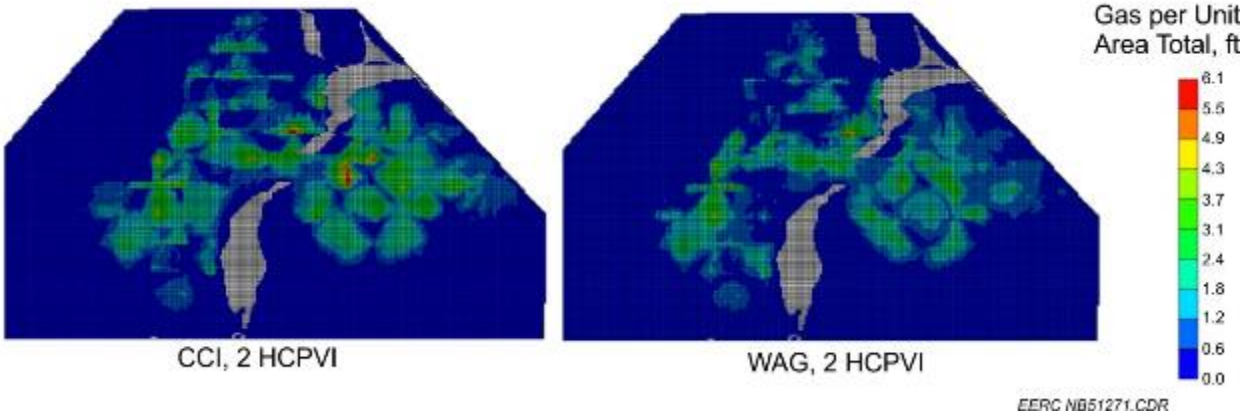

Figure 34. CO_2 plume distribution for CCI and WAG after 2 HCPVI.

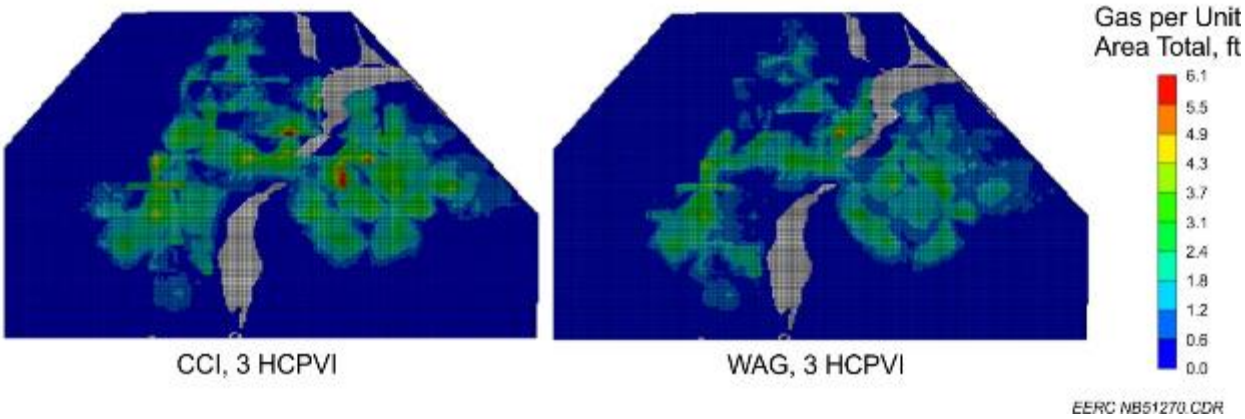

Figure 35. CO_2 plume distribution for CCI and WAG after 3 HCPVI.

V3 Geologic Model

Previous Modeling Efforts and Conventional Depositional Model

Two Bell Creek geologic models have previously been constructed by the EERC to provide the basis for numerical simulations to give predictive estimates of fluid flow and pressure effects during CO_2 injection. The first (V1) model encompassed an area slightly larger than the field's Phase 1 boundary. The second (V2) geologic model attempted to expand the area of review to encompass the entire field and a large portion of the surrounding area (some 200 square miles). Both the V1 and V2 models were developed with the conventional depositional model in mind and the understanding that Bell Creek Field, at the time of the Muddy Formation deposition (Early Cretaceous), was located at the eastern margin of the Cretaceous Interior Seaway.

Historical interpretations have characterized the Muddy sands of the Bell Creek Field as being part of a large, Galveston Island-style barrier bar along a shoreline trending approximately northeast to southwest, evidencing the lack of clean sand to the east (interpreted lagoonal deposits) and a general thickening of the Muddy sands to the west. Formation pressure tests revealed some compartmentalization of the reservoir, and phase boundaries were drawn up to approximate these permeability barriers.

Two major reservoir permeability barriers were noted in the field (well discussed in Spakiewicz and others, 1988), one trending approximately northwest to southeast along the northern edges of Phases 1 and 2 and the other trending approximately north–south along the boundary separating Phases 1 and 2 (Figure 36). These permeability barrier features were described as being shale-filled and explained in a couple of ways; the northwest–southeast-trending feature in northern Phases 1 and 2 was interpreted as an incised marine channel (incising from deeper seas at the west/northwest toward the shoreline in the east/southeast). The north–south-trending permeability barrier was thought to be related to either fluvial channel incision parallel to the overall barrier bar trend or simply a gap between barrier bar lobes related to a sudden shift in sea level (moving barrier facies rapidly so as to leave a separation between sand lobes). A third permeability barrier toward the southern end of the field was noted along the boundaries of Phases 8 and 9, interpreted as an incised arm of a paleodrainage (not fully incising through the field to the west) trending roughly northwest–southeast. Core and well log analysis from this feature indicated a different type of infill, usually containing coals near the bottom and varying amounts of sand and siltstone overlying.

The Muddy Formation of the Bell Creek Field has been divided into four informal members (based generally upon Molnar, 1990), including (from bottom to top) the Rozet member, the Bell Creek sand interval, Springen Ranch siltstone, and the Shell Creek shale (reservoir stratigraphy shown in Figure 37). The Rozet member has been described as unconformably overlying the Skull Creek Shale and consisting of a 0.5–3-foot sand marking the Skull Creek–Rozet contact and an overlying 5–10 feet of shale/siltstone. The sandstone interval overlying the Rozet member is referred to as the Bell Creek sand interval, and has been described previously as having up to three different sand lobes (vertically), termed the BC10, BC20, and BC30. The Springen Ranch member overlies the Bell Creek sand interval, generally silty with some sand content. Log analysis shows

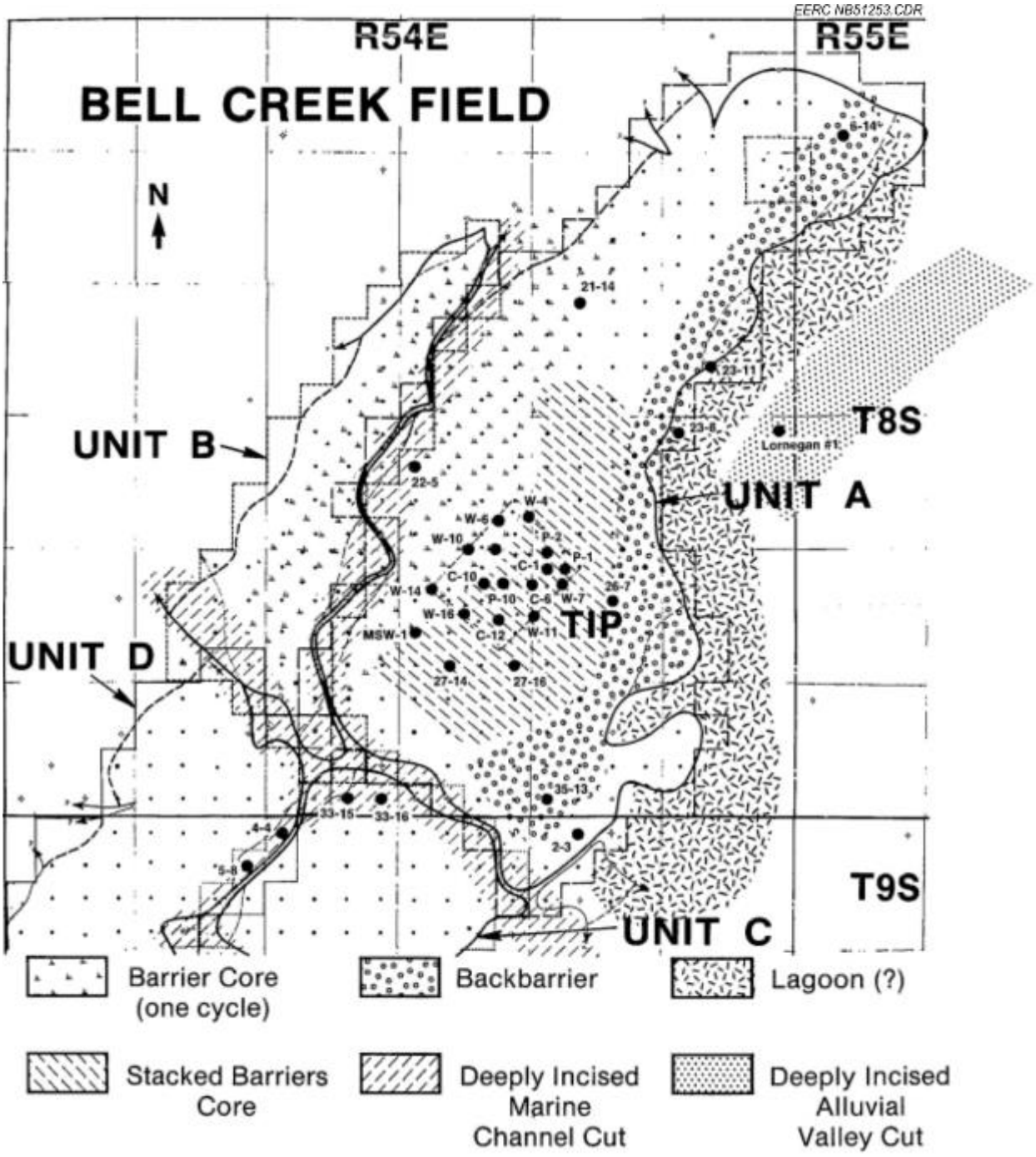

Figure 36. Historical illustration of interpreted depositional setting and facies distribution in the northern Bell Creek Field (from Spakiewicz and others, 1988).

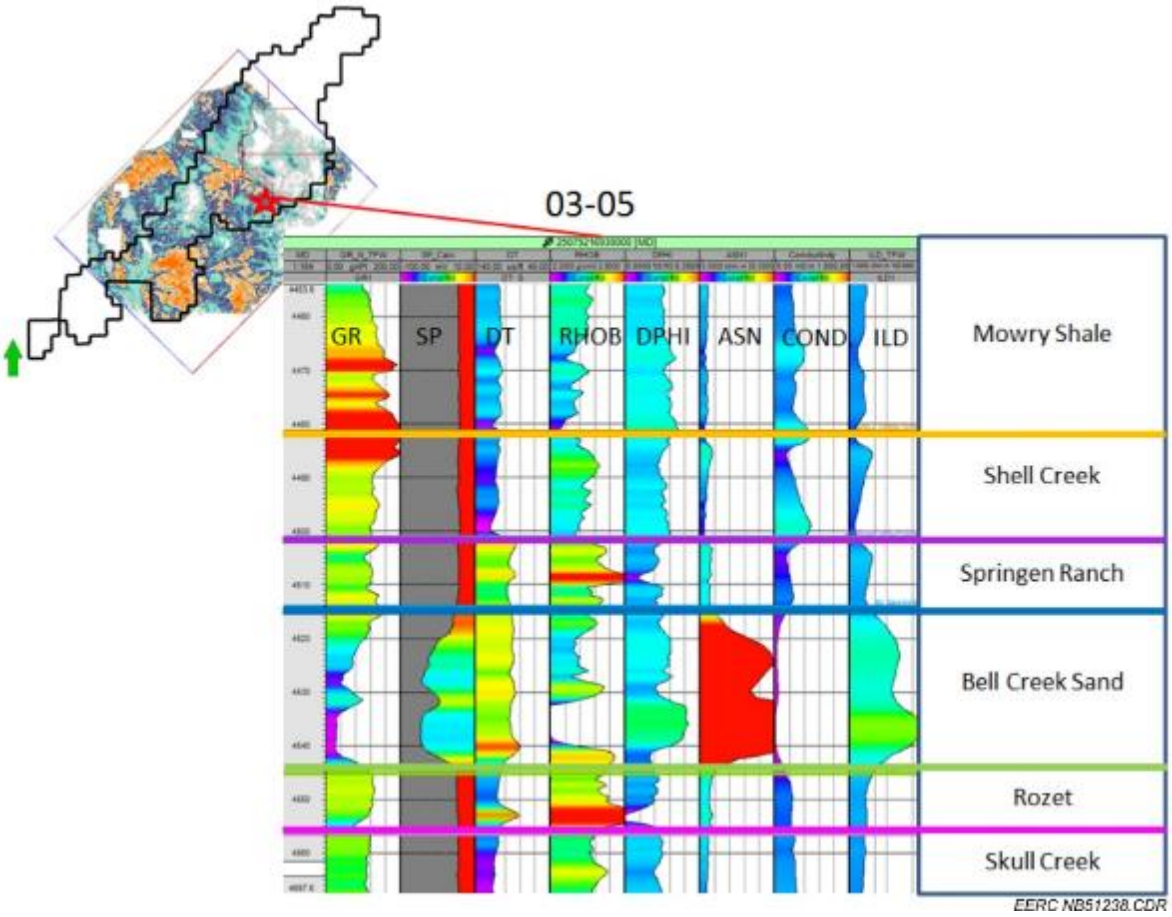

Figure 37. Well log display from Well 03-05 depicting the reservoir stratigraphy.

that some locations have a sandier interval at the top of the Springen Ranch member, possibly indicating a slight shallowing event. Overlying the Springen Ranch member is the Shell Creek shale (alternatively, some consider the Shell Creek shale as the lowest member of the Mowry Formation).

This understanding of the Muddy Formation within the Bell Creek Field was applied in the previously developed EERC reservoir models (V1 and V2). Geostatistical property distributions were achieved using variograms reflecting anisotropy trends consistent with a large-scale barrier bar oriented northeast–southwest (major range parallel to barrier bar trend [northeast to southwest] and minor range perpendicular to barrier bar trend [northwest to southeast]). As such, porosity and permeability trends were modeled with higher connectivity parallel to the strike of the interpreted barrier bar (northeast–southwest).

These models were used to run history-matching and numerical simulation efforts. As discussed in the history-matching section, there were substantial difficulties noted in the history-matching process, including adjustment of fluid flow boundaries; adjustment of near-wellbore fluid saturations, porosities, and permeabilities; and the necessity of additional pseudowells for

pressure support to achieve acceptable history-matched conditions. These difficulties indicated that the reservoir geology had not been captured accurately in the previous modeling efforts.

These issues spurred renewed efforts to understand the deposition of the Muddy Formation sands of the Bell Creek Field and develop of a new (V3) geologic model. This model has not been completed as of the writing of this report, but it incorporates important differences in approach and geological understanding, much of which has been enabled by the incorporation of newly acquired 3-D surface seismic data.

Seismic Data Interpretation and Revised Depositional Model

Surface 3-D seismic data were acquired in the Bell Creek Field in 2012 to characterize the geology prior to CO_2 injection activities and provide a baseline for comparison with repeat (4-D) seismic data in an effort to identify areas of the reservoir showing changes in fluid saturation and pressure effects related to CO_2 injection. This data set, which was not available during the development of the previous geologic models, has led to some interesting discoveries within the Muddy sands of the Bell Creek Field.

The 3-D seismic data from the Bell Creek Field have been analyzed using several different methods, including development of surface attribute maps (combining amplitude or signal character over an interval and displaying the result as a surface or map), development of volumetric attributes (applying a calculation to the seismic data to develop a new attribute volume), AVO, and seismic data inversion to create geomechanical properties. There are challenges in the analysis of the Bell Creek 3-D seismic data, most of which stem from the vertical seismic resolution (the vertical resolution of the seismic data is on the order of 60 feet [Burnison and others, 2014]) and relatively thin character of the Muddy sands (the Muddy Formation itself varies generally between 70 and 90 feet; the reservoir sands of the Muddy Formation are variable in thickness from a couple of feet to usually not much more than 30 feet). This makes most types of inversion to create reservoir properties ineffective, but the development of simple surface attributes, such as signal analysis or summation of positive amplitudes from the Skull Creek seismic horizon to the Springen Ranch seismic horizon (previously discussed in Burnison and others, 2014; see Figure 38), have been particularly useful in identifying important seismic geobodies, guiding well log and well cross-sectional analyses to better understand reservoir heterogeneity, and shedding light on active processes during the deposition of the Muddy Formation of the Bell Creek Field.

Referring to the amplitude summation surface attribute map discussed in Burnison and others (2014), there is a prominent high-amplitude, elongate, bow-shaped geobody (Figure 39, Geobody A) trending approximately northwest–southeast through Phases 1 and 2 of the Bell Creek Field. Bordering and mimicking the northern border of this geobody from northwest to southeast is a very low amplitude area (directly along the northern borders of Phases 1 and 2, precisely where a previously interpreted incised marine channel was inferred; see Geobodies B1 and B2 bounded in yellow in Figure 39). Perpendicular to these features, trending generally north–south, is a thin, sinuous, high-amplitude feature directly aligned with the boundary between Phases 1 and 2 (precisely where a prominent permeability barrier has previously been interpreted; see Geobody C1 in Figure 39). Another prominent dendritic feature in the southwest portion of the

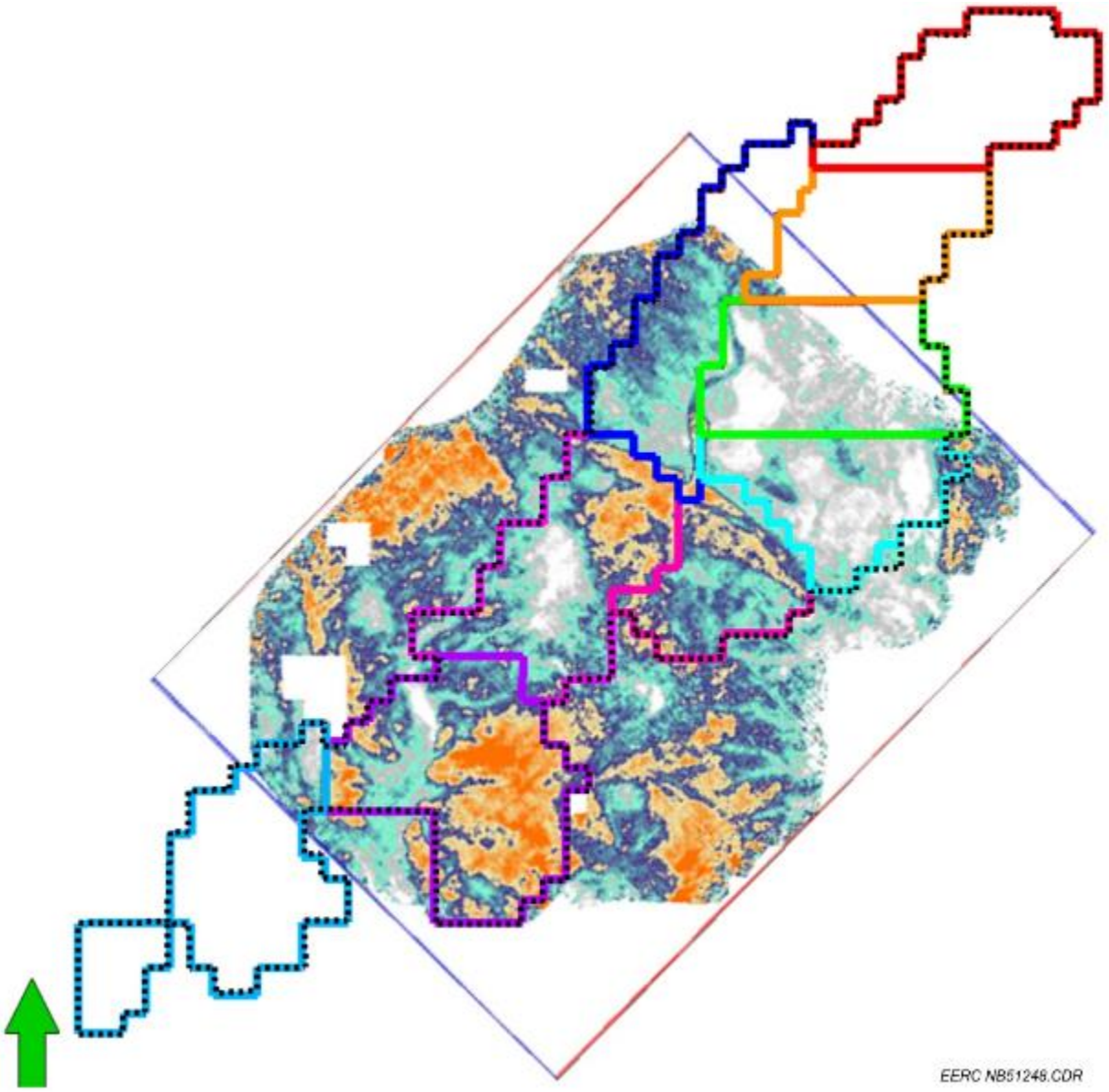

Figure 38. Map of Muddy Formation reflector amplitude with the Bell Creek phase boundaries overlain. This map was generated by and first discussed in Burnison and others (2014) through amplitude summation within the reservoir interval after a 90 degree phase rotation of the seismic data.

seismic survey coverage was previously interpreted as an incised drainage field trending to the southeast (see Geobody D in Figure 39). The information relayed in the surface attribute map regarding the location and morphology of these important geobodies enabled focused geologic investigations of reservoir character from well to well.

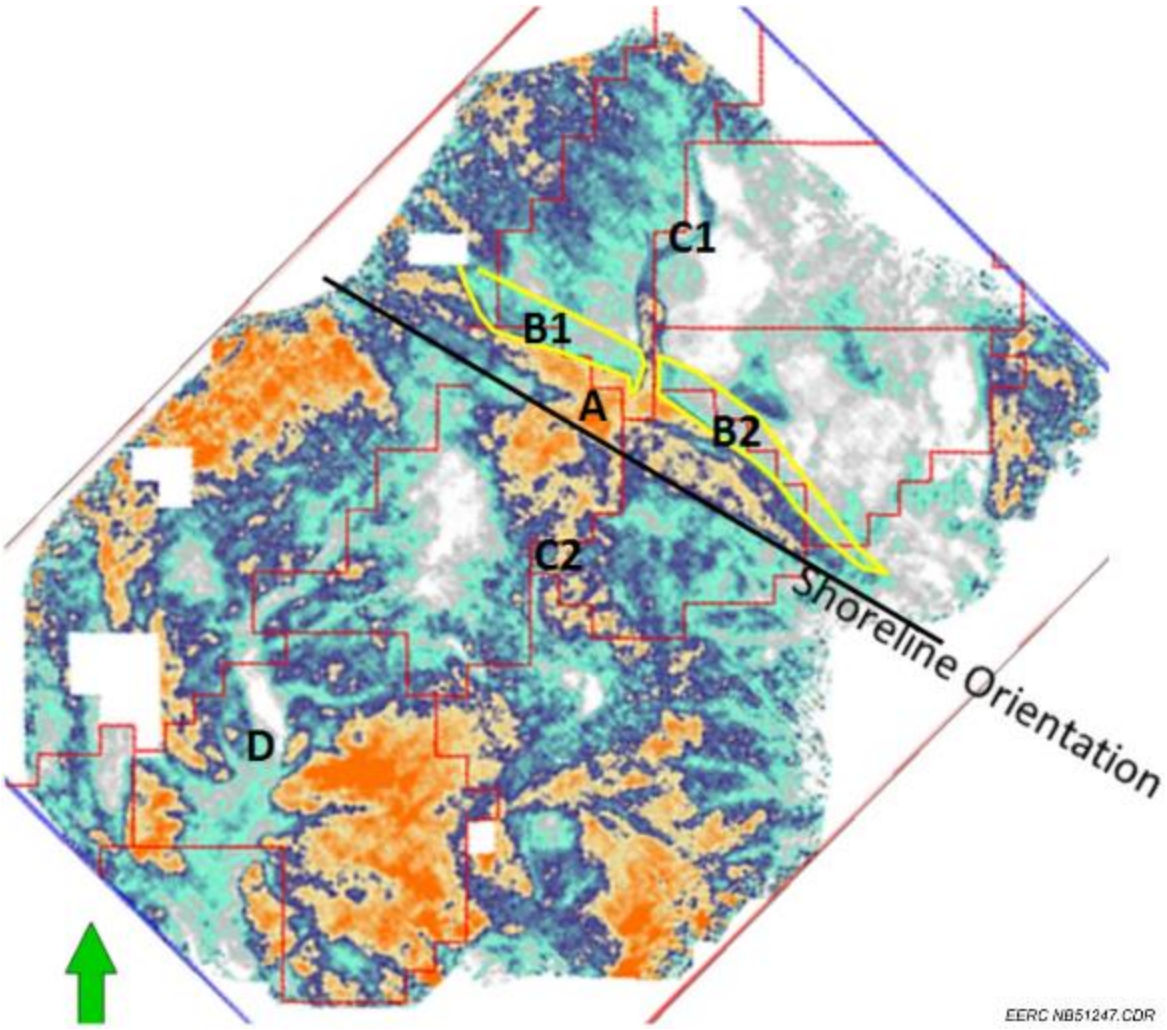

Figure 39. Bell Creek seismic amplitude map (from Burnison and others, 2014) with labeled geobodies. Geobody A represents the effect of interpreted back-barrier silty sands (evidenced in well logs and core samples). Geobodies B1 and B2, appearing to have little amplitude expression because of destructive interference in sonic velocity of well log-interpreted siltstones and shales, represents lagoonal deposits appearing to be offset by Geobody C1, an incised fluvial channel. Geobody C2 represents interpreted shallow marine channel deposits. Geobody D, containing coals and fine-grained sediments overlain by sand–silt cyclothems (seen both in well log and core samples; appearing to have similar geologic characteristics to Geobodies B1 and B2) may have started initially as a second (but earlier) lagoonal environment repurposed as a tidal channel system during relative sea level rise.

Cross-sectional investigation of the prominent geobody trending northwest–southeast through Phases 1 and 2 (well cross section perpendicular to the geobody, southwest–northeast) indicates the lower-amplitude area to the south is characterized by generally thick, clean sands, and the sand thickness seems to increase (correlating with increasing thickness of the upper sand within the Bell Creek sand interval) to the northeast, nearing the high-amplitude geobody. At the southern interface of the high-amplitude geobody, a silty sand interval is present at the top of the

Bell Creek sand member (overlying the clean upper sand); the upper Bell Creek sand interval thins moving north, with the silty sand interval increasing in thickness until it encompasses nearly all of the upper sand zone. The very low amplitude feature bordering to the north (the previously interpreted incised marine channel trending northwest–southeast) is characterized by a lower sand overlain by an interval with anomalously high radioactive character (noted in GR log), very low resistivity, flat-lined spontaneous potential (SP) response, and very low sonic velocity (very little clean sand present; the overall Bell Creek sand interval in this area is substantially thinner as well). Continuing along this well cross-sectional line to the northeast, the upper clean sand returns and the Bell Creek sand interval exhibits a more normal thickness (see well cross section in Figure 40).

This well cross section appears to transect a local barrier bar trending northwest–southeast, with cleaner bar front facies in the low-amplitude area to the southwest, silty back-bar sands within the high-amplitude geobody feature, lagoonal deposits along the north–northeast edge of the high-amplitude feature, and interpreted beach or mainland shorefront facies further to the northeast (all of these distinctly within the upper sand of the Bell Creek sand interval, with a separate lower sand interval below). These deposits, present in the upper Bell Creek sand interval, imply the barrier bar formation happened during the late stage of Muddy sand deposition; the barrier bar was likely transgressive in nature and preserved by burial during subsequent sea level rise. This interpretation gives a strong paleoshoreline indicator parallel to the barrier bar trend (northwest–southeast). Upon closer inspection, the interpreted local barrier bar seismic geobody has a very linear character along the southern margin, indicated by a wave-dominated shorefront. It also appears, from well logs within the interpreted bar front area, that it may be possible to determine lower-shoreface, middle-shoreface, and upper-shoreface zones from the log character, although further well log and core analysis are necessary to confirm this.

The high-amplitude feature with sinuous character, trending generally north–south along the boundary between Phases 1 and 2 (permeability barrier between Phases 1 and 2), intersects the interpreted local barrier bar and appears to change character after passing through to the south of the interpreted barrier bar geobody. This feature exhibits character very closely resembling the shape and scale of a fluvial incised valley and, as such, provides an explanation for the erosion of the Bell Creek sand interval. This interpreted channel's character change to the south of the barrier bar geobody (generally higher sinuosity, larger and more feathery appearance in the seismic data) is thought to represent a transition from a terrestrially confined channel in the north (thinner, more clearly defined channel) to longshore drift/marine channel facies in the south. However, this channel's terrestrial confinement expression can be found near the southern end of the seismic data to the southwest of the longshore drift/marine channel deposits. This lends support to the development of the fluvial system during subaerial exposure near the middle of the Bell Creek sand deposition (prior to transgression and barrier bar formation). The incised fluvial channel is mostly filled with fine-grained sediments (similar to the Springen Ranch member), indicating a rather rapid transgression nearing the end of the Bell Creek sand deposition. There is one important exception to the incised-channel, fine-grained infill just to the south of the high-amplitude barrier bar geobody. It appears that during barrier bar development, the longshore drift/marine channel deposits draped sands across the previously incised fluvial channel within the shallow marine environment before continuing to move the sediment further to the east and south. This sandy

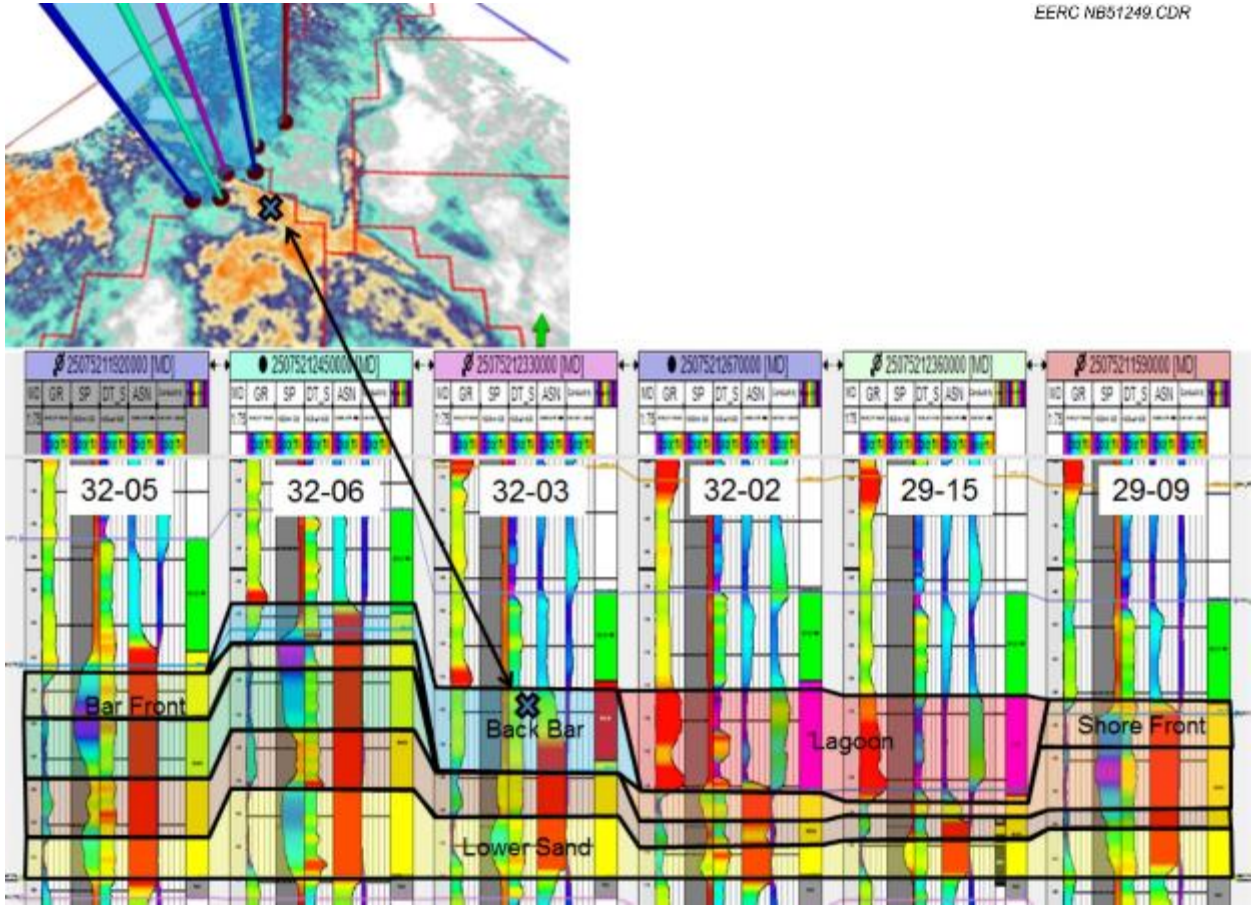

Figure 40. Interpreted well cross section (SW–NE) through the high-amplitude seismic geobody seen in Phases 1 and 2. Tracks are (from left to right) GR, SP, DT, ASN, conductivity, and facies logs. This cross section is located along the northwestern wing of the feature, but the same relationships in character are noted across the feature from northwest to southeast. The high-amplitude character seen in the seismic data appears to correlate with a silty sand interval in the upper Bell Creek sand and has been interpreted as back-barrier bar deposits.

incised-channel infill appears (from the repeat/4-D seismic surveys) to provide the only substantial hydraulic connection between Phases 1 and 2.

The prominent low-amplitude dendritic feature in the southwest portion of the seismic survey (previously interpreted as an arm of an incised drainage system) appears to exhibit similar log character to the lagoonal feature to the north (highly radioactive character noted in GR log, very low resistivity, flat-lined SP response, and very low sonic velocity) overlying a lower sand interval. Core analysis shows this character coinciding with coals and fine-grained sediments and may possibly have been deposited in another (earlier) lagoonal environment. Well cross section development perpendicular to this feature (southwest–northeast) agrees that this may be the case, with thicker, cleaner upper sands to the southwest grading and thinning into silty sand deposits within a higher-amplitude seismic feature (similar to interpreted back-bar silty sands in Phases 1 and 2), coal/shales lie laterally adjacent (possibly lagoonal facies) when progressing northeast before the clean upper sand returns (possibly beach/mainland shorefront facies). The dendrites trending from southwest to northeast appear to relate to interbedded cyclothems of sand and silt occurring at the top of the Bell Creek sand interval. These are likely related to the formation of a tidal channel system during a final transgressive event. Also, the seismic data display some linear character to features in the far southwest (trending north–northwest to south–southwest; well cross section analysis shows these are subparallel to parallel, thick, clean sand ridges in the upper Bell Creek sand interval separated by thin, silty sand troughs, which may be other (previous) paleoshoreline indicators. These features appear to have a high character resemblance and scale to modern baymouth bars, such as those of Perdido Bay along the Gulf Coast at the state boundaries of Alabama and Florida.

Furthermore, there appear to be trends in sand thickness within the Bell Creek Field and the surrounding area, generally from northwest to southeast (generally parallel to subparallel with the interpreted local barrier bar in Phases 1 and 2; as seen in the isopach in Figure 41). It should be noted that well control is substantially decreased outside of the field boundary, and as a result, the isopach map shown in this report has greater uncertainty in the outlying areas. However, there are multiple sand ridges separated by troughs (as many as six in the immediate area), which would seem to lend some support to their presence. There seems to be little possibility that these features could be related to faulting during deposition as investigation of the 3-D seismic data has shown no prominent structural influence persisting through or near the shallower strata (including the Muddy Formation). There is little discussion of these sand ridges in previous publications regarding formation and interpreted depositional environment. It is possible these features may be related to paleoshoreline processes at different points in time (facies migration with relative sea level rise and fall; sand ridges possibly formed during brief stillstands during the Muddy Formation deposition). If this is correct, the orientation implies deeper-water environments were generally to the southwest and terrestrial environments were to the northeast (pertaining to transgression–regression actions), rather than northwest and southeast, respectively, as previously thought.

This discussion has involved the prominent seismic features noted in the surface attribute map, but there are some other subdued, low-amplitude, curvilinear features in the northern portion of the seismic survey bounded by (relatively) higher-amplitude features. There are three such features laterally adjacent, subparallel, and approximately 0.25–0.5 miles wide in expression. Well

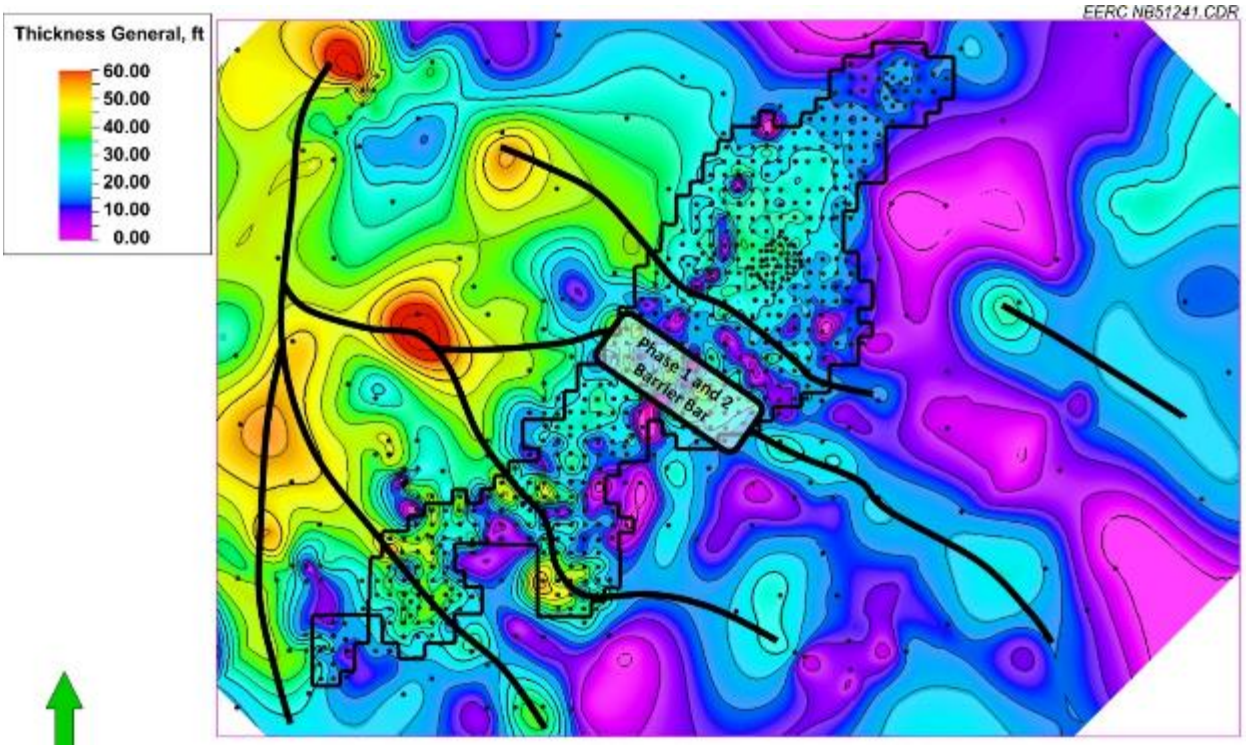

Figure 41. Bell Creek sand interval isopach with sand ridge trends approximated by black lines. Black dots represent well control in the development of the map. The Bell Creek Field boundary is shown as the black polygon. The contour interval is 5 feet. These sand ridges are roughly perpendicular to previous paleoshoreline interpretation but parallel to subparallel with the local barrier bar interpreted from the 3-D seismic data in the area of Phases 1 and 2. These sand ridges may have been formed during brief stillstand events during the Muddy Formation deposition, indicating shoreline may have been oriented generally northwest–southeast in the area of the Bell Creek Field.

cross section analysis indicates that these features are indicative of lower sand thickness (within the interpreted regressive deposits) and are likely not erosional in origin. The lower sand thickness appears to decrease toward the center of these features and thicken toward the bounding higher-amplitude areas and are, possibly, expressions of meandering deltaic channels traversing (generally) from north to south (thinning where water movement is greatest and thickening to the margins into levee deposits). If this interpretation is correct, further credence is given to the lower Bell Creek sand being deposited during an overall regressive event and the upper Bell Creek sand deposited during subsequent transgression.

In summary, the Muddy Formation sands within the Bell Creek Field appear to have been deposited during an overall regressive–transgressive sequence, with subaerial exposure and erosion occurring and separating the two sequence stratigraphic units. The barrier bar geobody noted in the seismic data as a paleoshoreline indicator suggests a shoreline orientation at the time of deposition approximately northwest–southeast. The fluvial channel expression in the seismic data indicates the updip (terrestrial environment) direction being to the north–northeast and deeper

marine direction to the south–southwest. Deltaic/shoreline progradation likely occurred at the beginning of the Bell Creek sand deposition (generally from north–northeast to south–southwest) during a relative sea level fall event. There may have been a brief deepening event (as evidenced by a relatively thin, silty sand–siltstone overlying the lower sand) before sea level lowering continued. Subaerial exposure and erosion occurred following relative sea level fall. It is likely that fluvial channel development and incision would have begun during this time as well. A subsequent transgression from the southwest likely resulted in barrier bar and lagoonal facies development in the southwest part of the field. Transgressive seas likely entered the associated southwestern lagoon and formed a tidal channel complex, with the dendritic channel features etching landward (north–northeast) as sea level continued to rise. The barrier bar noted in Phases 1 and 2 likely formed during a brief stillstand event. Fluvial sediments transported to the shallow marine environment to the south of the barrier bar were likely carried by longshore currents to the southeast, draping sands into the incised channel and providing a hydraulic link between Phases 1 and 2. Transgression continued to the north–northeast, rapidly burying (and preserving) these features observed in the seismic data in the fine-grained Springen Ranch sediments.

Reservoir Model Construction

The aspects of the new Bell Creek depositional model discussed above provide the foundation upon which the Version 3 geologic model is being built. The areal extent of this new model will encompass the entire Bell Creek Field (Phases 1–9). The stratigraphic content of the model includes the Muddy Formation (Rozet, Bell Creek sand, and Springen Ranch members) and the Shell Creek shale (lowermost upper seal for the Muddy interval). The initial static model is being developed at the same lateral resolution as the baseline 3-D seismic data set (82.5 feet × 82.5 feet), allowing for ease of seismic resampling and inversion efforts in property development. The initial vertical resolution of the reservoir model is 1 foot. Grid sensitivity analyses will be undertaken on the completed model to determine the final grid resolution (upon upscaling for simulation).

The area of baseline 3-D seismic coverage has been the focus in V3 model development thus far. The seismic data have provided an ability to extract geobodies (areas having similar lithologic properties) to focus investigation and property distribution, i.e., barrier bar, incised fluvial channel, and tidal channel system geobodies.

Well log and cross section development has been undertaken to develop an understanding of lateral and vertical facies associations, which are needed in the creation of facies logs and multiple point statistic (MPS) training images. These facies logs are upscaled within their respective geobody regions in the reservoir model and provide the control points (hard data) needed to guide an MPS facies distribution. MPS training images have been created for each of the different geobody regions (each region having its own particular facies associations and training image). Facies distribution using MPS has been achieved for each of the seismic geobody regions.

Current efforts are centered on facies modeling outside of seismic survey coverage area. The seismic data allow for the construction of a very specific model with relatively low uncertainty in facies distribution. Facies associations (pertaining to the new understanding of the Muddy Formation deposition) outside of the seismic survey coverage are not well understood and cannot be captured with the same level of uncertainty, providing a unique challenge. This obstacle will be overcome by revisiting specific cores for vertical facies associations and developing well cross sections to determine lateral facies associations and approximate geobody region bounds. The MPS method will be used to distribute facies similarly to the area of seismic survey coverage, although with increased uncertainty in comparison.

The resulting facies model will be used to constrain further property distributions (porosity, permeability, and water and oil saturations). Upon the completion of property modeling, the grid will be upscaled for simulation purposes. History-matching efforts will provide insight into the accuracy of the static model's property distributions. A comparison will be made with V2 model simulation efforts in an attempt to further support or deny the new Bell Creek depositional model.

SUMMARY

During the last year, modeling and simulation activities for the Bell Creek CO_2 EOR and Storage project were updated, including the evolution of the Bell Creek reference model, history-matching efforts on a combined Phase 1 and 2 model, and storage potential for the Bell Creek Field. In addition, efforts were undertaken to better understand factors that affect CO_2 EOR and to begin the development of a new (V3) reservoir model incorporating Bell Creek 3-D seismic data. The results of these efforts will assist with risk assessment and MVA planning for long-term storage. Key highlights and results of the current simulation activities include the following:

- The Bell Creek reference model was developed to enable consistency across various modeling efforts and contains all available pertinent modeling data (wells, well logs, formation tops, structural surfaces, previously developed V1 and V2 geologic models, near-surface model, etc.). The model has been updated as new data are acquired, including repeat PNLs and seismic data.

- Thirty-three baseline PNLs and 19 repeat PNLs provided confidence in updating the local stratigraphic column and thicknesses in the area of investigation from reservoir to ground surface. Moreover, changes in fluid saturations of CO_2, water, and oil were also identified through the repeat logs on certain injection and production wells. These results have been integrated into the ongoing modeling and simulation activities.

- Previous dynamic simulation activities on separate Phase 1 and Phase 2 models (from the V2 geologic model) indicate there is likely some hydraulic connectivity between the phases (previously reported).

- Individual Phase 1 and 2 simulation models have been combined to form a new simulation model. The new model enables simulated fluid flow between the phases. In this study, the simulation work includes 1) history-matching 47 years of field records with primary

depletion, waterflooding, and CO_2 EOR in the Phase 1 and 2 areas; 2) analyzing fluid saturation distribution in the reservoir and identifying cross-boundary fluid flow between Phases 1 and 2; and 3) predictive simulations of CCI and WAG in both Phase 1 and 2 areas to assess oil recovery, CO_2 storage, and CO_2 utilization factor, ultimately improving risk identification and MVA strategies.

- The WAG case results in less HCPVI than CCI for the same injection time (WAG results in 3 HCPVI, while CCI results in 4.65 HCPVI). This is because CO_2 has lower density and viscosity than water; more pore volumes of CO_2 can be injected into the reservoir than water under the same pressure conditions. Thus it may be better to compare the reservoir performance and evaluate sweep efficiency based upon HCPVI rather than injection duration for the two cases.

- The CCI case results in injection of approximately twice the amount of CO_2 in comparison to the WAG case and roughly 1.7 times greater mass of stored CO_2 (however, more CO_2 is produced with oil in CCI mode). Also, CCI requires more CO_2 to produce the same amount of oil in comparison to the WAG case.

- The CO_2 utilization factor (amount of CO_2 needed to produce one barrel of oil) for the WAG case drops below 10 MMscf/bbl after 1 HCPVI. This decreases to 7 MMscf/bbl when 3-HCPV fluids are injected in WAG mode, while the value remains above 10 MMscf/bbl even after 4 HCPVI in CCI mode.

- The incremental oil recovery from CCI and WAG is almost the same (although CCI seems to produce oil more quickly; see Appendix B, Figure B-16), while the HCPVI of WAG is 35% less than that of CCI. Thus WAG has higher sweep efficiency and can utilize CO_2 better than CCI in the EOR process.

- It should be noted that the previously developed Bell Creek reservoir models (V1 and V2) were developed supporting the large, Galveston Island-style barrier bar depositional model and proved challenging in the history-matching process. Comparison of modeled oil saturations and PNL-measured oil saturations shows substantial differences as well. This indicates the reservoir heterogeneity has not been captured in previous models and provides impetus to develop a new (V3) geologic model.

- Integration and interpretation of the Bell Creek 3-D baseline surface seismic data give support to a new depositional model, with an interpreted local, transgressive (as seen to be related to character in the upper Bell Creek sand interval) barrier bar in Phases 1 and 2, indicating a shift in shoreline orientation from previous studies (approximately northwest to southeast).

- Important permeability barriers noted in previous studies appear to be related to sinuous fluvial channel incision trending north–south along the boundary between Phases 1 and 2 and lagoonal deposits trending northwest–southeast along the northern boundaries of Phases 1 and 2.

- Simulation history-matching efforts have indicated that there may, in fact, be some hydraulic connectivity between Phases 1 and 2. Interpretation of initial results developed from repeat/4-D seismic data surveys in Phases 1 and 2 seem to agree, indicating fluid saturation and pressure (plume) effects related to CO_2 injection making an east–west connection between Phases 1 and 2. This has been interpreted as being related to local infill of fluvial channel incision with draped, sandy longshore drift/shallow marine channel deposits, whereas the remainder of the infill elsewhere appears to be more closely related to Springen Ranch fine-grained sediments.

- Other features noted in the seismic data include possible deltaic meanders (well cross-sectional analysis indicates these features are probably resulting from topographic character in the lower Bell Creek sand interval, indicating deposition during regression/relative sea level fall), linear sand ridges and silty sand troughs in the southwest portion of the seismic data (subparallel to the interpreted local barrier bar in Phases 1 and 2 and possibly representative of a second barrier–baymouth bar complex), and an unusually shaped, dendritic channel system in the southwest portion of the seismic data survey (appearing to be related to coals and shales within the upper Bell Creek sand interval and overlain by varying amounts of sand and sand–silt cyclothems, possibly beginning as a lagoonal environment but appearing to have tidal channel character near the end of deposition).

- The features interpreted from the Bell Creek 3-D seismic data support a depositional model of facies migration during an overall regressive–transgressive event occurring generally from northeast–southwest and vice versa, respectively.

- Facies modeling, leveraging seismic geobody extraction and MPS, is currently under way to capture reservoir heterogeneity. Property distributions will be conditioned to the resulting facies model before being prepared for history matching and predictive simulations.

LIMITATIONS

Although meaningful simulation results have been presented here, they are primarily based on the V2 geologic model. This version, while still useful, does not contain certain data that have been collected in the past year. As a result, the V3 model currently under development will further reduce uncertainty by incorporating petrographics, outcrop fieldwork, 3-D and 4-D seismic surveys, PNLs, and additional core characterization data. Improvements will be made in the distribution of petrophysical facies, which will be correlated to both PNLs and core petrographic descriptions and distributed with conditioning to the new understanding of the reservoir heterogeneity. PNLs (and a potential tracer study) will provide a better understanding of preferential fluid flow and changes in reservoir fluid volumes and ensure CO_2 containment.

Although several scattered reservoir pressure data points were matched, a limitation of this dynamic simulation work remains the history matching of average reservoir pressure, since only

the initial and limited average pressures are available. More historical reservoir pressure data would lead to more accurate calculated pressure; however, these data are not available.

During the predictive simulation of CO_2 flooding, the relative permeability hysteresis and CO_2 solubility in the aqueous phase were considered for only select cases, so the estimated associated CO_2 storage capacity values for different cases may appear to be on the lower side overall. The WAG ratio of 1:1 was used in all of the simulation cases, but in future predictive simulation, other injection ratios may be evaluated for their effects on associated CO_2 storage and incremental oil recovery.

ONGOING AND FUTURE WORK

Reference Model

The Bell Creek reference model has been developed in this study in an effort to provide a consolidated data source for future geologic modeling efforts. Created and intended as such, the model will be updated continually with various pertinent data sets as they become available in the future.

Fluid Model and Reservoir Simulation

Although the V2 model can match the overall reservoir performance, individual wells need more effort to match (the static model properties are likely decreased in accuracy because of previously developed depositional assumptions). Fluid saturation property distributions in the V2 model were based on geologic assumptions in line with the conventional depositional model (Galveston Island-style deposition from east to west, which we now know may not be the case). This is apparent when comparing modeled fluid saturation properties with properties measured from PNLs. The history match has captured general trends noted in historical field data, but some localized points are missed because the reservoir has stronger heterogeneity (in both vertical and horizontal directions) than was captured in the V2 model as a result of a complicated depositional process. The V3 geologic model will incorporate these findings to achieve informed property distributions, which will enable a more accurate history match (and likely mean increased accuracy in predictive estimates gained from future dynamic simulations).

EOS and Relative Permeability Curves

Through the special core analysis being conducted by Core Laboratories, the relative permeability curves will be updated and the revised versions used in the next cycle of activities. The new simulation model version may have up to five sets of relative permeability curves. The new measured relative permeability curves will provide additional insight into CO_2 EOR efficiency, which will be used to improve predictive scenarios.

History Matching of CO_2 Flood

Automatic history-matching techniques, e.g., CMG's CMOST, automatically vary reservoir parameters until criteria are achieved and a history match of field performance is obtained.

Computer-aided history matching by CMOST, which minimizes the global objective function error (the difference between observed reservoir performance and simulation results), is planned for future rounds of dynamic simulations.

The production and injection history of the CO_2 flood from the start of CO_2 injection through April 2015 was added to the previous history-matched simulation model, and the history-matching work of newly added CO_2 injection is under way. After a satisfactory history match of CO_2 flood is achieved, the matched model will be used for the predictive simulation of other CO_2 injection scenarios.

Integrated History Matching of Phases 1 and 2

V3 simulation efforts will be combined similarly to achieve an integrated model comprising both the Phase 1 and 2 areas. The experience derived from the history matching of the V2 (combined Phase 1 and 2) model will be used to ensure the quality of the new combined model and speed up the history-matching process. In addition to the regular indices to be matched, the combined model will partially focus on the fluid communication between phases.

Grid Refinement

Gridding alternatives are also being explored for the V3 model, including local grid refinement to better capture near-wellbore phenomena. For instance, PNL calculated oil saturations (as a history match validation data set) are measured from tool responses indicative of near-wellbore conditions; however, upscaled simulation models use quite large cells with averaged reservoir properties to calculate the saturations. This creates difficulty in achieving a good history match as the scale and range of values may be very different from PNL to simulation model. To overcome this challenge, detailed local reservoir characterization and grid refinement for wells will be attempted in the V3 model to better capture the localized phenomena. This will likely prove necessary for better understanding and predicting reservoir performance, especially for CO_2 flooding.

Predictive Simulations

Numerous theoretical studies and field cases have shown that WAG is an effective way to improve CO_2 sweep efficiency and enhance oil recovery (Harpole and Hallenbeck, 1996; Zhou and others, 2012; Braunberger and others, 2013; Han and Gu, 2014). Thus the WAG process will be simulated in future efforts to predict reservoir performance under different operational schedules. In addition, CO_2 plume distribution will be simulated to evaluate the storage capacity and long-term fate of CO_2 in the reservoir.

V3 Geologic Model

The V3 geologic model (currently under construction) plans to incorporate large data sets acquired in recent and ongoing characterization and monitoring efforts, including PNLs, structural and seismic interpretation, core analysis, and history-matching results. These data have important roles in improving the structural, petrophysical, and saturation models of the Bell Creek Field that

will build upon V2 to reduce uncertainty in numerical simulations of fluid flow, saturation changes, and pressure effects. This is of increasing importance as CO_2 injection begins to take place in other phases of the Bell Creek Field.

The V3 structural model will update surfaces created from the results of the PNLs, 3-D seismic survey interpretation (including both the baseline and repeat 3-D seismic surveys), and a potential tracer study aimed at enhancing the lateral structural resolution between wells. This enhanced resolution will provide a more accurate calculation of pore volumes and help identify structural features and thickness uncertainties that may inhibit (or unexpectedly allow) flow throughout the reservoir, as well as above and below, to ensure CO_2 containment.

Facies modeling, informed by the seismic data where available, will be completed using advanced geostatistical methods (including MPS) to develop geologic understanding throughout the field and expanded area of review. An associated petrophysical model will be constructed using results from the PNLs, recent core analysis, and future lithologic (core and outcrop) descriptions and interpretations (with a new understanding of the deposition of the Muddy Formation of Bell Creek in mind). Fluid saturations and other key rock properties will then be populated based on field tests and PNLs. An upscaling process will be followed to prepare an appropriate simulation model.

3-D Mechanical Earth Model

In order to assess the state of stresses and reservoir mechanical properties (e.g., rock strength, pore pressure, in situ stress, and elastic properties) caused by injection and production, a 3-D mechanical earth model (MEM) is being created for the Bell Creek Field. The 3-D MEM will aid in the understanding of reservoir response to various stress states, assisting with the prediction of formation deformation, permeability variation, and the maximum injection rate and pressure that can be used without compromising the integrity of the reservoir and confining units.

The 3-D MEM is being created based on the existing 1-D MEM while incorporating several additional wells with geomechanical property logs, wells with PNLs run to the near-surface, and 3-D seismic data. The 3-D MEM will contain a combination of stress states, geologic structure, seismic inversion-derived lithofacies, and reservoir elastic properties. All of the geomechanical properties are being populated into the whole field by the petrophysical modeling process in Petrel, with the 3-D seismic property as the secondary data.

This fieldwide 3-D MEM will, in next steps, be used to conduct geomechanical simulations. The dynamic simulations of the rock mechanical properties and reservoir conditions will provide more accurate support for the prediction of wellbore instability, fault reactivation, and potential leakage of CO_2 during injection, production, and long-term storage.

CONCLUSIONS

Over the past year, Bell Creek modeling and simulation activities have included a PNL campaign, updating of a reference model, history-matching of the production/injection data and

selected available reservoir pressures in a combined Phase 1 and 2 simulation model, and initial efforts in the construction of the V3 geologic model.

The PNL campaign, with 33 baseline PNL and 19 repeat logs, has built confidence in identifying changes in fluid saturations of CO_2, water, and oil. These results have been integrated into a reference model, along with other updated well data, and are being used to track the presence of CO_2, directly benefitting the monitoring and risk assessment activities of the project.

The Phase 1 and 2 area model was clipped from the 3-D full-field geologic model (V2) and validated by matching the historical production/injection and reservoir pressure data. The overall trends of the historical data have been captured in the history-matching efforts, but some localized points and individual wells have proven difficult to match, indicating the modeled geology may not be an accurate representation of the actual reservoir character.

The V3 geologic model currently under construction aims to address the shortcomings of the V1 and V2 models by integrating a new understanding of the reservoir depositional model, previous simulation results, newly reprocessed baseline surface seismic data, repeat/4-D surface seismic data, and advanced geostatistical methods (including MPS for facies distribution) to more accurately capture and model reservoir heterogeneity in unsampled locations. These static modeling upgrades will enable more efficient history-matching and increased accuracy in predictive simulations. This will, in turn, contribute vital information for adaptive management plans, risk assessment in containment effectiveness analyses, and future MVA efforts and technology deployment.

REFERENCES

Bennion, D.B., Thomas, F.B., and Bietz, R.F., 1996, Hysteretic relative permeability effects and reservoir conformance—An Overview. Hycal Energy Research Laboratories Ltd.

Braunberger, J.R., Pu, H., Gorecki, C.D., Bailey, T.P., Bremer, J.M., Peck, W.D., Gao, P., Ayash, S.C., Liu, G., Hamling, J.A., Steadman, E.N., and Harju, J.A., 2013, Bell Creek test site – simulation report: Plains CO_2 Reduction (PCOR) Partnership Phase III Task 9 Deliverable D66 Update 2 for U.S. Department of Energy National Energy Technology Laboratory Cooperative Agreement No. DE-FC26-05NT42592, August.

Burnison, S.A., Burton-Kelly, M.E., Zhang, X., Gorecki, C.D., Steadman, E.N., and Harju, J.A., 2014, Bell Creek test site – 3-D seismic and characterization report: Plains CO_2 Reduction (PCOR) Partnership Phase III Task 4 Deliverable D96 for U.S. Department of Energy National Technology Laboratory Cooperative Agreement No. DE-FC26-05NT42592, March.

Burt, R.A., Haddenhorst, F.A., and Hartford, J.C., 1975, Review of Bell Creek waterflood performance – Powder River, Montana: Journal of Petroleum Technology, v. 27.

Chewaroungroaj, J., Varela, O.J., and Lake, L.W., 2000, An evaluation of procedures to estimate uncertainty in hydrocarbon recovery: Proceedings of SPE Asia Pacific Conference on Integrated Modelling for Asset Management, Yokohama, Japan, April 25–26, SPE 59449.

Ettehadtavakkol, A., Lake, L.W., and Bryant, S.L., 2014, CO_2 EOR and storage design optimization: International Journal of Greenhouse Gas Control, v. 25, p. 79–92.

Fatemi, S.M., Sohrabi Sedeh, M., Jamiolahmady, M., and Ireland, S., 2012, Experimental and theoretical investigation of gas/oil relative permeability hysteresis under low oil/gas interfacial tension and mixed-wet conditions. Energy Fuels, Vol. 26, p. 4366-4382.

Gorecki, C., Hamling, J., Klapperich, R., Steadman, E., and Harju, J., 2012, Integrating CO_2 EOR and CO_2 storage in the Bell Creek oil field: Presented at Carbon Management Technology Conference, Paper 151476.

Hamling, J.A., Gorecki, C.D., Klapperich, R.J., Saini, D., and Steadman, E.N., 2013, Overview of the Bell Creek combined CO_2 storage and CO_2 enhanced oil recovery project: Energy Procedia, v. 37, p. 6402–6411.

Han, L., and Gu, Y., 2014, Optimization of miscible CO_2 water-alternating-gas injection in the Bakken Formation: Energy Fuels, v. 28.

Harpole, K.J., and Hallenbeck, L.D., 1996, East Vacuum Grayburg San Andres unit CO_2 flood ten year performance review—evolution of a reservoir management strategy and results of WAG optimization: Proceedings of SPE Annual Technical Conference and Exhibition, Denver, Colorado, October 6–9, SPE-36710.

Huang, E.T.S. and Holm, L.W., 1988, Effect of WAG injection and rock wettability on oil recovery during CO_2 flooding. SPE-15491-PA, SPE Reservoir Engineering, vol. 3, no. 1, February.

Jin, L. and Wojtanowicz, A.K., 2014, Progression of injectivity damage with oily waste water in linear flow. Pet. Sci. vol. 11.

Liu, G., Braunberger, J.R., Pu, H., Gao, P., Gorecki, C.D., Ge, J., Klenner, R.C.L., Bailey, T.P., Dotzenrod, N.W., Bosshart, N.W., Ayash, S.C., Hamling, J.A., Steadman, E.N., and Harju, J.A., 2014, Bell Creek test site – simulation report: Plains CO_2 Reduction (PCOR) Partnership Phase III Task 9 Deliverable D66 Update 4 for U.S. Department of Energy National Energy Technology Laboratory Cooperative Agreement No. DE-FC26-05NT42592, August.

Molnar, P.S., 1990, Geologic reservoir study of the Bell Creek Field, Carter and Powder River Counties, Montana: Exxon Company, Midland, Texas.

Pu, H., Hamling, J.A., Bremer, J.M., Bailey, T.P., Braunberger, J.R., Ge, J., Saini, D., Sorensen, J.A., Gorecki, C.D., Steadman, E.N., and Harju, J.A., 2011, Bell Creek test site – simulation report: Plains CO_2 Reduction (PCOR) Partnership Phase III Task 9 Deliverable D66 for U.S.

Department of Energy National Energy Technology Laboratory Cooperative Agreement No. DE-FC26-05NT42592, August.

Rogers, J.D., and Grigg, R.B., 2000, A literature analysis of the WAG injectivity abnormalities in the CO_2 process. SPE 59329, Proceedings of SPE/DOE improved oil recovery symposium, Tulsa, OK, Apr. 3–5.

Saini, D., Braunberger, J.R., Pu, H., Bailey, T.P., Ge, J., Crotty, C.M., Liu, G., Hamling, J.A., Gorecki, C.D., Steadman, E.N., and Harju, J.A., 2012, Bell Creek test site – simulation report: Plains CO_2 Reduction (PCOR) Partnership Phase III Task 9 Deliverable D66 Update 1 for U.S. Department of Energy National Energy Technology Laboratory Cooperative Agreement No. DE-FC26-05NT42592, August.

Shook, M., Li, D., and Lake, L.W., 1992, Scaling immiscible flow through permeable media by inspectional analysis: In Situ, v. 4.

Spakiewicz, M., Shatzinger, R., Honarpour, M., Tham, M., and Tillman, R., 1988, Geological and engineering evaluation of Barrier Island and Valley-Fill Lithotypes in Muddy Formation, Bell Creek Field, Montana: Rocky Mountain Association of Geologists Guidebook, p. 159–182.

Steadman, E.N., Anagnost, K.K., Botnen, B.W., Botnen, L.S., Daly, D.J., Gorecki, C.D., Harju, J.A., Jensen, M.D., Peck, W.D., Romuld, L., Smith, S.A., Sorensen, J.A., and Votava, T.J., 2011, The Plains CO_2 Reduction (PCOR) Partnership—developing carbon management options for the central interior of North America: Energy Procedia, v. 4, p. 6061–6068.

Wood, D.J., Lake, L.W., Johns, R.T., and Nunez, V., 2008, A screening model for CO_2 flooding and storage in Gulf Coast reservoirs based on dimensionless groups: SPE Reservoir Evaluation & Engineering, v. 11.

Zhou, D., Yan, M., and Calvin, W.M., 2012, Optimization of a mature CO_2 flood – from continuous injection to WAG: Proceedings of SPE Improved Oil Recovery Symposium, Tulsa, Oklahoma, April 14–18, SPE-154181.

APPENDIX A

BELL CREEK REFERENCE MODEL

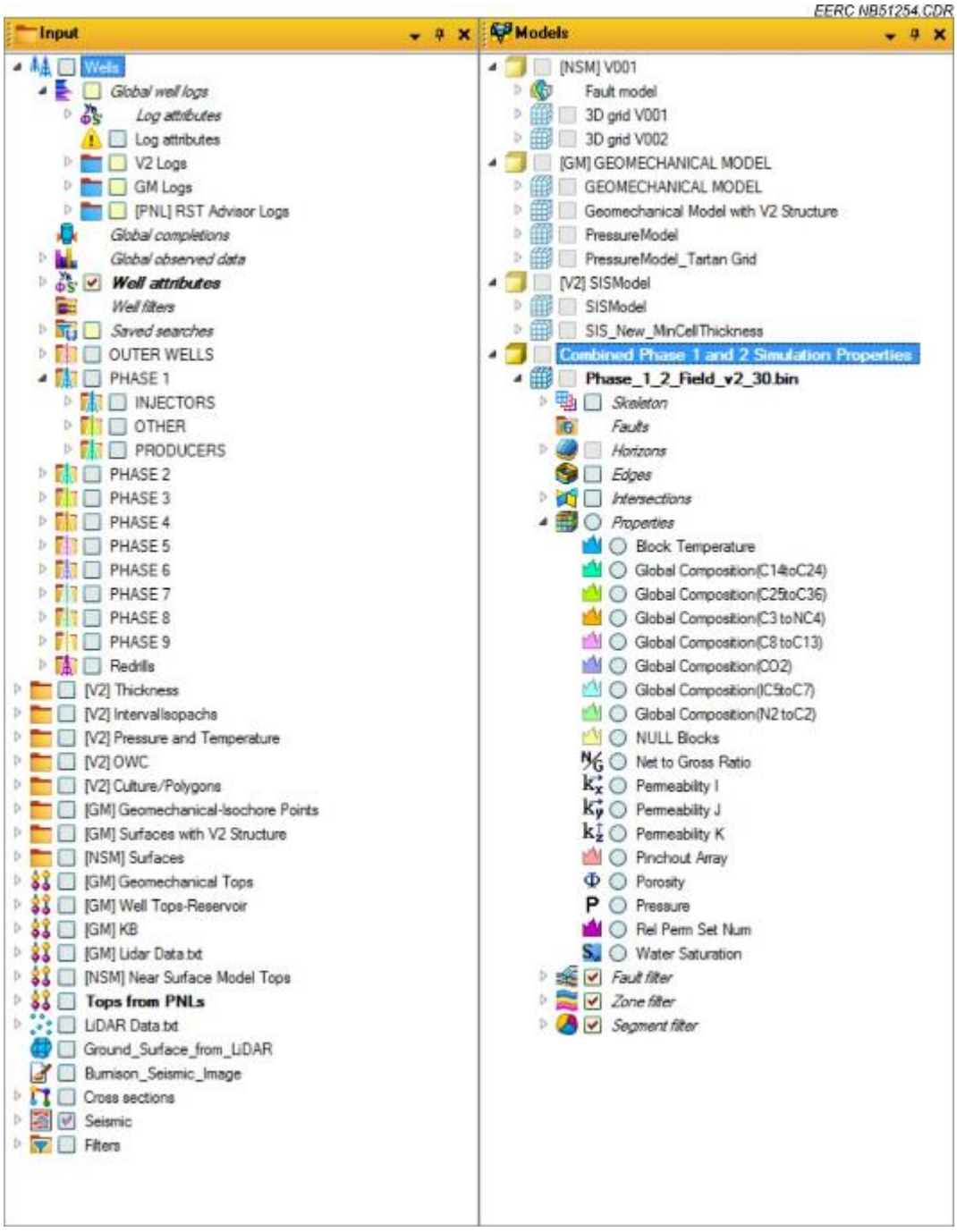

Figure A-1. Input and Modeling Interfaces from the Reference Model Made with Schlumberger's Petrel ([V2] represents data from the Version 2 model, [GM] represents data from the geomechanical model, and [NSM] represents data from the near-surface model).

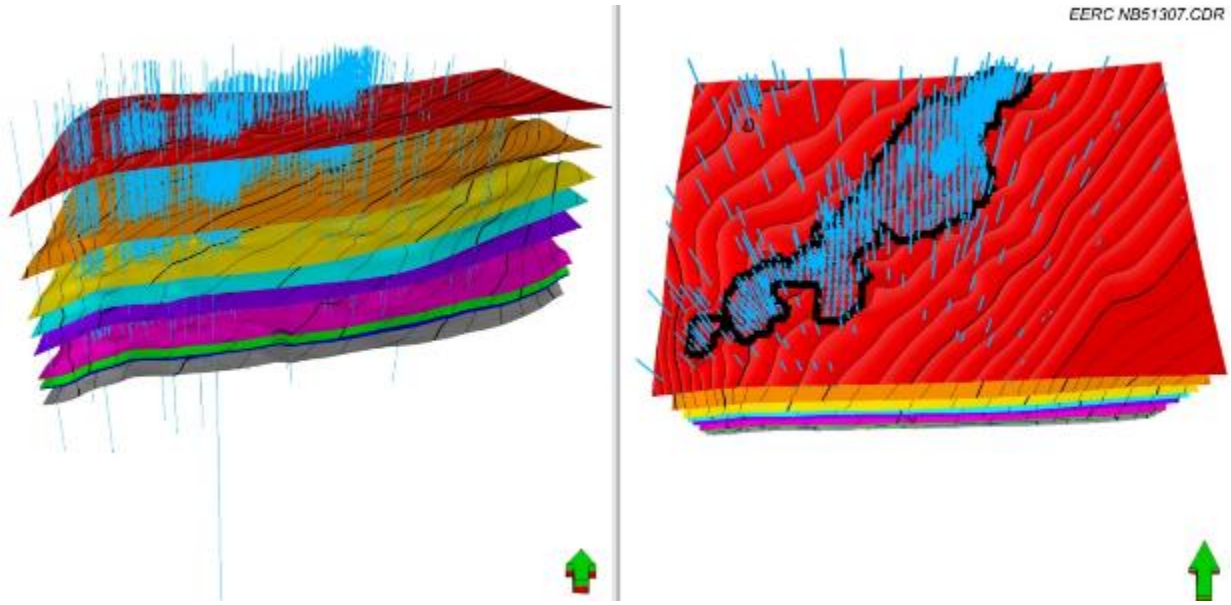

Figure A-2. Select structural surfaces within the Bell Creek reference model, well traces (blue vertical lines), and Bell Creek Field boundary polygon (black). The structural surfaces are (in descending order): Pierre (red), Shannon Sand (orange), Niobrara (yellow), Turner Sand (light blue), Belle Fourche (purple), Mowry Shale (pink), Springen Ranch (green), Skull Creek Shale (dark blue), and Lakota (gray) top surfaces (view is oblique from the south; vertical exaggeration is 10×).

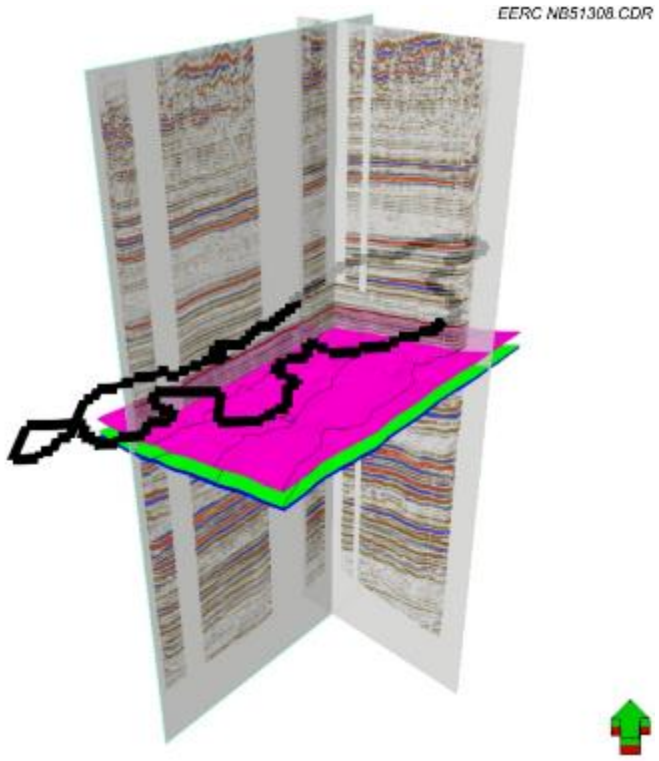

Figure A-3. Semitransparent 3-D baseline surface seismic in-line and crossline with the Bell Creek Field boundary polygon and select structural surfaces displayed (clipped to seismic data extent; Mowry (pink), Springen Ranch (green), and Skull Creek (dark blue) top surfaces; view is oblique from the south; vertical exaggeration is 10×).

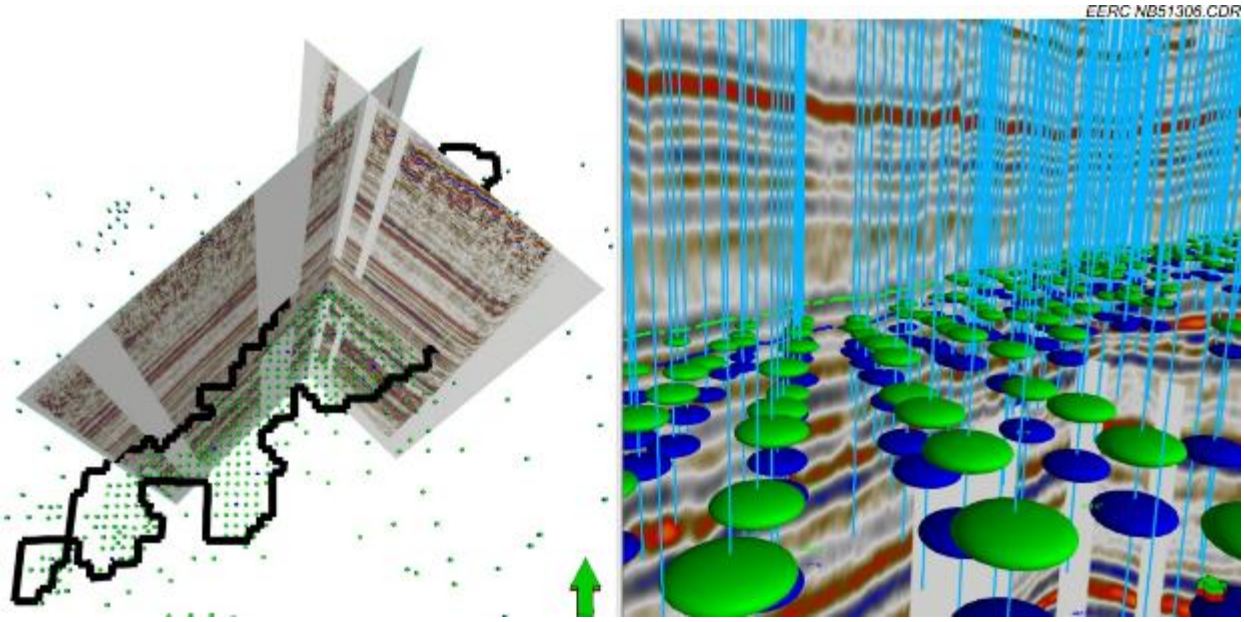

Figure A-4. At left: oblique map view from the south of a 3-D baseline surface seismic in-line and crossline with the Bell Creek Field boundary polygon and reservoir well tops (Springen Ranch – green; Skull Creek – dark blue). At right: view from near reservoir depth of well trajectories (vertical blue lines), well tops (Springen Ranch – green; Skull Creek – dark blue), and 3-D seismic in-line and crossline with interpreted horizons (Springen Ranch – green; Skull Creek – dark blue).

APPENDIX B

RESERVOIR SIMULATION RESULTS: COMBINED PHASES 1 AND 2

RESERVOIR SIMULATION RESULTS: COMBINED PHASES 1 AND 2

A systematic history match methodology using dimensionless groups was applied in this study to analyze the reservoir conditions and match the field data. The first step is to reduce the input, in this case by minimizing the uncertainty in free parameters (reservoir properties). This reduction of parameters is conducted by generating scaled variables (dimensionless groups), which cluster several dimensional parameters to a single dimensionless number (Chewaroungroaj and others, 2000). This method has been widely used to scale waterflooding and enhanced oil recovery (EOR) processes, as it directly correlates the parameters involved in the dynamic modeling process. Because both waterflooding and carbon dioxide (CO_2) flooding have been carried out in the field, dimensional analysis was used in the history match.

Shook and others (1992) derived five basic dimensionless groups for scaling waterflooding in a simplified homogeneous reservoir structure, as shown in Figure B-1. These groups were found to be sufficient to describe waterflooding performance in a 2-D, Cartesian, dipping reservoir with oil/water (two-phase) flow. Table B-1 shows the expressions of these groups: effective aspect ratio, mobility ratio (water), dip angle group, buoyancy number (water), and capillary number.

Wood and others (2008) used these groups as an initial basis to screen reservoir candidates for CO_2 flooding and storage in the Gulf Coast region. They found that these groups were not sufficient to describe CO_2-flooding behavior. The reason is that a complete set of dimensionless groups is derived from the most fundamental differential equations that govern the physical process, but waterflooding and CO_2 flooding belong to different categories. Waterflooding is an immiscible displacing process where water maintains reservoir pressure and drives oil from the

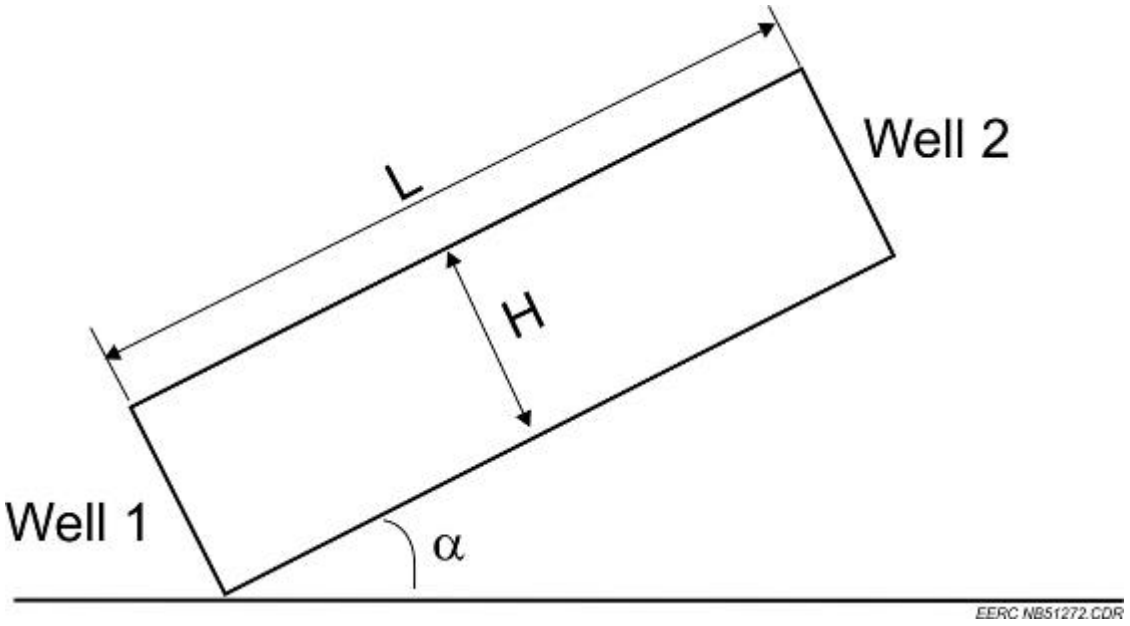

Figure B-1. Schematic of waterflooding in a dipping reservoir (from Shook and others, 1992).

Table B-1. Dimensionless Groups for Waterflooding (Shook and others, 1992)

Name	Expression
Effective Aspect Ratio	$R_L = \frac{L}{H}\sqrt{\frac{k_z}{k_x}}$
Mobility Ratio (water)	$M_w^* = \frac{k_{rw}^* \mu_o}{k_{ro}^* \mu_w}$
Dip Angle Group	$N_\alpha = \frac{L}{H} tan\ \alpha$
Buoyancy Number (water)	$N_w^* = \frac{k_x \lambda_{r2}^* \Delta\rho g cos\ \alpha}{u_T} \frac{H}{L}$
Capillary Number	$N_{Pc} = \frac{\lambda_{r2}^* \sigma}{L u_T} \sqrt{\phi k_x}$

reservoir to wells. In CO_2 flooding, the situation becomes much more complicated; both immiscible and miscible flooding may be the mechanisms for incremental oil production. When the reservoir pressure is lower than the minimum miscible pressure (MMP), immiscible flooding dominates the EOR process as CO_2 does not mix with oil. When the reservoir pressure rises above the MMP, CO_2 dissolves into the oil and changes the oil properties (density and viscosity are reduced, volume expands, and residual oil saturation decreases). As a result, miscible flooding becomes the main mechanism for incremental oil production.

In order to assess the CO_2-flooding process, Wood and others (2008) modified the governing equations and boundary conditions of Shook and others (1992) and rederived the dimensionless groups using inspectional analysis. Ten groups were derived for CO_2 flooding, as shown in Table B-2. The capillary number was dropped, and six new groups were added: injection pressure group, producing pressure group, mobility ratio (CO_2), initial oil saturation, residual oil saturation to water, and residual oil saturation to CO_2.

Table B-2. Dimensionless Groups for CO_2 Flooding (Wood and others, 2008)

Name	Expression	Name	Expression
Effective Aspect Ratio	$R_L = \frac{L}{H}\sqrt{\frac{k_z}{k_x}}$	Mobility ratio (water)	$M_W^* = \frac{k_{rw}^* \mu_o}{k_{ro}^* \mu_w}$
Dip Angle Group	$N_\alpha = \frac{L}{H} tan\ \alpha$	Mobility ratio (CO_2)	$M_g^* = \frac{k_{rg}^* \mu_o}{k_{ro}^* \mu_g}$
Buoyancy Number (gas)	$N_g^* = \frac{H \Delta\rho g cos\ \alpha}{\Delta P}$	Initial oil saturation	S_{oi}
Injection Pressure Group	$P_{injD} = \frac{P_{inj}}{P_{MM}}$	Residual oil saturation to water	S_{orw}
Producing Pressure Group	$P_{pD} = \frac{P_p}{P_{MM}}$	Residual oil saturation to gas	S_{org}

By reducing 20+ parameters to ten groups with clear physical meanings, the problem becomes much easier to analyze. The effective aspect ratio measures the rate of communication between fluids in the horizontal direction versus that in the vertical direction. Lower aspect ratio means that fluids flow easier in the vertical direction relative to the horizontal direction, which leads to segregation of fluids in the reservoir. Increased segregation means a smaller swept zone and lower flooding efficiency. Thus it is favorable to have larger aspect ratios in the reservoir. The dip angle group is a purely geometrical group without any rock or fluid properties. Long and thin reservoirs have high values of the dip angle group, which is favorable for both water and CO_2 flooding, as it reduces the impact of gravity override. The buoyancy number is a ratio of gravity force to viscous force; a higher value in this category means larger density difference between fluids and, therefore, higher potential for fluids to segregate in the reservoir and smaller sweep efficiency. Injection and producing groups are the measurements of pressure control in the wells. Both of them relate to the MMP, which is the lowest pressure for CO_2 and oil to be miscible. Miscibility is a function of temperature, pressure, and oil composition. The greater the miscibility between CO_2 and oil, the greater the displacement efficiency of the CO_2 flooding.

The five groups from the left-hand column of Table B-2 (discussed in the preceding paragraph) are closely related to reservoir geometry and operational constraints, which are more deterministic than the following rock–fluid related groups (right-hand column of Table B-2). The initial oil saturation and residual oil saturations to water and gas were measured from lab experiments, but the accuracy of their distribution in the reservoir remained uncertain. A mobility ratio characterized the moving abilities of fluids in the reservoir as the ratio of the viscous forces of one fluid to the viscous forces of another. The water/CO_2 mobility ratios were functions of fluid viscosities and relative permeability curves, which had higher uncertainty but considerable impact on oil recovery. Thus relative permeability and end point fluid saturation of fluids were the major parameters for adjustment in the history match process. Also, skin factor was used to mimic the formation damage/stimulation effects near wellbores.

REFERENCES

Chewaroungroaj, J., Varela, O.J., and Lake, L.W., 2000, An evaluation of procedures to estimate uncertainty in hydrocarbon recovery: Proceedings of SPE Asia Pacific Conference on Integrated Modelling for Asset Management, Yokohama, Japan, April 25–26, SPE 59449.

Shook, M., Li, D., and Lake, L.W., 1992, Scaling immiscible flow through permeable media by inspectional analysis: In Situ, v. 4.

Wood, D.J., Lake, L.W., Johns, R.T., and Nunez, V., 2008, A screening model for CO_2 flooding and storage in Gulf Coast reservoirs based on dimensionless groups: SPE Reservoir Evaluation & Engineering, v. 11.

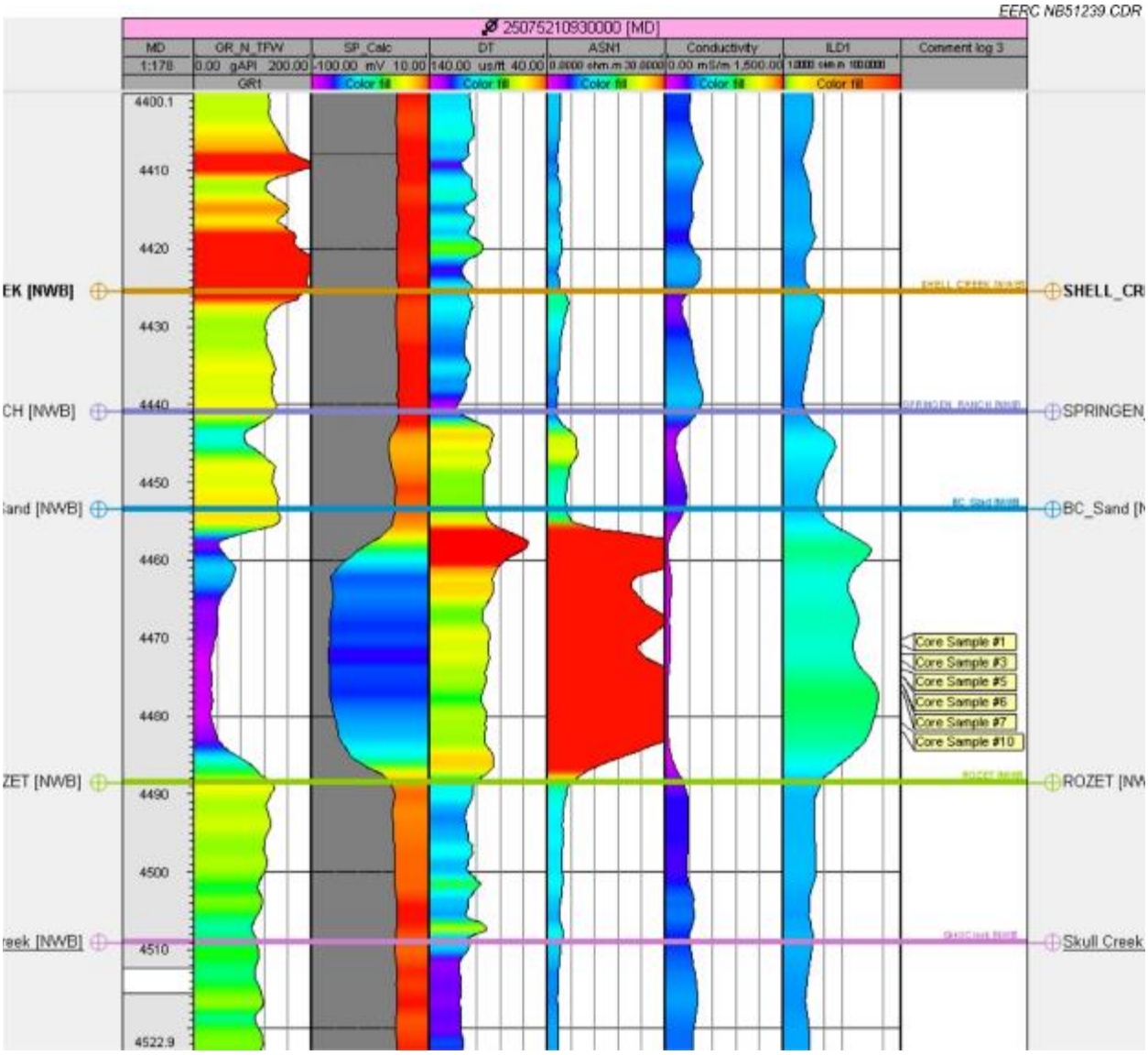

Figure B-2. Well 22-03 log display with relative permeability core sample depths plotted. Tracks are (from left to right) index (measured depth), GR, SP, DT, ASN, conductivity, ILD, and a comment track approximating sample depths. Well tops shown (from top to bottom) are Shell Creek shale, Springen Ranch, Bell Creek sand, Rozet, and Skull Creek Shale.

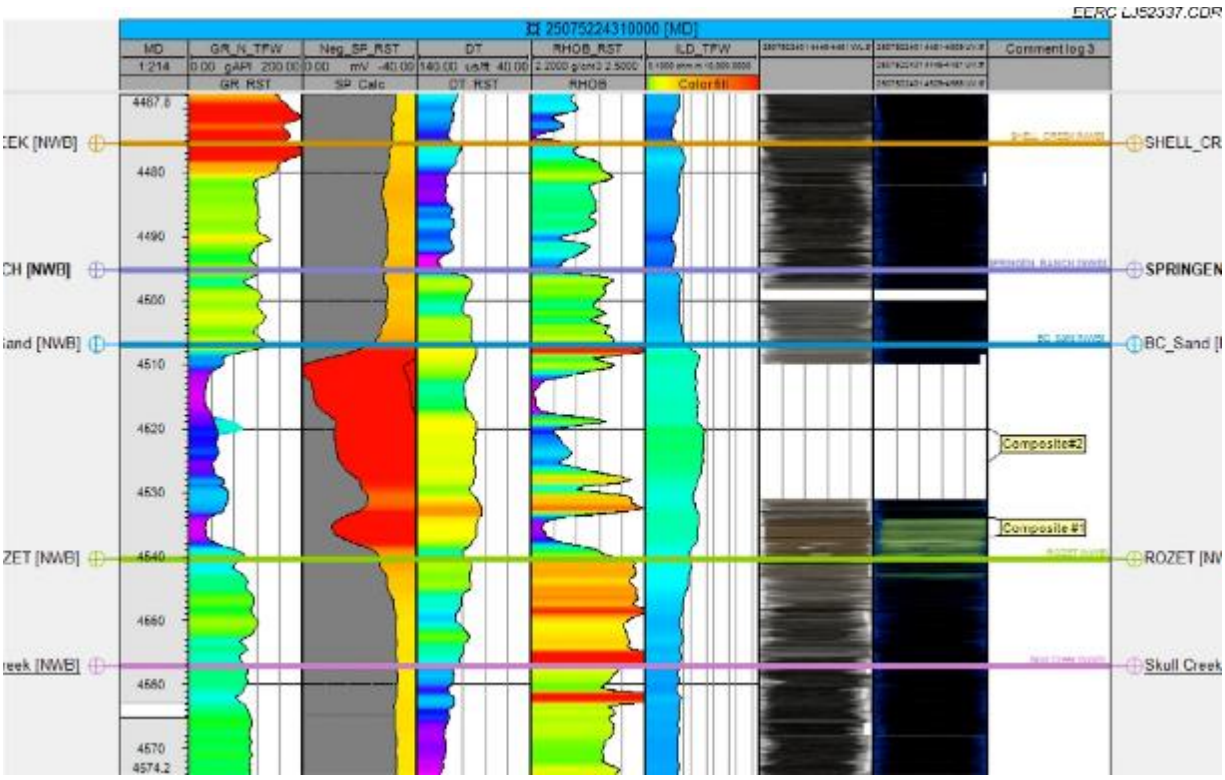

Figure B-3. Well 05-06 log display with relative permeability core sample depths plotted. Tracks are (from left to right) index (measured depth), GR, SP, DT, RHOB, ILD, white light core photo log, ultraviolet light core photo log, and a comment track approximating sample depths. Well tops shown (from top to bottom) are Shell Creek shale, Springen Ranch, Bell Creek sand, Rozet, and Skull Creek Shale.

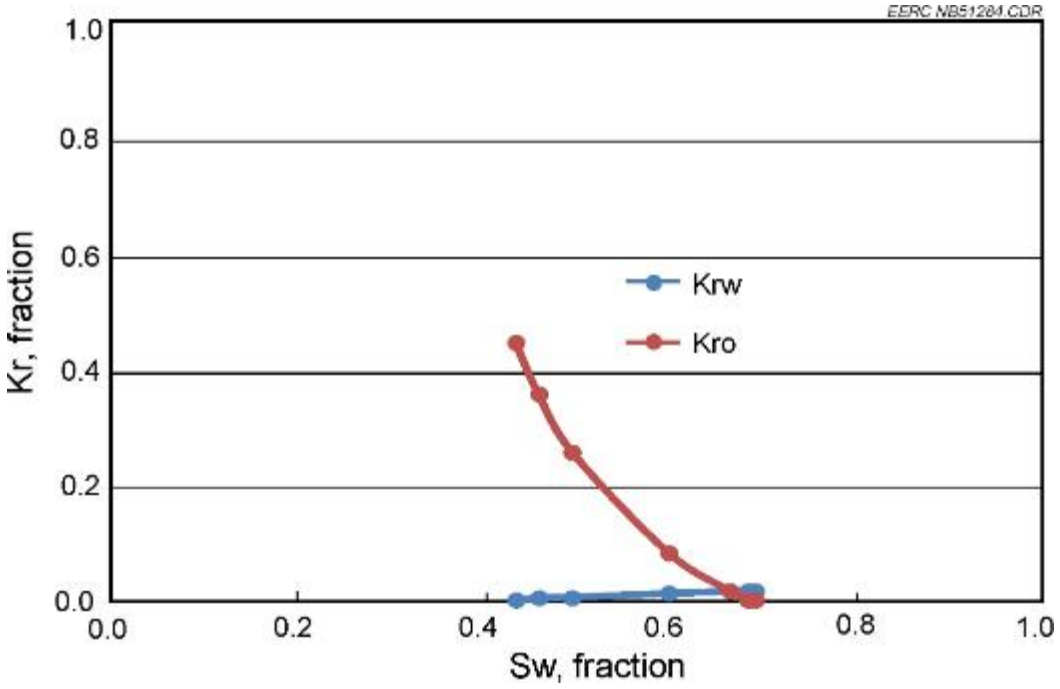

Figure B-4. Oil–water relative permeability curves for Well BC 22-03, Core Sample 1.

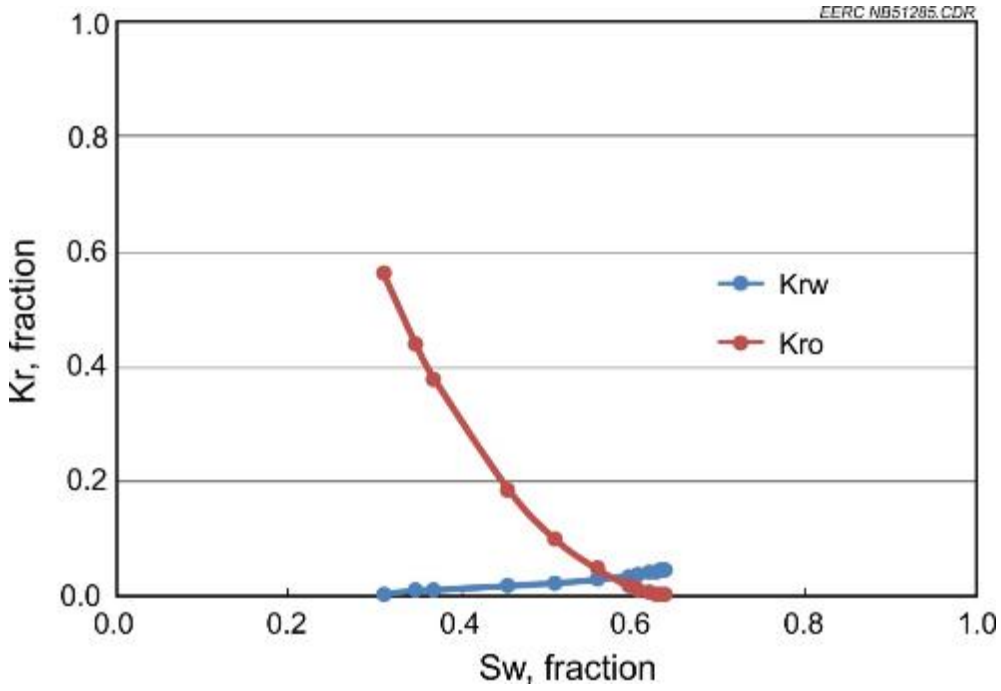

Figure B-5. Oil–water relative permeability curves for Well BC 22-03, Core Sample 5.

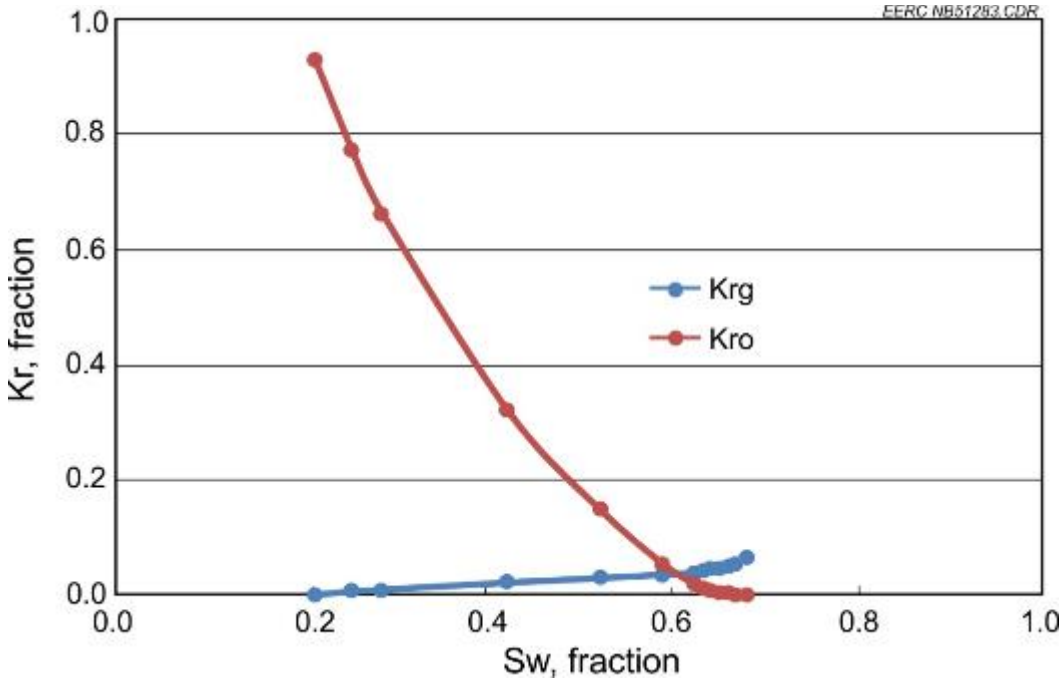

Figure B-6. Oil–water relative permeability curves for Well BC 22-03, Core Sample 6.

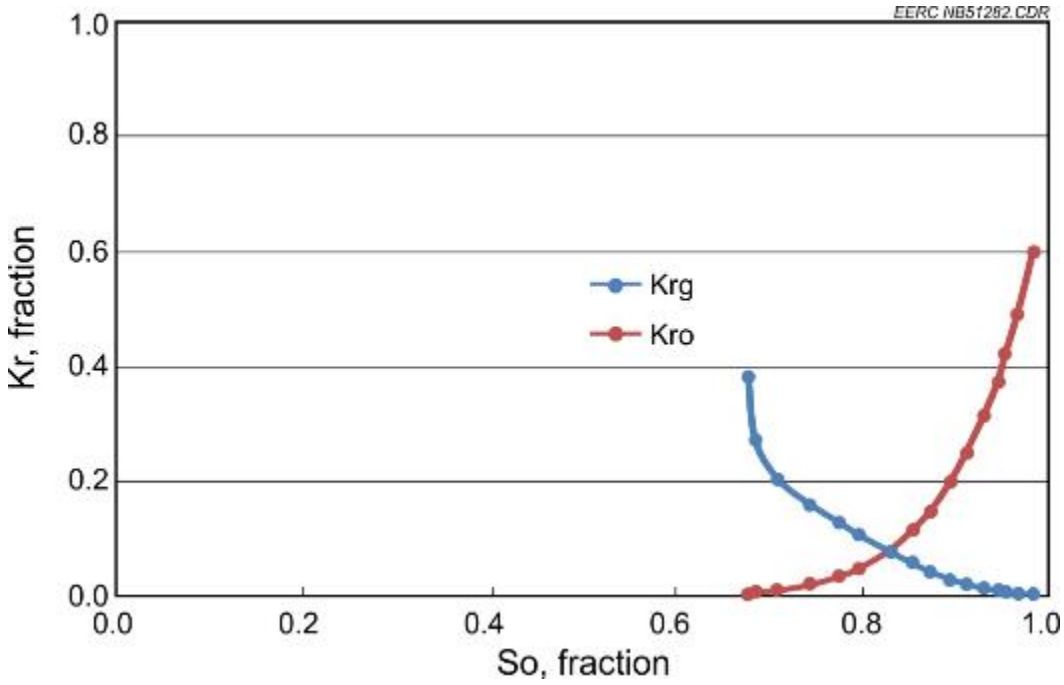

Figure B-7. Gas–liquid relative permeability curves for Well BC 22-03, Core Sample 3.

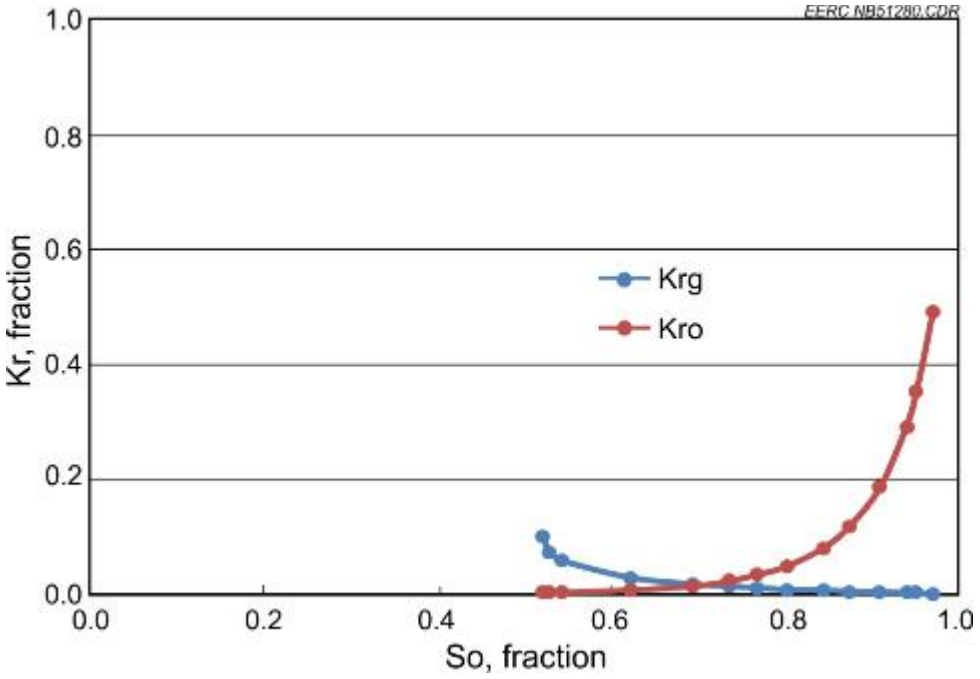

Figure B-8. Gas–liquid relative permeability curves for Well BC 22-03, Core Sample 7.

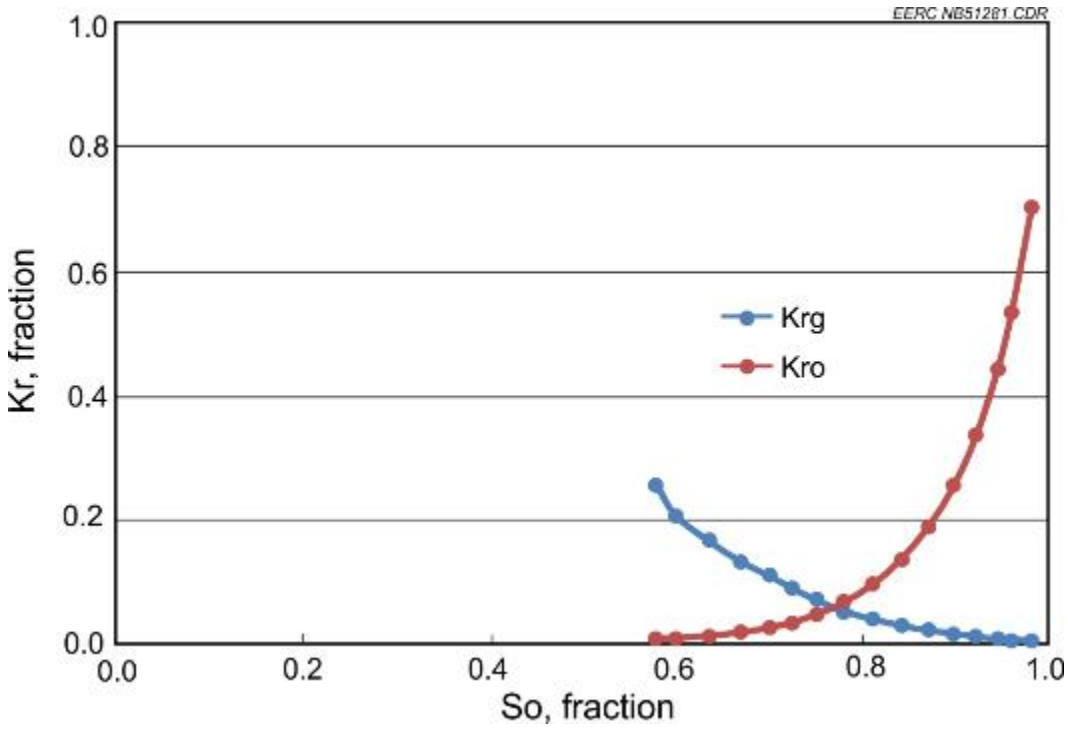

Figure B-9. Gas–liquid relative permeability curves for Well BC 22-03, Core Sample 10.

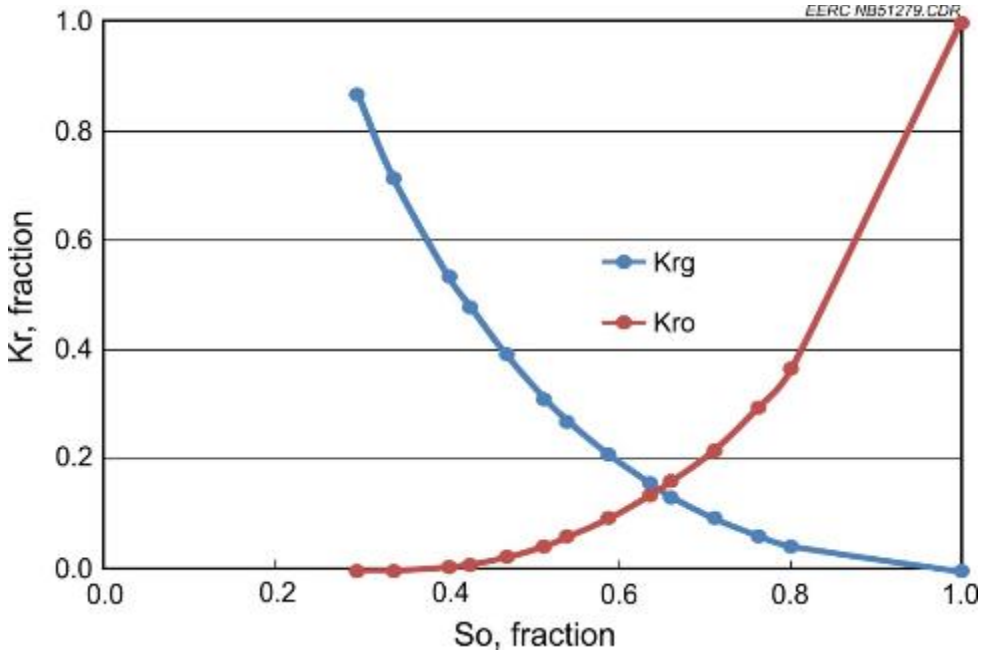

Figure B-10. Gas–liquid relative permeability curves for Well BC 05-06 OW, Composite Core 1.

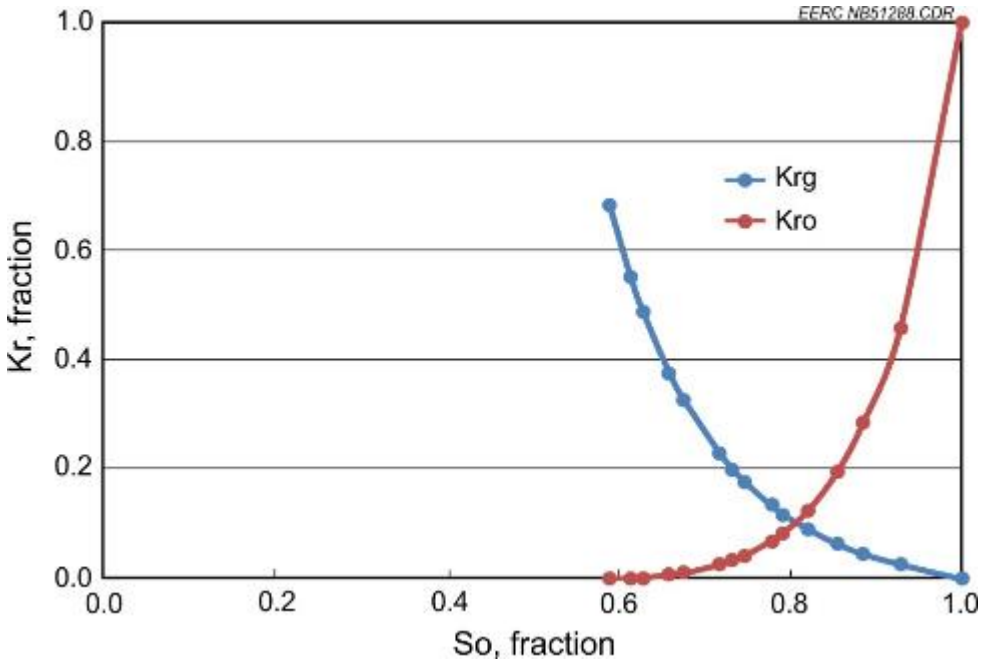

Figure B-11. Gas–liquid relative permeability curves for Well BC 05-06 OW, Composite Core 2.

Table B-3. Simulation Parameters for Predictive Cases

Case	Flood Style	Injector Pressure, psi	Producer Pressure, psi	Injected Time, year	CO_2 Injected, HCPV	Water Injected, HCPV	Cycle Length
1	WAG	2800	2300	45	2.5	0.5	3 month
2	CCI	2800	2300	45	4.7	–	–

Table B-4. Results of Simulation for Produced and Injected Water and CO_2 Volumes in 45 Years

Case	Cumulative CO_2 Injected, Bscf	Cumulative Water Injected, MMbbl	Cumulative CO_2 Produced, Bscf	Cumulative Water Produced, MMbbl	Stored CO_2, Bscf	Stored CO_2, Mt
1	662	120	600	123	62	3.30
2	1334	–	1228	15	106	5.65

Table B-5. Results of Simulation for Produced Hydrocarbons and Flood Performance

Case	Cumulative Oil Production, MMbbl	Peak Oil Production Rate, bbl/day	Average Reservoir Pressure, psi	Recovery Factor, %	Net Utilization Factor, Mscf/bbl
1	12.1	2428	2356	13.51	7.02
2	12.8	2470	2340	14.26	10.21

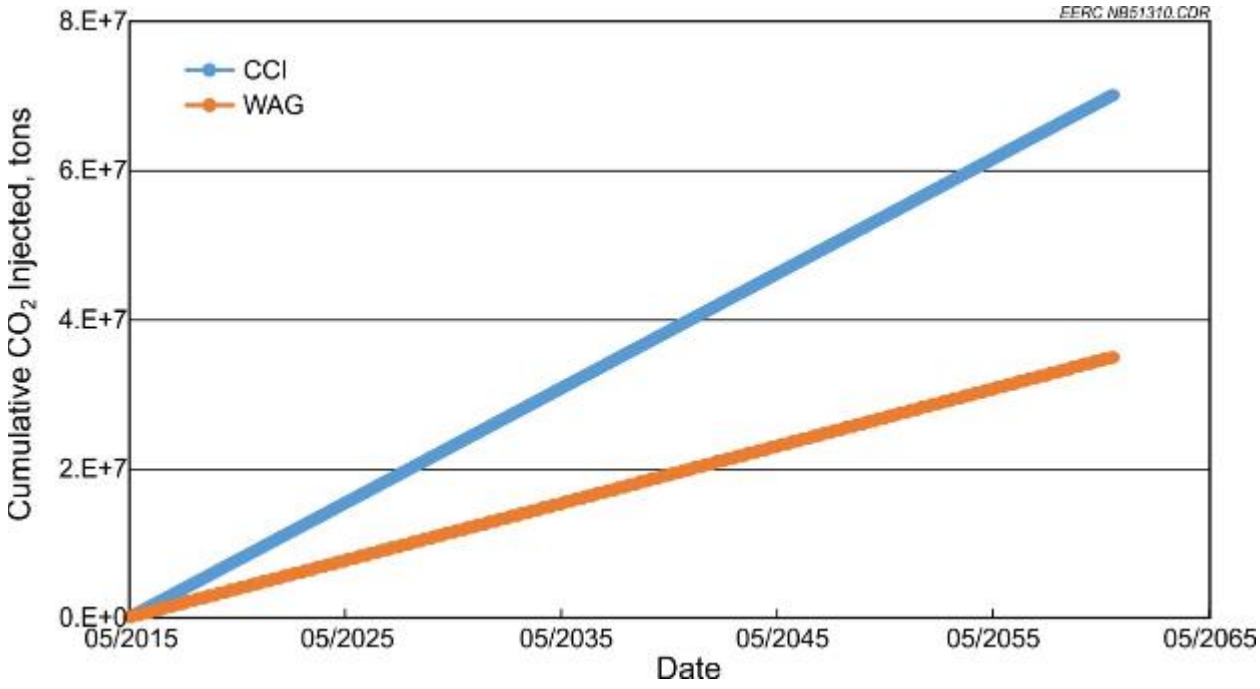

Figure B-12. Cumulative CO_2 injected during CCI and WAG over the simulation time frame.

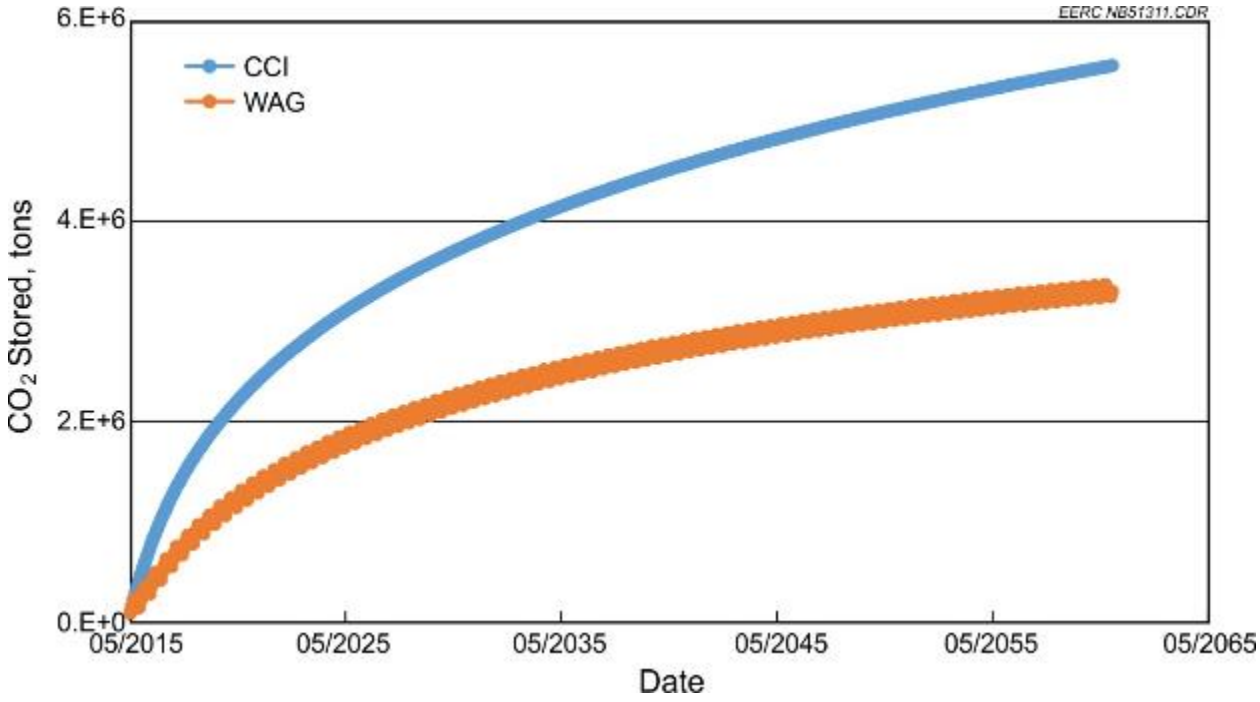

Figure B-13. Cumulative CO_2 stored during CCI and WAG over the simulation time frame.

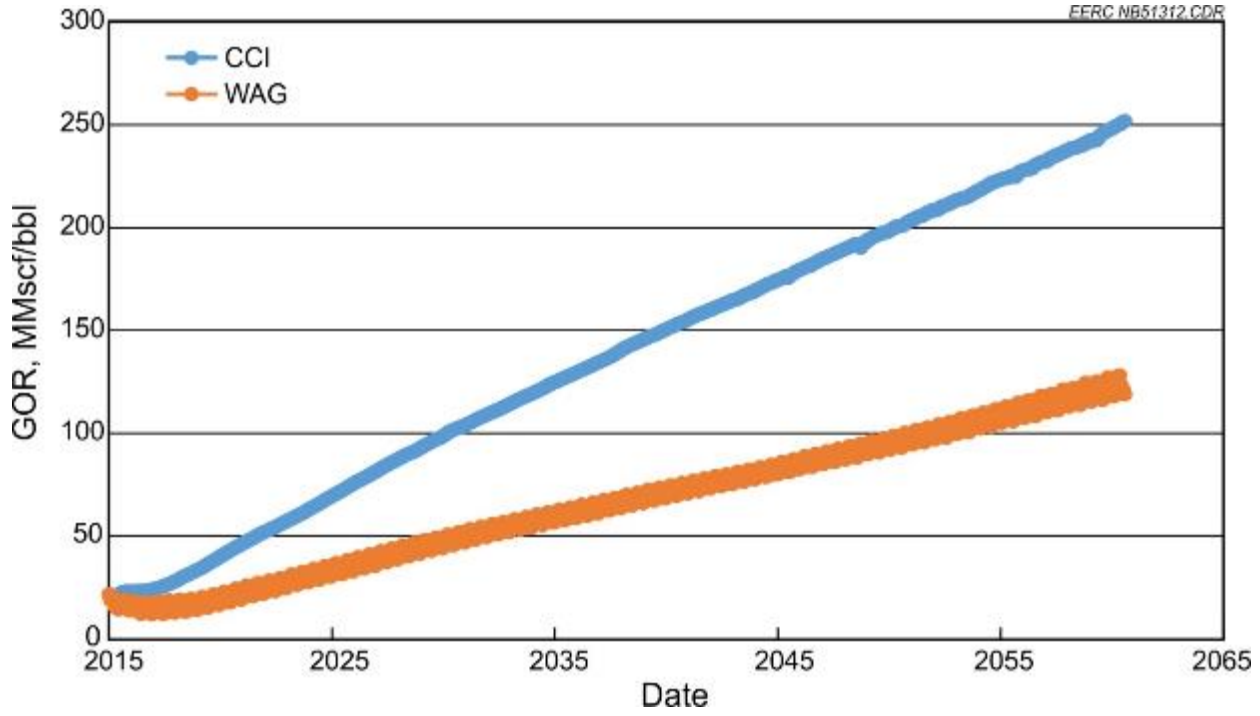

Figure B-14. GOR during CCI and WAG over the simulation time frame.

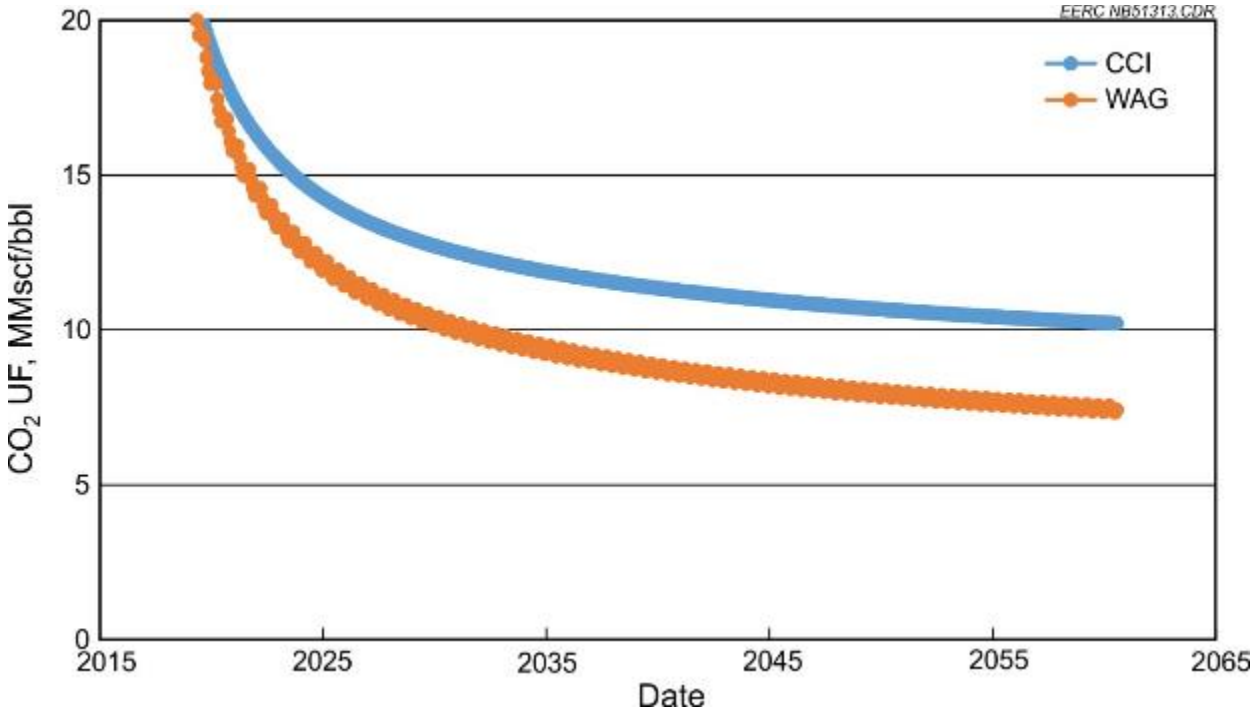

Figure B-15. CO_2 utilization factor during CCI and WAG over the simulation time frame.

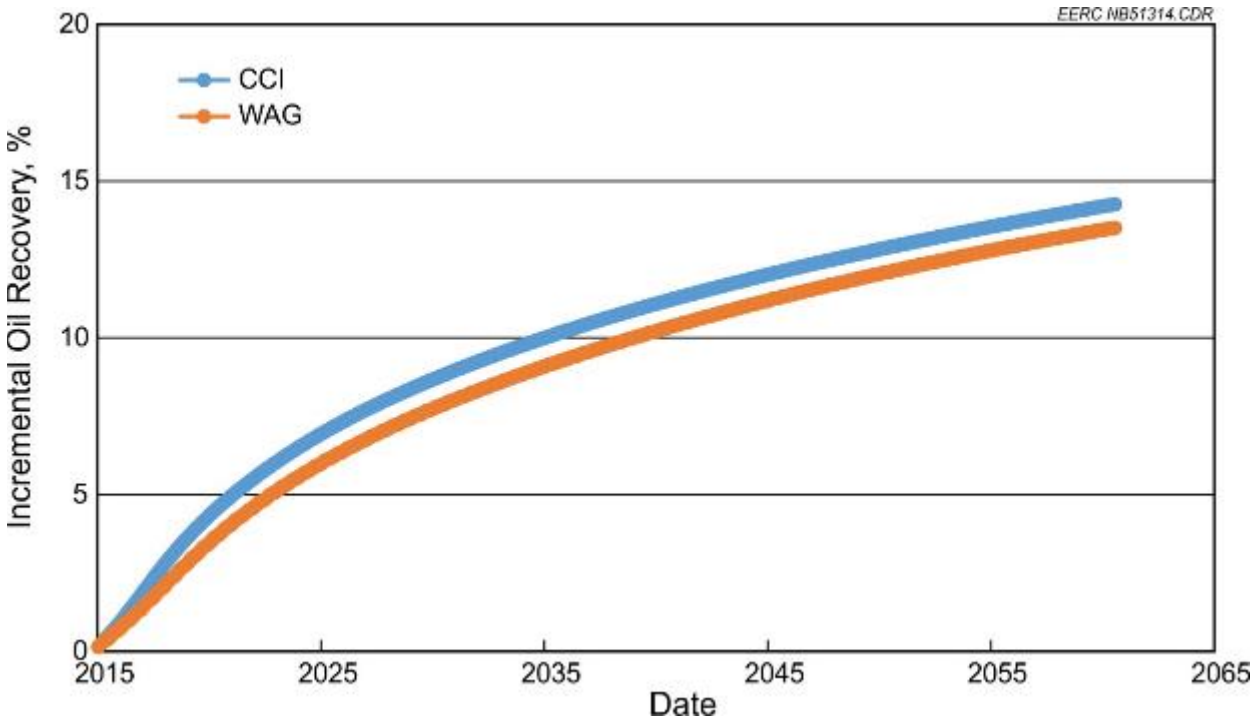

Figure B-16. Incremental oil recovery during CCI and WAG over the simulation time frame.